OXIDATION OF IRON

OXIDATION OF IRON

by

Albert Gilbert GOURSAT, M.Sc., Ph.D.

A Thesis

Submitted to the Faculty of Graduate Studies

in Partial Fulfilment of the Requirements

for the Degree

Master of Science

McMaster University

August 1972

MASTER OF SCIENCE (1972)   McMaster University
(Materials Science)   Hamilton, Ontario.

TITLE: OXIDATION OF IRON.

AUTHOR: Albert Gilbert GOURSAT, M.Sc. University of Limoges.
                                 Ph.D. University of Poitiers.

SUPERVISOR: Professor W. W. Smeltzer.

NUMBER OF PAGES: xiv, 122.

SCOPE AND CONTENTS:

        The main objective of this study was to gain an understanding

of the oxidation properties of iron at low oxygen pressures and at

high temperature.

        A thermogravimetric technique was employed to investigate

the oxidation of iron in oxygen over the pressure range 2.5×10^{-3} -

3.0×10^{-1} torr at temperatures ranging between 750° and 1000°C. The

oxidation curves exhibited distinct intervals of linear kinetics

followed by transition to intervals of parabolic kinetics during

exposures extending to 125 min. Linear kinetics governed the growth

of uniformly thick wustite scales; the linear rate constants showed

a proportional dependence on oxygen pressure due to reaction control

by a phase boundary reaction involving non-dissociation adsorption

of oxygen. Parabolic kinetics governed growth of wustite-magnetite

scales containing magnetite as outermost layers. The value of the

parabolic rate constants were independent of oxygen pressure since

scale growth was directly dependent on the iron vacancy gradient in

(ii)

wustite established by the oxygen activities at the Fe/FeO and
FeO/Fe$_3$O$_4$ interfaces.

Scanning electron microscopy techniques were used to gain
information on the growth of magnetite and hematite layers in the
multilayer scale consisting largely of wustite formed at high
temperature in the pressure range 2.5×10^{-3} to 760 torr.

ACKNOWLEDGMENTS

TABLE OF CONTENTS

LIST OF TABLES

LIST OF FIGURES

CHAPTER I

INTRODUCTION

One of the major alloys in use today is steel, especially
mild steel. An understanding of the oxidation properties of this
steel can be gained by learning in detail the oxidation behavior of
the simpler systems: iron, iron-carbon alloys, iron-silicon alloys,
iron-manganese alloys. Studies on the high temperature oxidation of
iron have been conducted in recent years with the result that this
process is well understood and a first part of our work consisted
with a review concerning this important literature. However diverse
features of oxidation based upon interfacial rate control remain
outstanding. In order to solve this problem several investigations
have been carried out to determine the influence of oxygen pressure
on the oxidation properties of iron at temperatures in the range
200°-500°C (131-136). The early oxidation stage involves processes
for nucleation and growth of magnetite. Growth of hematite on a
developed magnetite layer or separation of this layer from the metal
leads to a decrease in the oxidation rate. Detailed information is
not available, however, on iron oxidation properties at temperatures
sufficiently high for formation of wustite as a scale constituent
(64, 78, 94-96, 197). Nucleation and growth of wustite occurred in
the early stage of the reaction at temperatures exceeding 600°C; it
grows as a layer being controlled during exposures of short duration
by an oxide/gas phase boundary reaction. Growth of a wustite scale

1

at long exposures or the growth of a multilayer scale containing wustite, magnetite and hematite is associated with diffusional processes. Iron diffuses through wustite and magnetite whilst both iron and oxygen diffuse through hematite (86, 41, 42).

Large discrepancies occur among results reported for the influence of oxygen pressure on the form of oxidation curves obeyed and the magnitudes of the reaction rates at temperatures in the range 600°-1000°C. The results obtained at low pressures appear to be strongly affected by the iron purity and different transport limiting factors dependent upon experimental conditions (138). We have therefore systematically investigated the oxidation of high purity iron in oxygen atmospheres at pressures ranging from 2.5×10^{-3} to 760 torr and at high temperature.

The following section presents a literature survey on the subject of high temperature oxidation of iron, description of the experimental techniques, experimental results and discussion. Further, the experimental results are used to understand the oxidation mechanism.

CHAPTER II

REVIEW OF THE LITERATURE

Introduction

Iron exposed to oxygen represents a complex reaction system because oxidation usually leads to growth of more than one oxide on a metal which exhibits three allotropic forms. Since these reviews deal with high temperature properties of materials, we survey the oxidation properties of iron found at temperatures in the range 570° to 1371°C. These lower and upper temperatures correspond to the eutectoid and the melting points of wustite. It is necessary, in spite of these limitations, to select for review representative papers from the scientific literature leading to our present understanding of oxidation mechanisms. The reader is referred for additional information to the review by Paidassi (1) and to several monographs (1-5).

Parabolic and linear scaling kinetics may be regarded as representing ideal oxidation curves for growth of wustite scales or multilayer scales consisting of wustite, magnetite and hematite layers. Consequently, we first survey several aspects of iron-oxygen thermodynamics, the lattice defect structures and the diffusional properties of the various oxides because knowledge of these subjects is essential for formulating oxidation mechanisms. A survey is then presented of contributions dealing with nucleation and growth of wustite on iron and the mechanisms for linear and parabolic scaling kinetics. We finally are concerned with a topic of practical implication whereby anomalies from the ideal oxidation curves lead to more rapid scaling kinetics and development of diverse

3

scale morphologies.

Thermodynamics of the Iron-Oxygen System

The Fe-O phase diagram constructed by Hansen (6) from a critical appraisal of the literature available to 1957 is shown in Fig. 1. Iron exists in three allotropic forms: b.c.c. α-Fe at temperatures to 910°C, f.c.c. γ-Fe from 910° to 1390°C, and as b.c.c. δ-Fe from 1390° to its melting point of 1534°C. Although oxygen solubility in solid iron is very small, it has been determined for temperatures exceeding 800°C (7,8,9). This solubility in each allotrope increases with increasing temperature: its value is only 2-3ppm at 881°C and 83ppm at 1510°C.

Homogeneity regions for wustite, magnetite and hematite differ significantly as illustrated in Fig. 1. Also, the degree of nonstoichiometry and crystal structures of the oxides are dependent upon temperature and oxygen pressure. Wustite, the oxide of lowest oxygen content, has a NaCl structure. It exists from approximately 560°C to its melting range 1371-1424°C as a solid solution containing a large excess of oxygen in comparison to the stoichiometric formula. Magnetite is a spinel and the smaller degree of nonstoichiometry ranges from Fe_3O_4 to a small oxygen-excess. On the other hand, hematite supports a very small degree of non-stoichiometry toward the metal-excess side and it is of rhombehedral structure. The dissociation pressures of these oxides have been recently compiled (10,11).

Detailed information has become available only on the composition and thermodynamic solution behavior of wustite despite considerable work since the early intensive studies by Darken and Gurry (12) to define the stability ranges of the oxides. Some work has been completed by Schmahl et al (13) on magnetite-hematite equilibria and they summarize available results on this system. A representative phase diagram for wustite given
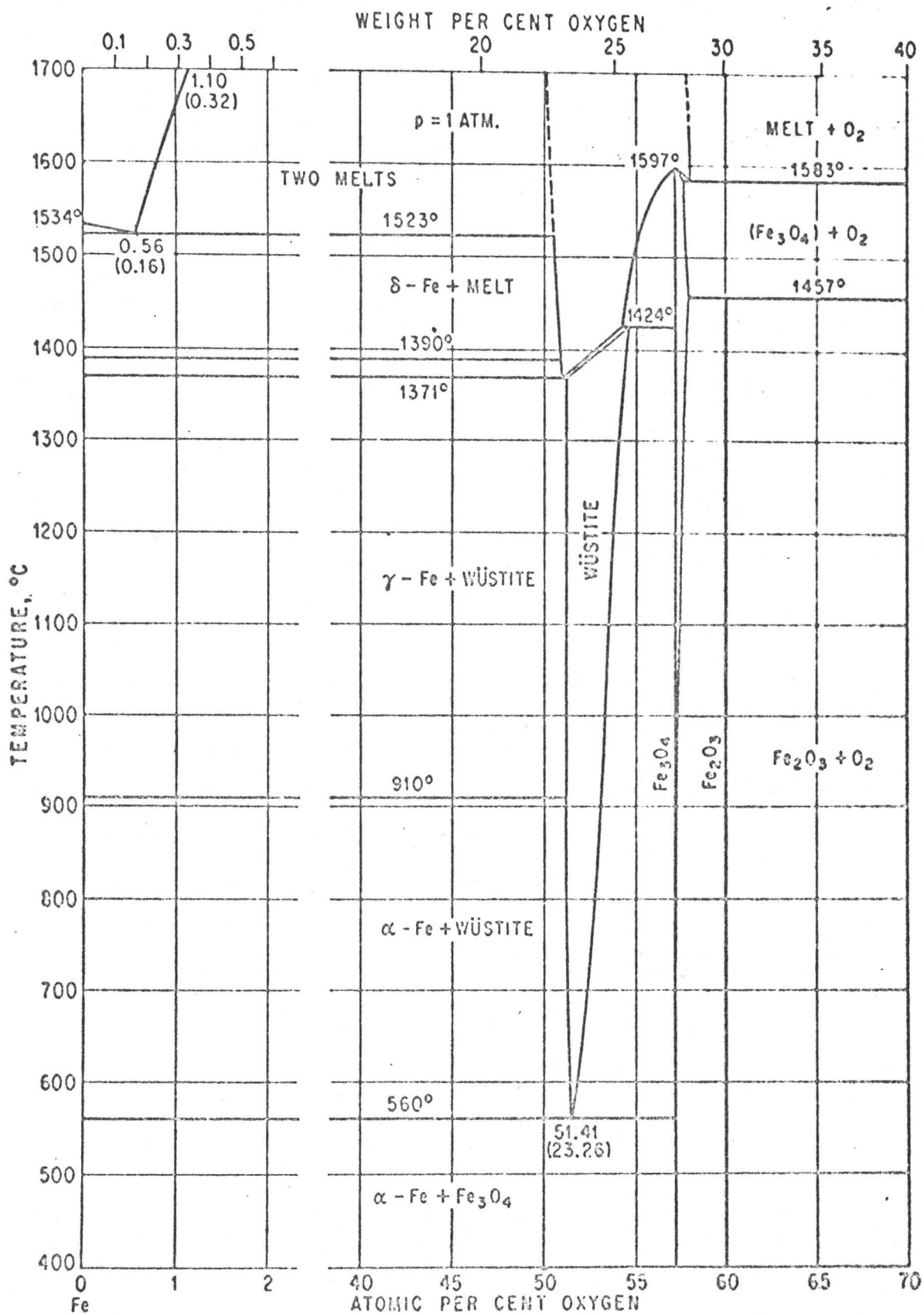
Figure 1

Iron-Oxygen Phase Diagram. (From Reference 6)

by Fender and Riley (14) is illustrated in Fig. 2; compilations of the experimental results are presented by Campserveux et al (15) and Lehmann (16). The wustite eutectoid temperature is stated to be 570°C, but it remains reported as lying in the range 560-610°C. It is apparent, nevertheless, that wustite does not exist as a stoichiometric compound and that the large variation in oxygen excess with temperature is determined mainly by the position of the wustite/magnetite boundary. Its phase extent is unusually large Manenc et al (17), Vallet and Raccah (18), Kleman (19), Carel et al (20) and Fender and Riley (14) have advanced oxygen activity and structural measurements which may be interpreted to show that wustite actually consists of three regions separated by order-disorder transitions. These regions are designated wustite I, II and III in Fig. 2.

Oxide Defect Structures

Investigations on the oxide defect structures have dealt mainly with wustite. Wagner and Koch (21) suggested in 1936 that the defects in this oxide could be interpreted as doubly charged iron vacancies (V''_{Fe}) and an equivalent concentration of ferric ions behaving as positive holes ($\oplus$). Accordingly, oxygen dissolves into the lattice as follows,

$$\tfrac{1}{2} O_2 = O_o + V''_{Fe} + 2\ \oplus \tag{1}$$

where O_o represents ions in normal lattice positions. Nonstoichiometry and the electrical conductivity are therefore proportional to the sixth root of the oxygen pressure if the defects exhibit ideal or Henrian solution behavior (22-24). However, this model is inadequate for interpreting the observed solid solution behavior especially at high levels of nonstoichiometry where thermoelectric measurements indicate a transition from p to n type conductivity (25). Geiger et al (26) and Swaroop and Wagner (27) have generalized this approach by suggesting that the dependence of vacancy concentration on oxygen pressure appears to satisfy the more general relationship,

Figure 2

Wustite Phase Field.(From Reference 14)

$$\tfrac{1}{2} O_2 = O_o + V_{Fe}^{'m} + m\,\theta \tag{2}$$

where m is the degree of vacancy ionization. Upon expressing the mass law in terms of concentrations and activity coefficients for the point defects,

$$K = \gamma_V \gamma_\theta^m [V_{Fe}][\theta]^m \Big/ (P_{O_2})^{\tfrac{1}{2}} \tag{3}$$

it was found that the parameter $\gamma_V \gamma_\theta^m$ collectively changed from the ideal value of unity to larger values at higher levels of nonstoichiometry. They suggested that this behavior possibly arises from the ordering of vacancies and electron holes to the ordered phases previously designated I, II and III. In contrast to this approach, Laptev (28) has attempted to determine variations in the properties of wustite by a statistical thermodynamic method in which the iron ions in different valence states are not distinguished.

Another approach has been suggested by Libowitz (29) and Kofstad and Hed (30) based upon structural determinations of quenched wustite by Roth (31). Clusters were found which were assumed to arise from complexes consisting of two iron vacancies in neighboring octahedral sites and an iron interstitial in a tetrahedral site. Electronic exchange may occur between ions in octahedral and tetrahedral sites (32,33). To correlate nonstoichiometry with lattice defects, Libowitz postulated that these complexes are stable at high temperatures. Hence, the defect equilibrium may be written as,

$$\tfrac{1}{2} O_2 + 2Fe_{Fe} = O_o + [2V_{Fe}Fe_i]' + \theta \tag{4}$$
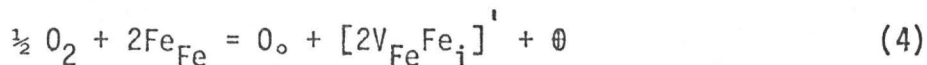
where Fe_{Fe} and Fe_i represent cations in octahedral and interstitial positions. A more general scheme was adopted by Kofstad and Hed by taking into account the concentrations of all atoms and sites and considering different degrees of ionization for the complexes. The most reasonable equilibria to account for nonstoichiometry were,

$$\tfrac{1}{2} O_2 + Fe_{Fe} + V_i = O_o + [2V_{Fe}Fe_i] \tag{5}$$

$$Fe_{Fe} + [2V_{Fe}Fe_i] = [2V_{Fe}Fe_i]' + \theta \tag{6}$$
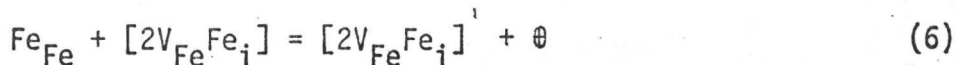
where V_i represents an empty tetrahedral site and the complexes have been represented as existing in the neutral and singly ionized states. Seltzer and Hed (34) analyzed the conductivity and Seebeck coefficient in terms of these complexes but with limited success. One must therefore conclude that general features of the defect structure of wustite have been elaborated but that more refined measurements with different techniques on nonstoichiometry, oxygen activities, electronic and structural properties are required for establishment of an appropriate model.

The crystal structures of wustite and magnetite are interrelated (35). Verwey and Haayman (36), and Bhatt and Merchant (37) have shown that nonstoichiometry of magnetite is caused by the presence of iron vacancies presumably over octahedral sites whilst Smut (38) has concluded that the proportion of ferric ions on the tetrahedral sites in stoichiometric magnetite is proportional to the iron/oxygen ratio as for wustite. Due to the paucity of results, investigators believe that eqn.(1) approximately describes defect equilibrium. It is usually assumed that hematite is slightly oxygen deficient since ferrous and ferric states are readily available to iron. This property would lead to the presence of either anion vacancies or interstitial cations. Hematite does behave as an n-type semiconductor (39) and the model has been favored for nonstoichiometry determined by oxygen vacancies and free electrons,

$$\tfrac{1}{2} O_2 + V_O'' + 2e^- = O_o \tag{7}$$

Diffusional Properties

A substantial amount of work to determine the diffusion coefficients of iron and oxygen in the solid phases has been carried out in order to interpret oxide defect structures and the oxidation mechanisms

for iron. Oxygen diffuses rapidly in iron albeit its very small solubility (8,9). Iron acts as the mobile species in wustite and magnetite at rates conspicously more rapid in wustite (40); iron and oxygen both migrate at relatively low rates in hematite (41,42). These characteristics are illustrated by the Arrhenius plots of the self-diffusion constants in Fig.3.

The diffusional properties of wustite have been more fully studied than for any other oxide. In 1953, Himmel et al (40) determined the rates of iron self-diffusion in artificially prepared wustites of different compositions using a radio-active iron tracer. They found that the value of the self-diffusion constant was directly dependent on the concentration of iron vacancies at 800°, 897°and 983°C. Hembree and Wagner (43) also found this dependence at 1100°C. These linear relationships are shown by the plots of the self-diffusion constant versus iron vacancy concentration in Fig. 4. This simple dependence, moreover, indicates that the chemical diffusion constant and mobility of iron vacancies is independent of nonstoichiometry since,

$$D_{Fe}X_{Fe} = D_{\square}X_{\square} \tag{8}$$

where $D_{\square}$ is the iron vacancy diffusion constant and X_{Fe} and $X_{\square}$ are the atom fractions of metal sites filled and devoid of iron, respectively. Engell (44) has shown that the hypothesis is consistent with the above results and that it is valid for the vacancy gradient across wustite in a growing scale. He found the diffusivities for iron vacancies determined from the results of these two different types of experiments to be in good agreement,

$$D_{\square}(cm^2/min) = 1.22 \times 10^{-1} \exp.-29,700/RT \tag{9}$$
$$D_{\square}(cm^2/min) = 2.35 \times 10^{-1} \exp.-30,500/RT \tag{10}$$

More later measurements, however, demonstrate that these relationships must be regarded as first approximations. Desmarescaux and Lacombe (45,46) have shown that a linear dependence of self-diffusion on vacancy
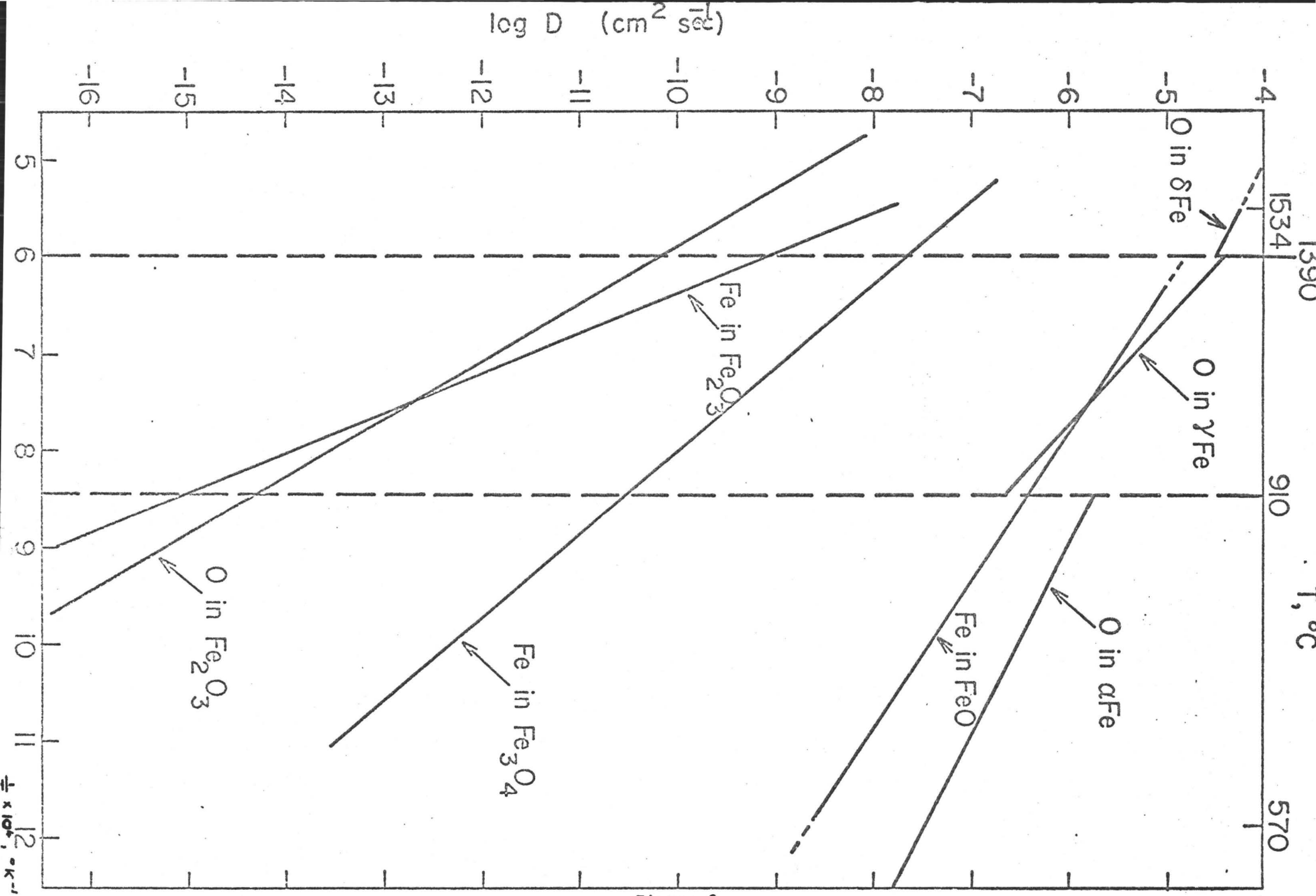
Figure 3

Arrhenius Plots for Iron and Oxygen Self-Diffusion Constants in

Iron and Iron Oxides. (From References 9,40,42,50)
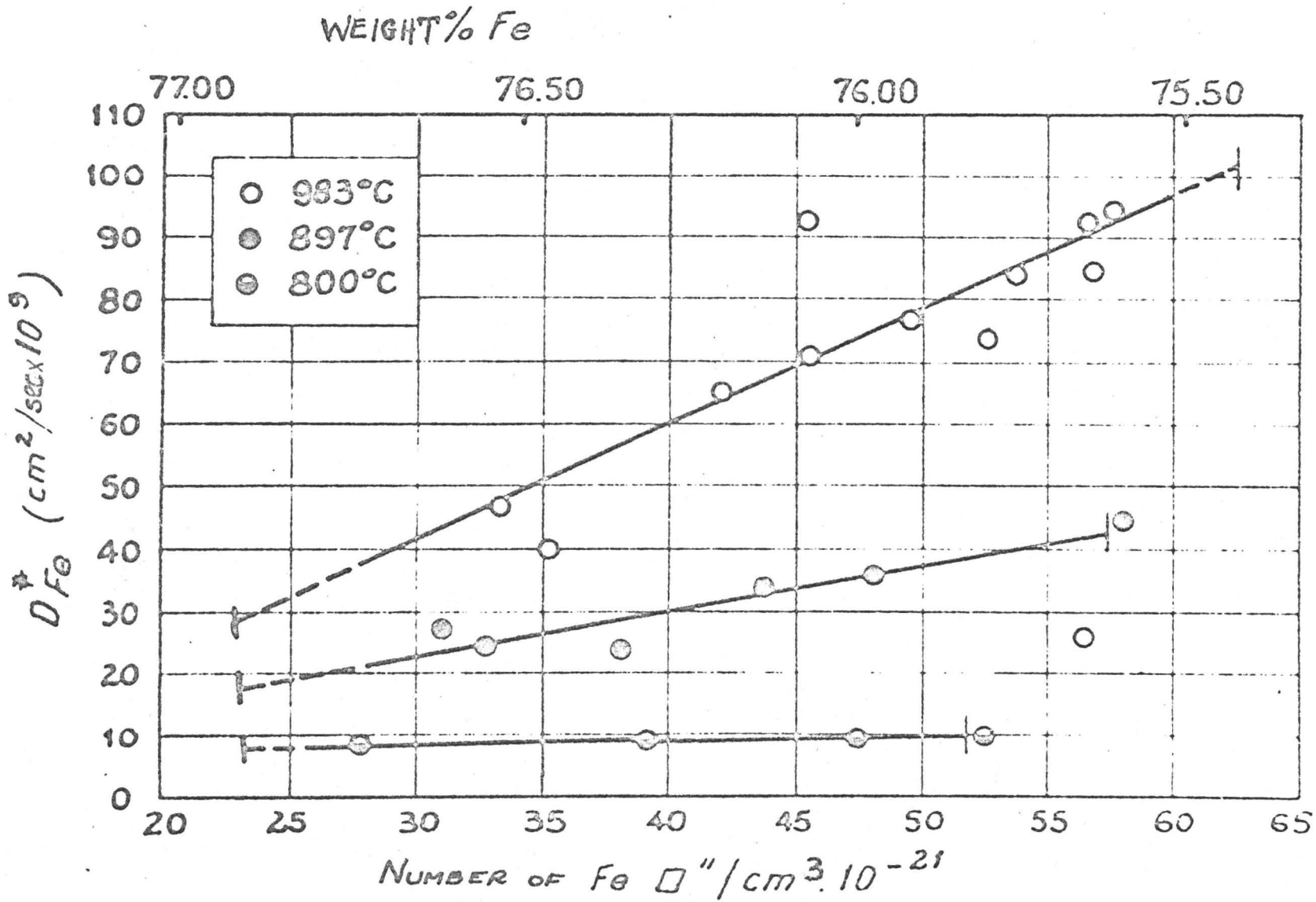
Figure 4

Variation of Self-Diffusivity of Iron with Temperature and

Composition of Wustite. (From References 40)

concentration may not be obeyed at low temperatures as a result of their interaction. The measurements demonstrate, nevertheless, that approximate agreement is obtained between the diffusion parameters determined by radio-tracer and by electrical coulometric techniques. Childs et al (47) have critically appraised the experimental results which indicate that the diffusion constant for iron vacancies slightly decreases as the wustite field is traversed to higher oxygen contents. We must therefore conclude that the diffusion mechanism as well as the defect structure of wustite have not yet been completely defined.

Diffusivities of the ionic species in magnetite and hematite have been determined but the broad scatter of results suggests that diffusion in these oxides of small nonstoichiometry is strongly influenced by impurity contents and structures of the materials examined. These results are summarized in Table 1 from a compilation by Harrop (48) of self-diffusion in oxides. Iron migrates most rapidly in magnetite, the activation energy being of the order 53-85 kcal/mole compared to the value of 100-112 kcal/mole for hematite. Oxygen diffusion in magnetite is negligible, whereas in hematite, oxygen diffuses at approximately the same rate as for iron at high temperatures. Mobility of oxygen in hematite becomes largest at low temperatures.

Nucleation and Growth of Oxides

It has been amply demonstrated by Bardolle and Bénard (53-55) in the early 1950's that the very first stage of oxidation is a discontinuous process. The initial reaction steps involve oxide nucleation at active sites on the metal surface. Growth of these nuclei, which are monocrystalline, leads to oxide oriented to the underlying metal grains. Fig. 5 represents the number of wustite nuclei as a function of the crystallographic orientation of iron, this number is maximum on the (100) plane and minimum on the (110) plane. These results were extended

TABLE 1

Self-Diffusion Constants of Iron and Oxygen in Magnetite and Hematite.

The diffusivities are expressed in Arrhenius form: $D(cm^2/sec) = D_0 \exp - E/RT$

Oxide	Material	Diffusing Element	Temperature Range (°C)	D (cm^2/sec)	E (kcal/mole)	Reference
Fe_3O_4	single crystal	iron	850 - 1075	6.0×10^5	84.0	49
	polycrystalline	iron	850 - 1075	104	74.7	49
Fe_3O_4	polycrystalline	iron	750 - 1000	5.2	55	40
Fe_3O_4	polycrystalline	iron	770 - 1200	0.25	53.9	51
Fe_2O_3	single crystal	iron	1000 - 1217	4.0×10^5	112	40
Fe_2O_3	polycrystalline	iron	750 - 1300	4.0×10^4	112	41
Fe_2O_3	polycrystalline	iron	950 - 1050	1.3×10^6	100	51
Fe_2O_3	polycrystalline	oxygen	1150 - 1250	10^{11}	146	52
Fe_2O_3	polycrystalline	oxygen	900 - 1250	2.0	77.9	42

TABLE 2

Measured and Calculated Parabolic Rate Constants for Oxidation of Iron to Wustite. (From Reference 40)

Pressure: 1 atm Temp. (°C)	$K_p (g.O/cm^2-sec^{1/2})$		
	Experimental	Calculated	$K_p(exptl)/K_p(calcd)$
800	2.3×10^{-4}	2.3×10^{-4}	1.0
897	5.0×10^{-4}	4.8×10^{-4}	1.04
983	8.2×10^{-4}	7.7×10^{-4}	1.07
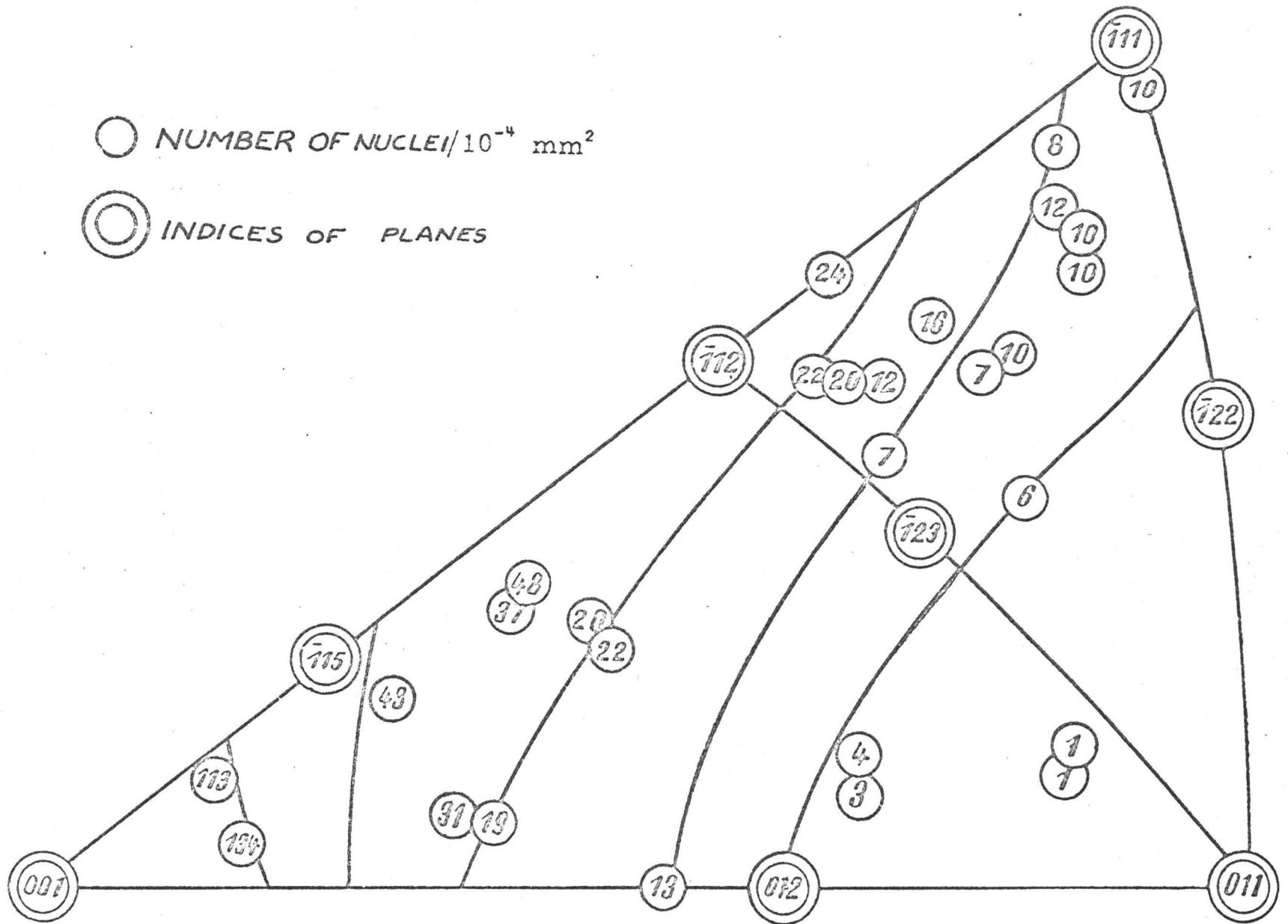
Figure 5

Influence of the Crystallographic Orientation of Iron on

the Density of Wustite Nuclei.(From Reference 55)

by Gulbransen et al (56,57) and their conception of the initial reaction stages is represented by the model in Fig. 6. At the beginning of oxidation, the nuclei grow laterally and vertically until the metal is covered by a film of small oxide crystallites. Oxide then continues to form preferentially at certain growth centres until relatively larger crystals cover the surface as an oriented uniform mosaic. Several authors have advanced results to show that the cube plane of wustite grows on the cube plane of α-Fe while the <100> directions of the oxide lie parallel to the <100> directions in the metal (58).

Growth mechanisms in the early stages of oxidation are still a matter of conjecture. Rhodin et al (59) elaborated a model by taking into account and analysing the various partial processes involved: for example, adsorption, nucleation, surface diffusion and capture of oxygen. Following the concepts of Bénard (60), Rhead (61) developed a model in which the growth rate of nuclei is assumed to occur by surface diffusion.

Chittum (62) has analyzed these processes in terms of an electro-chemical mechanism for preferential oxide growth at anodic sites on the surface.

The only quantitative investigations which have been done so far concerning wustite nucleation and growth kinetics were realized in dry oxygen by Charbonnier et al (63,64). They found that a distinction must be made for the crystallographic, temperature and oxygen pressure dependences of the parameters governing nucleation and growth. With respect to formation of nuclei, the number and the induction period for their appearance was dependent upon the crystallographic orientation of the metal face. The micrograph in Fig. 7 illustrates the variation in number and size of the oxide crystals on differently oriented iron grains. The number of these crystals on a given metal face decreased with temperature and increased with oxygen pressure. Oxide growth followed
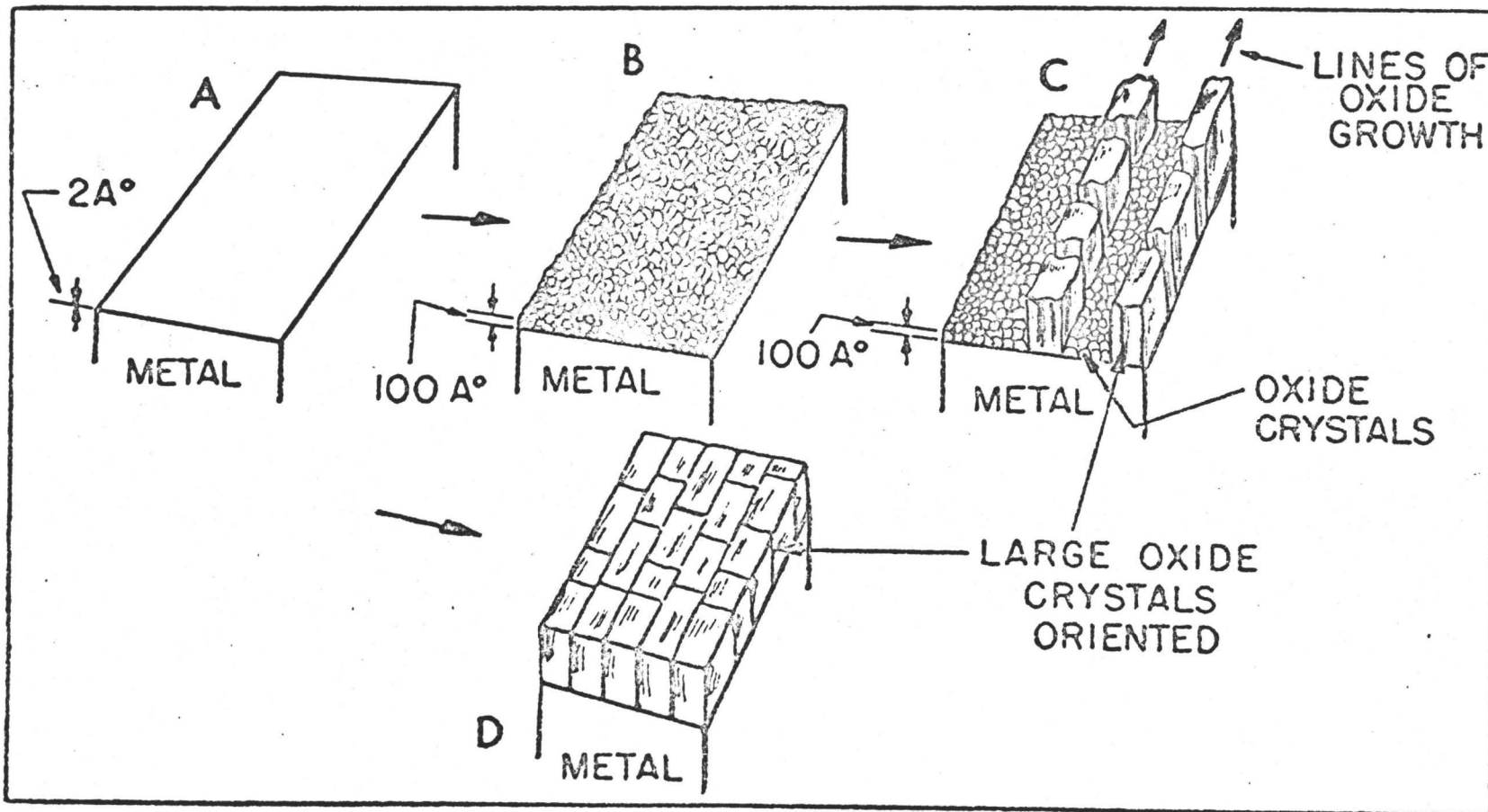
Figure 6

Oxidation Model: (A) Adsorbed Oxygen Film, (B) Fine Mosaic

Structure of Crystals, (C) Growth Centers of Large Crystals,

(D) Uniform Oxide Layer.(From Reference 56).
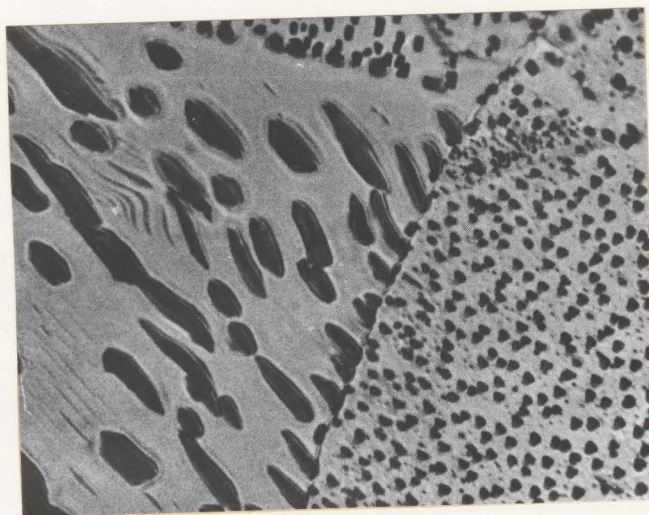
Figure 7

Wustite Growth Centers on Zone-Refined Iron Exposed
to Oxygen at 950°C,(650X).(Reference 64)

the relationship,

$$\frac{\Delta m}{A} = Kt^n \qquad\qquad (11)$$

where Δm is the weight gain of a specimen of area A, t is the time and K and n are constants. Typical oxidation curves for zone-refined iron are shown in Fig. 8. As illustrated by these curves, the reaction rates are strongly dependent on oxygen pressure. These rates were found to be also affected by trace amounts of carbon in the metal. The values of the constants K and n varied with metal orientation and exhibited different variations with temperature and oxygen pressure. Formation of wustite nuclei have also been observed upon oxidizing iron in water-hydrogen atmospheres (65).

Several examples on nucleation and growth of wustite at temperatures near the wustite eutectoid point have been reviewed by Paidassi (1) which upon their extension may give a more accurate evaluation of this transformation temperature. One example is concerned with oxidation in air over the range 570°-625°C (66). In this case, wustite was not observed in the scale formed at 585° even after 24hr. Nevertheless, at 604°C, wustite islands appeared on the metal surface and they grew into a layer covered by magnetite. Since wustite may be quenched to room temperature, a carefully controlled investigation on the growth and equilibration of their scales formed at small temperature intervals could lead to a more accurate determination of the eutectoid temperature.

Nucleation of the higher oxides, magnetite and hematite, on wustite is a relatively slow process even though investigated oxygen pressures greatly exceed the dissociation pressure of hematite. Since iron migrates rapidly through wustite, it grows until a complete layer covers the metal. Magnetite is not nucleated until the supply of oxygen adsorbed exceeds the amount of iron diffusing to the wustite surface.
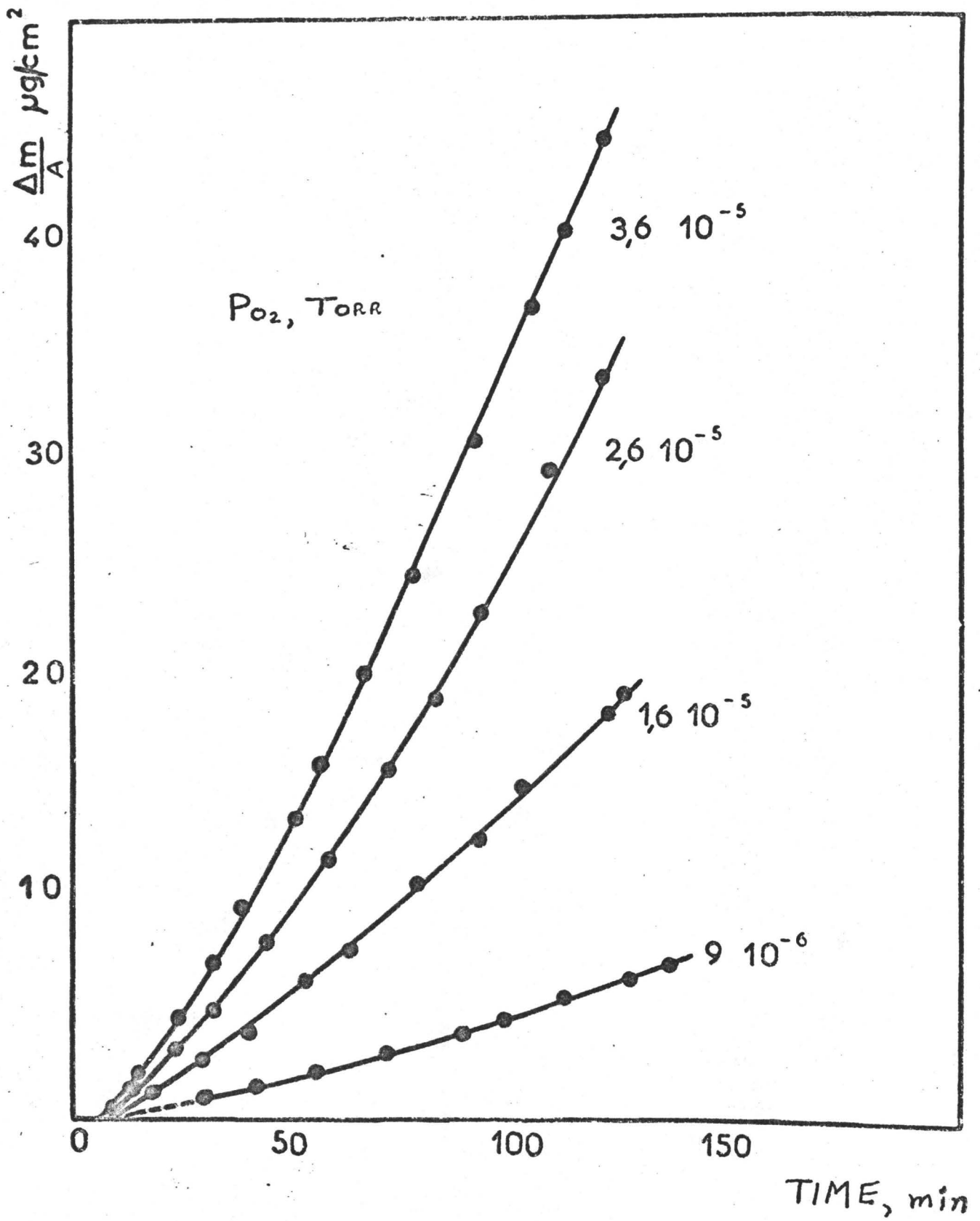
Figure 8

Influence of Oxygen Pressure on the Oxidation Kinetics of Zone-
Refined Iron to Wustite at 850°C. (From Reference 64)

Under this condition, Paidassi et al.   (67) have observed that magnetite nucleates as small isolated crystals on wustite upon exposing iron to water vapor and carbon dioxide at elevated temperatures.

Phase Boundary Kinetics

A region of an oxidation curve corresponding to linear kinetics can be identified after a uniformly thick wustite layer has grown on iron exposed to an atmosphere containing oxygen at low thermodynamic activity. This feature was observed by Fischbeck et al (68) in 1934 upon oxidizing iron in carbon dioxide. They concluded that the reaction was controlled by the passage of iron into the scale. This premise was accepted until 1953 when Hauffe and Pfeiffer (69) demonstrated that reaction control was actually associated with chemisorption processes at the wustite/gas interface. This latter behavior, however, does not appear to be inclusive since the results from several investigations indicate that the reaction step at the metal/wustite interface plays a role in early-stage oxidation kinetics.

Basic studies to elaborate linear kinetics have been mainly confined to the oxidation of iron in CO_2-CO (67-75) and H_2O-H_2 atmospheres (76,77). Some work has been reported of oxidation in oxygen at low pressures (64,78). For the former atmospheres, the reaction rates show a direct dependence on the partial pressure of the gaseous reactant. This behavior is illustrated by the plots in Figs. 9 and 10, the reaction rate constants in H_2O-H_2 atmospheres being larger than those for CO_2-CO atmospheres under equivalent oxygen activities.

Pettit et al (73), Turkdogan et al (76), and Morris and Smeltzer (79) have advanced mechanisms to account for these linear kinetics based upon steps for dissociation of the triatomic reactant and incorporation of chemisorbed oxygen into the wustite lattice. If for example, carbon dioxide is considered as the gaseous reactant, the linear rate constant
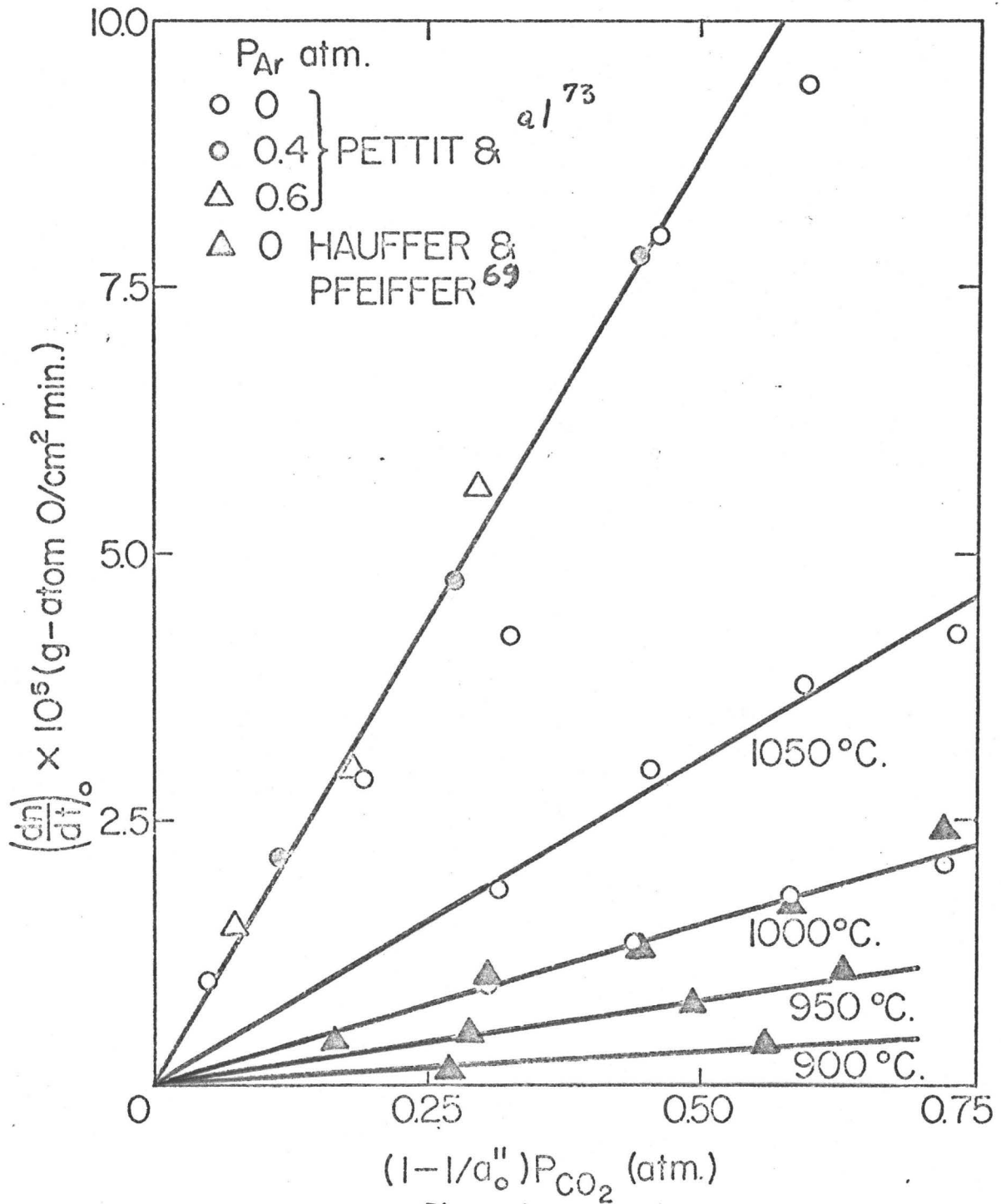
Figure 9

Variation of the Initial Linear Oxidation Rate of Iron

with the Product $(1-\frac{a_o'}{a_o''})P_{co_2}$. Oxidizing Atmosphere

is $P_{co_2}+P_{co}+P_{Ar}=1$ atm. $a_o'=1$. (From Reference 76)
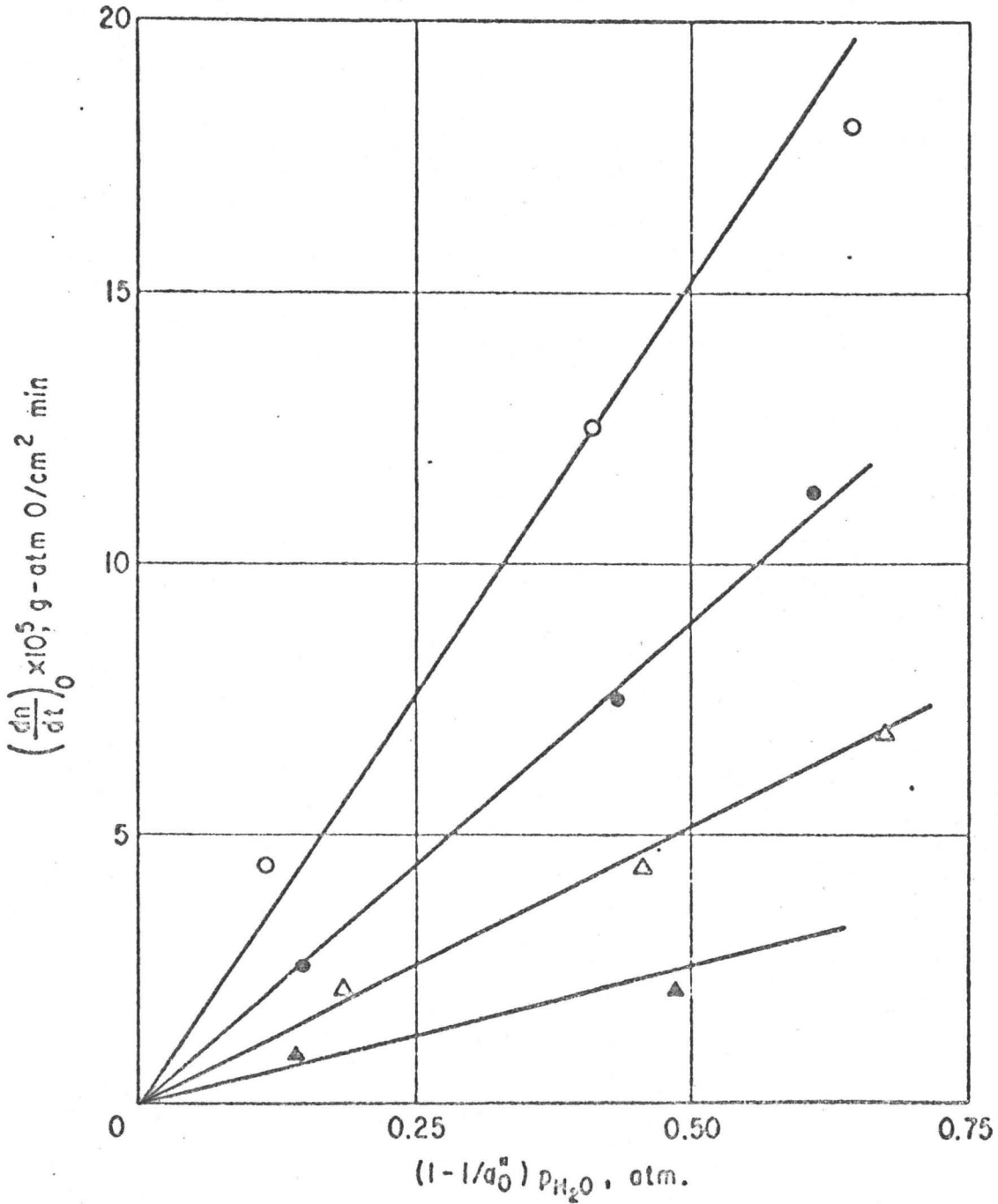
Figure 10

Variation of the Initial Linear Oxidation Rate of Iron

with the Product $(1-\frac{a_o^!}{a_o^"})P_{H_2O}$. Oxidizing Atmosphere

is $P_{H_2O}+P_{H_2}=1$ atm. $a_o^!=1$ (From Reference 76)

becomes,

$$K_L = k_i \theta_v (1 - a_o^*/a_o) P_{CO_2} = k_i \theta_v (1+K)(P_{CO_2} - P_{CO_2}^*)$$ (12)

when the reaction rate is controlled by the rate constant k_i for dissociation of carbon dioxide at the wustite surface to yield adsorbed oxygen. In these expressions, θ_v is the fraction of the wustite surface devoid of adsorbed oxygen, P_{CO_2} and a_o are the carbon dioxide pressure and oxygen activity of the gas phase, K, $P_{CO_2}^*$ and a_o^* are the equilibrium constant, carbon dioxide pressure and oxygen activity, respectively, required for equilibration of wustite with iron. It is seen from the plots in Fig. 10 that eqn.(12) accounts for the pressure dependence of the linear rate constants for CO_2-CO atmospheres. A similar expression may be shown to apply for the formation of wustite in the H_2O-H_2 atmospheres. Activation energies for this type of oxidation have been reported as 24-53 kcal/mole and 19 kcal/mole for wustite formation in the CO_2-CO and H_2O-H_2 atmospheres, respectively.

Grabke (75) has more recently demonstrated that the values of the linear rate constant in case of the CO_2-CO atmospheres closely agree with those obtained for the surface exchange of oxygen on wustite equilibrated with iron. He and his coworkers (80) have summarized the results from their intensive investigations on oxygen exchange from CO_2-CO and H_2O-H_2 atmospheres with surfaces of iron, wustite and magnetite. These rate constants are shown as a function of oxygen activity in Figs. 11 and 12. Exchange rates decrease with increasing oxygen activity by an exponential constant, its value being dependent upon the atmosphere considered and the temperature. They have interpreted these parameters by assuming that oxygen adsorption follows Langmuir or Freundlich isotherms.

There are meagre results for wustite growth in oxygen atmospheres. Pfeiffer and Laubmeyer (78) have reported that the linear reaction rate is proportional to the oxygen pressure raised to the power 0·7 at
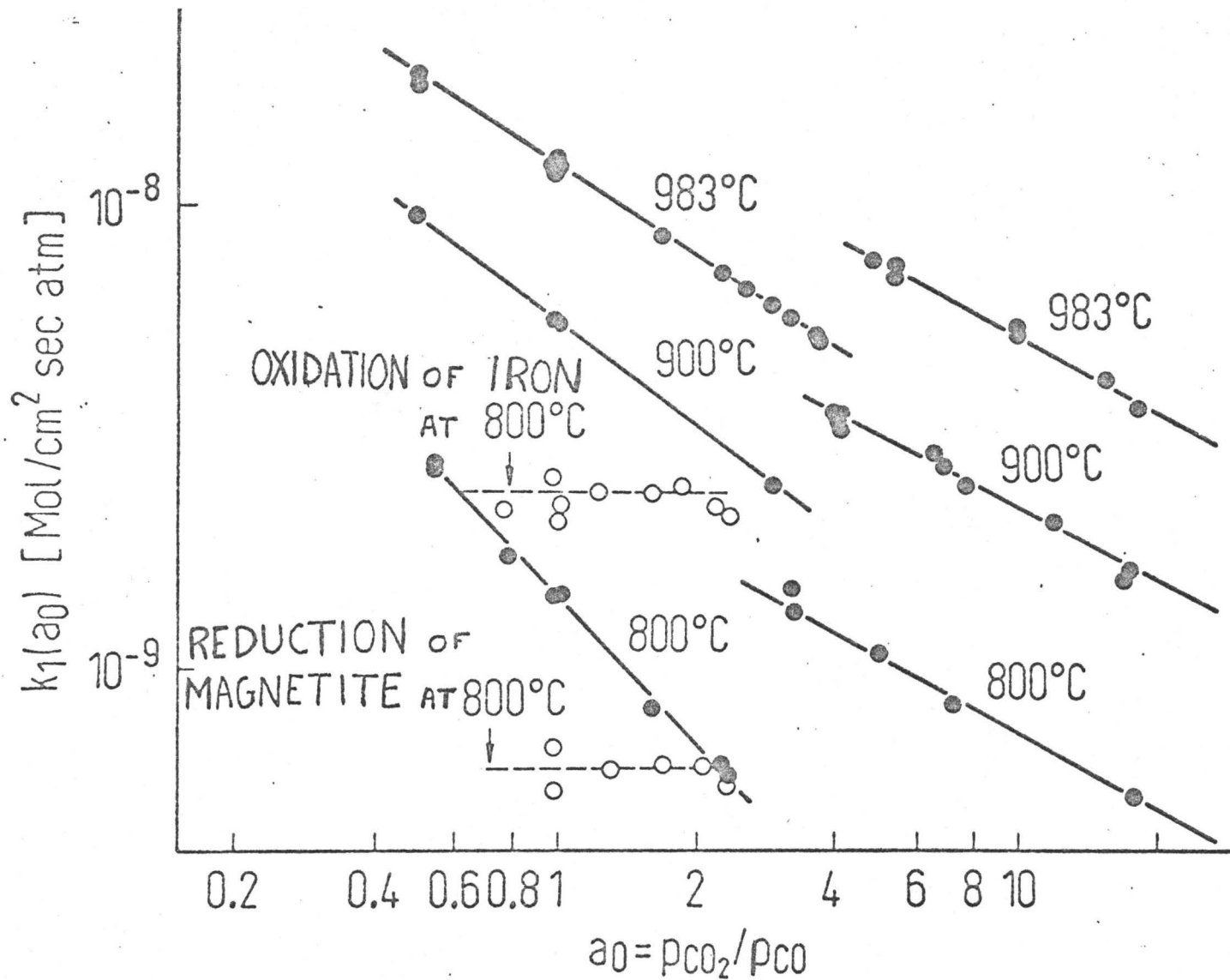
Figure 11

Representation by Double Logarithmic Plots of the Oxygen Exchange

Rate Constants from CO_2-CO Atmospheres at Surfaces of

Wustite and Magnetite under Equilibrium and during

Oxidation of Iron or during Reduction of

Magnetite (O) (From Reference 80)
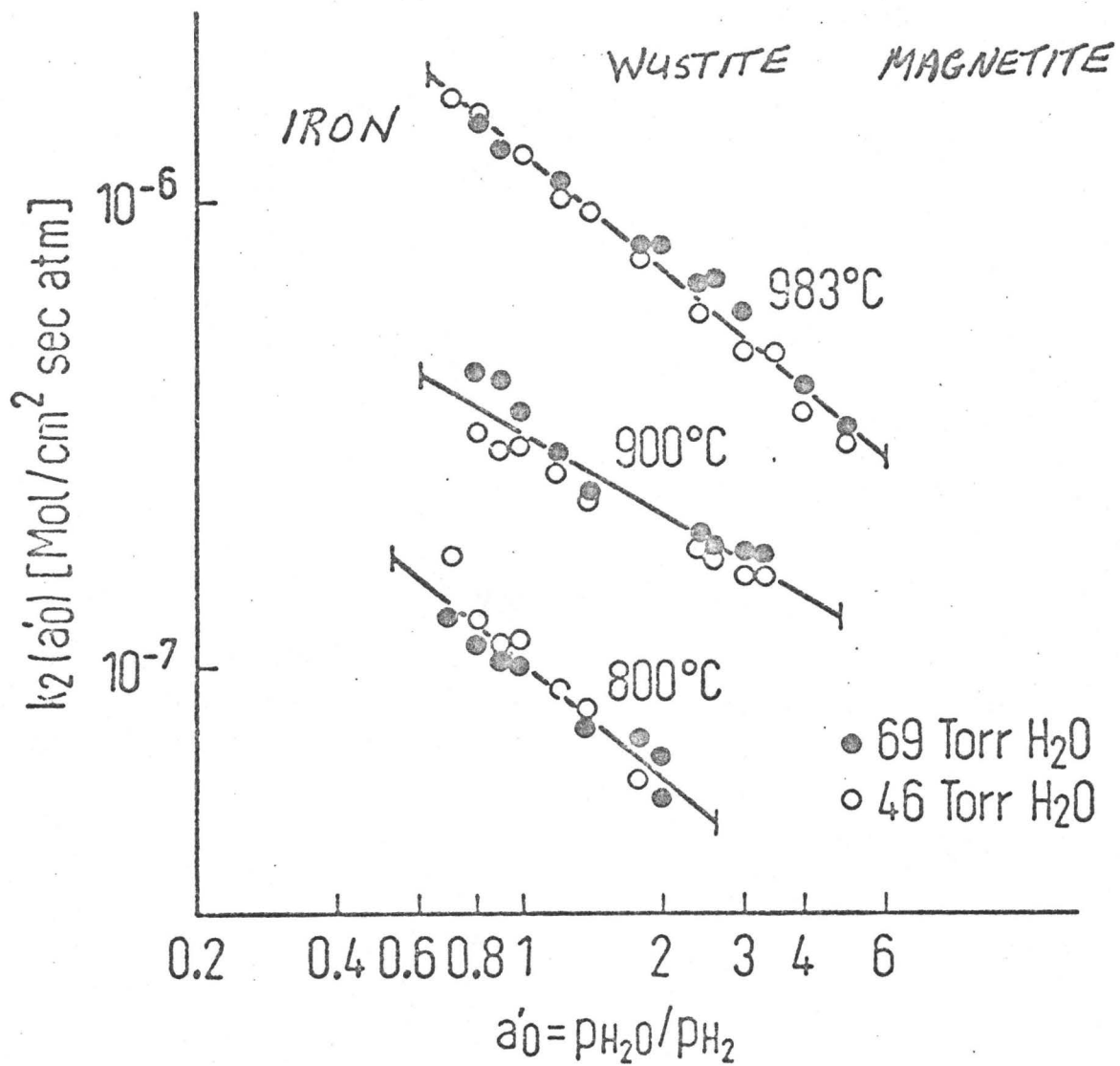
Figure 12

Representation by Double Logarithmic Plots of the Oxygen Exchange Rate

Constants from H_2O-H_2 Atmospheres at the Surface of

Wustite.(From Reference 80)

1000°C and at pressures ranging from 10^{-3} to 1 Torr;whereas Charbonnier and Bardolle (64) found the rate to be directly dependent on pressure at 850°C and at pressures less than 10^{-4} Torr. Although the mechanism has not been established, these findings indicate that oxidation is controlled at the wustite/gas interface. These considerations, however, may not apply to the kinetics obtained in oxygen at higher pressures (81-83). For examples, Bénard and Talbot (81), and Chattopadhyay and Measor (82) upon oxidizing iron in oxygen at pressures near 1atm found that plots of the initial linear rate and modified parabolic rate constants showed a discontinuity and anomally, respectively, at the α-γ allotropic transformation temperature. The former authors interpreted their results as showing that the passage of iron into wustite plays a transient role in controlling oxidation. The latter authors suggested that the anomalous behavior is associated with the metal/oxide interface in γ-iron and the oxide/oxygen interfacial reaction in α-iron. Accordingly, diverse features of oxidation based upon interfacial rate control remain outstanding which will only be resolved by additional experimentation carried out under conditions where overheating of the specimen does not occur during the early stages of reaction.

Parabolic Oxidation Kinetics

A multilayer scale consisting of the three common oxides is formed when iron is exposed at elevated temperatures to oxygen or dry air at normal pressure. In the 1920's, Pilling and Bedworth (84) and Pfeil (85) established that scale growth obeyed a parabolic law related to a diffusional mechanism. Subsequent research on this scaling reaction during the past half-century has been more extensive than for any other metal. Since Paidassi (1) has reviewed this literature, we restrict our remarks to the investigations bearing on the oxidation mechanism.

Curves for the parabolic growth of a scale at temperatures in the range 700°-1000°C are shown in Fig. 13. Growth proceeds rapidly and scales become several microns thick within a few minutes. The micrograph in Fig. 14 shows that uniformly thick layers form, the thickness of wustite greatly exceeding the combined thickness of magnetite and hematite. There occurs a non-steady state of oxidation during the very early stage of the reaction but relative thicknesses of these layers remain unchanged during parabolic oxidation. As illustrated in Fig. 15, magnetite and hematite account for approximately 5% of a scale at temperatures exceeding 700°C.

Davies et al (86), Paidassi (87) and Schmahl et al (88) have presented a large body of results on parabolic scaling amenable to theoretical analysis when combined with the previously discussed results on Fe-O thermodynamics, defect structures and diffusional properties of wustite. Himmel et al (40) first applied the Wagner theory (89) to this scaling reaction in 1953. This theory may be applied in a straight-forward manner since wustite is the major scale constituent and iron acts as the mobile species for growth of the wustite and magnetite layers (85,90-92). If an oxide exhibits metal transport and its conductivity is predominately electronic, Wagner (93) has shown that the parabolic rational rate constant may be expressed as,

$$k_r = \bar{c}_2 \int_{a_o^!}^{a_o} z_1^2 \left| \frac{}{z_2} \right| D_1 \, d\ln a_o \qquad (13)$$

where D_1 is the self-diffusion coefficient of metal $\bar{c}_2$ is the average oxygen concentration, a_o is the oxygen activity, z_1 and z_2 are the valencies of metal and oxygen. The integration is carried out from the inner to outer scale surfaces. Himmel et al used their determinations of the iron self-diffusion constants and results from the Fe-O phase diagram on wustite compositions versus oxygen activity to evaluate k_r from eqn. (13). As shown in Table 2, the calculated values are in close
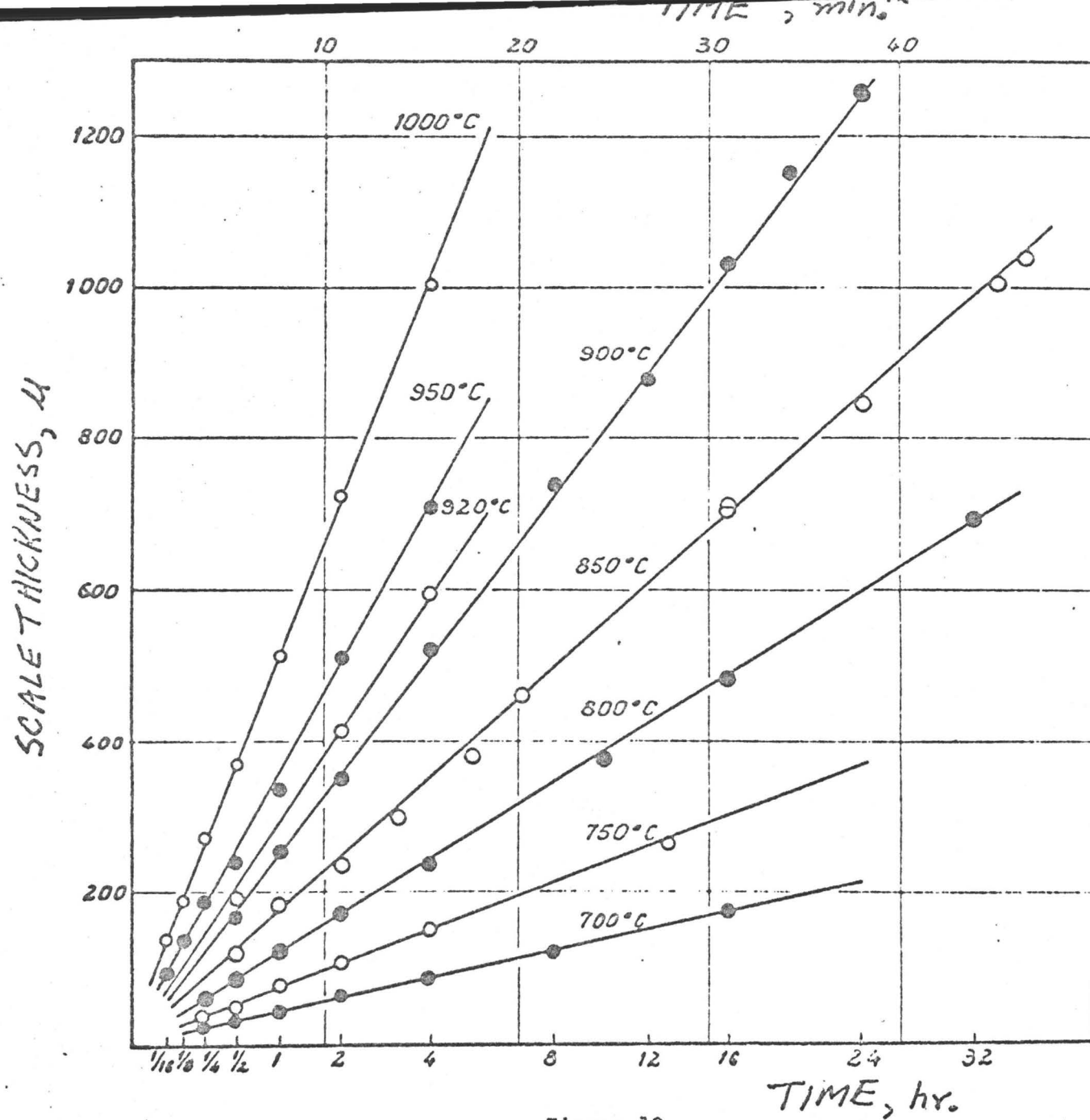
Figure 13

Parabolic Plots for the Isothermal Growth of the Scale

on Iron exposed to Air.(From Reference 87)
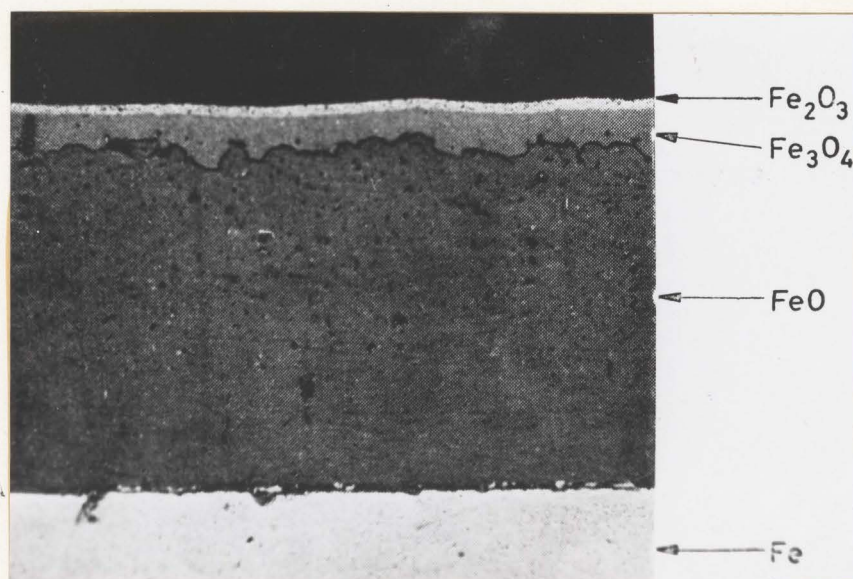
Figure 14

Microsection of Scale formed on Iron in Air.
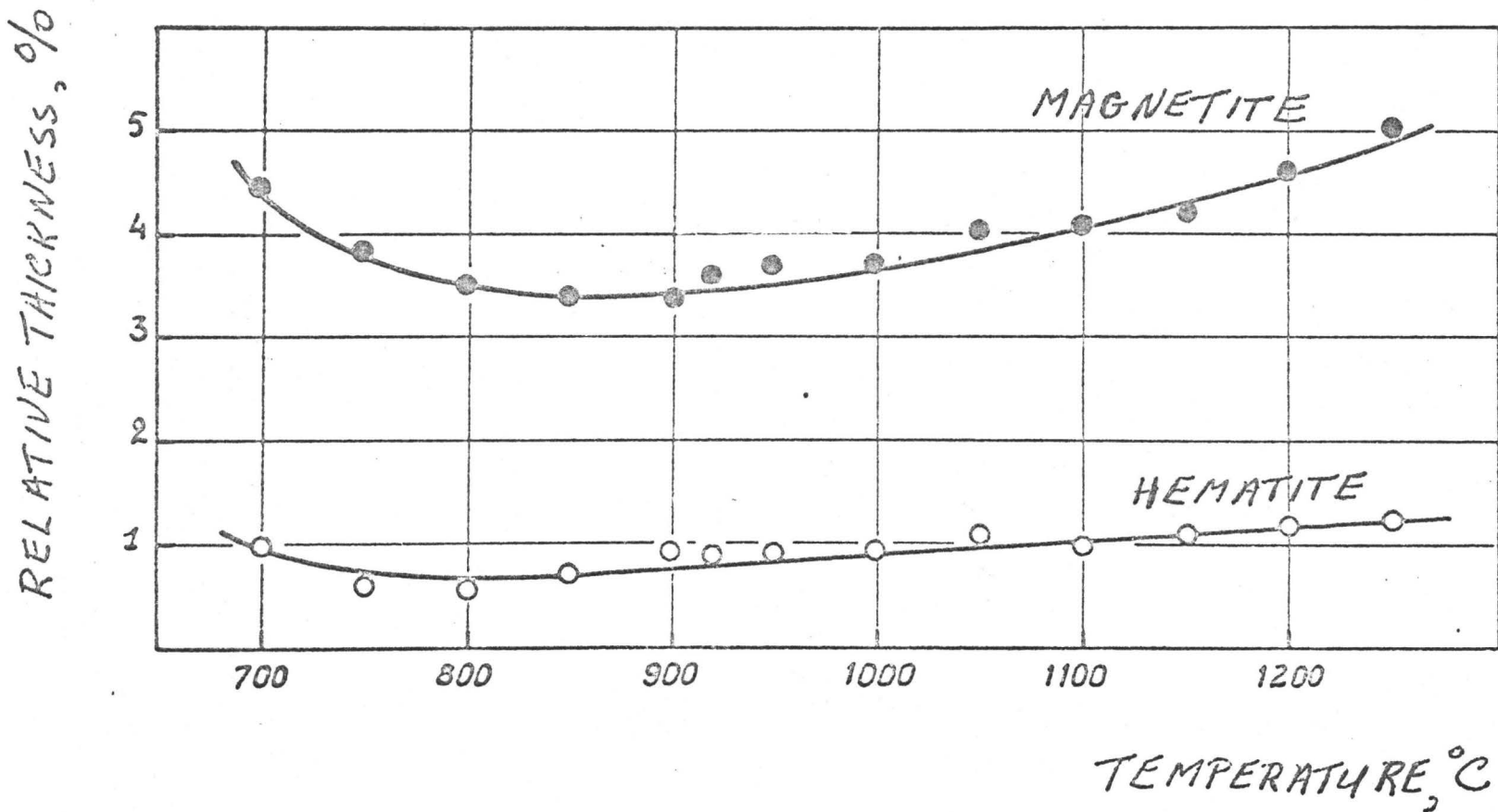
(From Reference 87)

Figure 15

Variation as a Function of Temperature of the Relative Thicknesses

of Magnetite and Hematite in the Scale formed on

Iron in Air.(From Reference 87)

agreement with measured values.

A more simple test has been made to correlate many of the experimental results with theory. Engell (44), as previously discussed, determined the diffusion constant for iron vacancies in wustite. Since the mobility of vacancies was not dependent on non-stoichiometry, the flux of iron can be expressed by the low gradient approximation,

$$j = 3D_{\square}[C_{\square}'' - C_{\square}']/x \qquad\qquad (14)$$

Here, x is the scale thickness and the double and single primes indicate the iron vacancy concentrations in wustite at its outer and inner surfaces. As shown in Fig. 16, the temperature coefficients calculated for the parabolic rate constant are in good agreement to the measured values for iron oxidation over the range 700°-1100°C. The deviations at low temperatures show the limitation of this analysis which possibly arise from the influence of vacancy interaction on iron mobility.

These calculations are but a good first approximation for relating theoretical to measured values of parabolic oxidation constants as account was not taken of the small amounts of higher oxides formed in the multilayer scale. A scale consisting entirely of wustite, nevertheless, is formed when iron is exposed to CO_2-CO and H_2O-H_2 atmospheres of controlled oxygen activity. The rate for diffusion controlled oxidation is readily calculable using eqn. (13) for any given oxygen activity at the wustite/gas interface. Pettit and Wagner (74) and Turkdogan et al (76) have shown that the portion of an oxidation curve exhibiting parabolic kinetics subsequent to the period of linear oxidation in these atmospheres agree with theoretical predictions. This correlation for the case of oxidation in H_2O-H_2 atmospheres is shown in Fig. 17. Some preliminary attempts have been made to elaborate the parabolic oxidation of iron exposed to atmospheres containing oxygen at
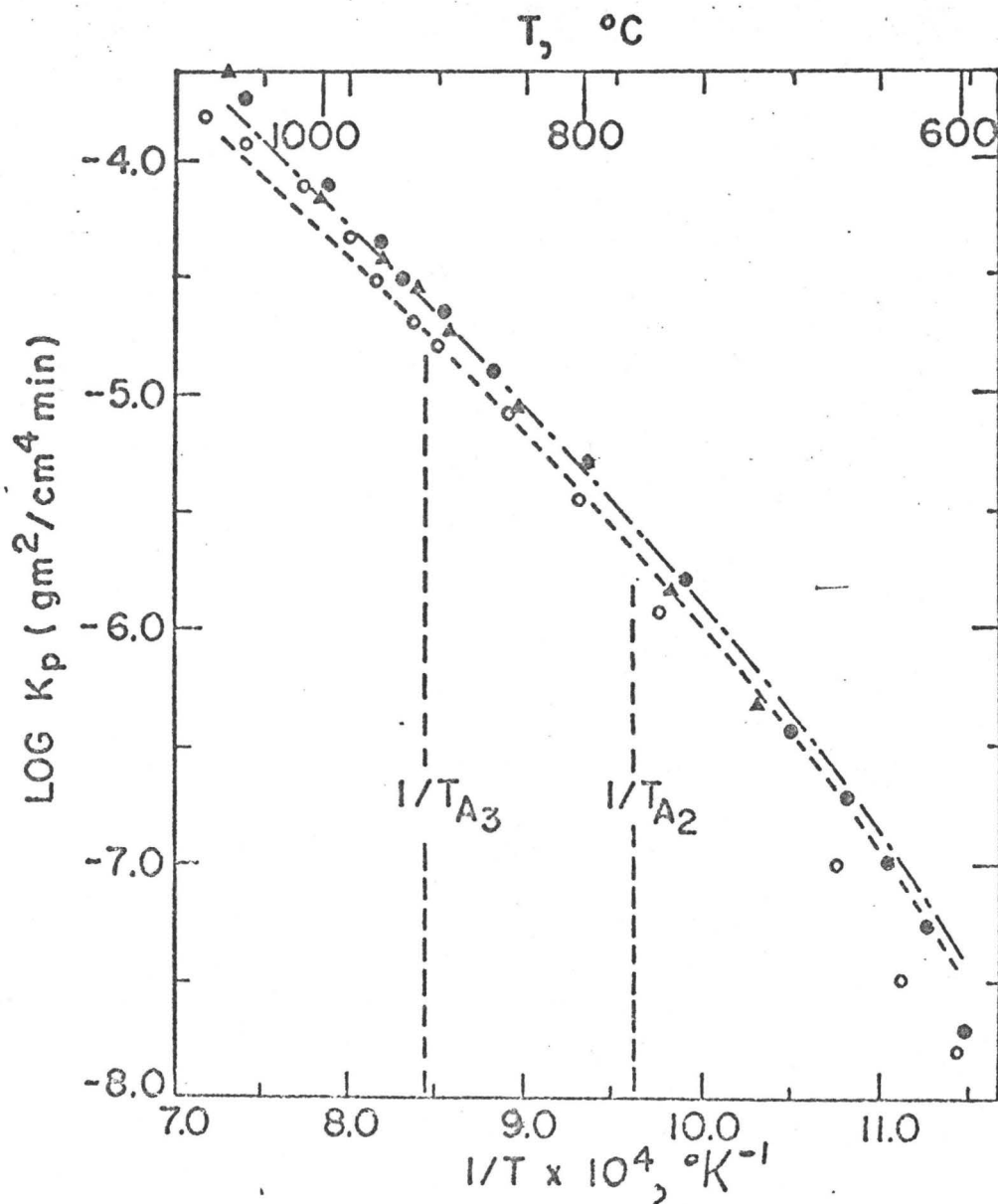
Figure 16

Arrhenius Temperature Coefficients of Parabolic Oxidation Constants for
Wustite Formation on Iron. Theoretical Coefficients calculated
from Eqn.(14) using the Values for the Diffusivities of Iron
Vacancies from Eqns.(9)- - -and(10)— - —· (From References
86(0), 87(▲), 88(●)).
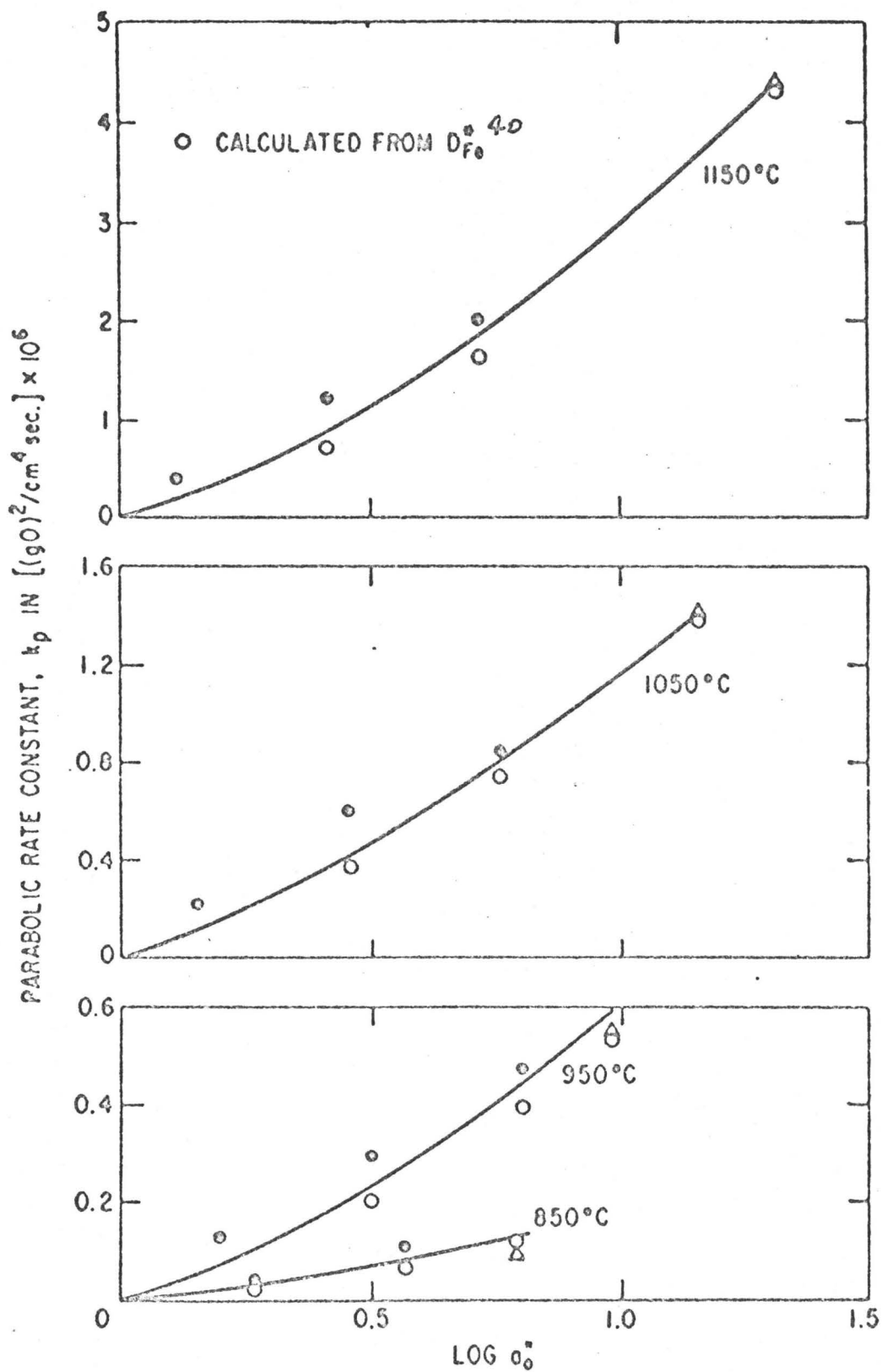
Figure 17

Variation of the Parabolic Rate Constant for Wustite Formation on Iron with

Oxygen Activity at the Surface of the Oxide.(From Reference 76)

low pressures but simple correlations have not been obtained due to interfacial parameters for appearance of the higher oxides (94-96).

A model for the mechanism of multilayer scale growth involving outward migration of iron through cation vacancies in the wustite and magnetite layers and inward migration of oxygen through anion vacancies in the external hematite layer has been proposed by Hauffe (97). A diffusion analysis by Tikhomirov (98) describes the rate constant for growth of this multilayer scale on iron in terms of average diffusivities and concentration gradients across the individual oxide layers. The preceeding analysis and qualitative calculations by Himmel et al for growth of magnetite on wustite support the premise for growth of the two inner oxide layers by iron diffusion. Hagel (42) has suggested from an analysis of the diffusion results for hematite that iron or oxygen would act as the predominant diffusing species in this oxide dependent upon the temperature. Structural evidence has been placed forward, however, by Arkharov and Agapova (99) which indicates that iron is the predominant migrating species in hematite when it is formed as the external layer in a scale containing wustite. Thus, it would appear that scaling at high temperatures may be attributed to outward diffusion of iron across the entire scale.

Anomalies in the Oxidation Curves and Scale Morphologies

The relationships discussed so far for the growth of scales by linear interfacial and parabolic diffusional kinetics are ideal and observed under particular and carefully controlled conditions. Under steady-state, formation of a uniform, compact and adherent wustite or multilayer scale may occur. Paidassi (1) has given a model based upon a survey of experimental results for the multilayer scale. The wustite layer contains large grains and their various orientations may correspond to matching of closest atom packing directions in the metal and oxide (54).

The magnetite and hematite layers are of finer structure, the hematite grains being smallest and only a few microns in size. These latter layers contain oxide exhibiting different planes parallel to the metal surface dependent upon exposure time and temperature (100). Also, the crystal structure of hematite has been reported to exist in a distorted rhombohedral habit (101). The scale can therefore be considered as a textured structure.

Many anomalies from linear and parabolic kinetics occur, especially in the early stages of the reaction and after prolonged exposures when the scales reach thicknesses of the order of 100μ. In the early stages of an oxidation test, it is very difficult to avoid specimen overtemperature resulting from the exothermicity of the chemical reaction. In practice, also, oxide growth may lead to formation of non-uniform scales resulting from the occurrence of pores, blisters and cracks.

Investigations on the "heating effect" upon exposing the metal to oxygen at normal pressure have been carried out by Schmahl et al (102) and Caplan (103). It is difficult to obtain an accurate evaluation of the transient overtemperature but values of some 40° to 50°C have been measured during the first few minutes. A simplified theoretical treatment of this phenomenon which is not very well known is given by Valensi (104).

The Pilling and Bedworth rule based upon the chemical equivalent volume ratio of metal to oxide for stress generation cannot be applied to the scale on iron since outward cation migration predominates. Notwithstanding, Dankov and Churaev (105) and Moreau and Cagnet (91) demonstrated that compressive stress is to be found in a growing multilayer scale since oxide formed only on one side of a thin metal foil caused a bending moment to develop. If the stress is sufficiently high, relief may occur by oxide fracture or by plastic deformation of either the scale or of the metal substrate. Bruce and Hancock (106) have shown by a

vibrational technique that the multilayer scale can undergo microscopic cracking during its growth. Lateral compression, in the absence of plastic deformation, can also lead to blistering of a scale if interfacial adhesion is weak. Stress generated during cooling also leads to fracture of thick scales since the dilation coefficients of the metal and oxides are different and can vary with temperature (107). Our present knowledge on the complicated mechanisms for stress generation and relief have been recently surveyed by Douglass (108) and Stringer (109).

Mackenzie and Birchenall (110) have shown that wustite behaves plastically over the temperature range in which it is stable whereas the higher oxides remain relatively rigid. Stress in the layers of these latter oxides have been suggested to play a role in two observed features of scale development. Whiskers and fine platelets have been observed to grow from the external hematite surface at temperatures less than 850°C (85,111,112). Also, blisters of temporary nature form during direct heating of iron in air due to detachment of hematite from the underlying magnetite layer (113). These features, however, appear to play a minor role in scaling compared to formation of microscopic defects at the metal/ wustite interface.

When an iron atom is transferred from the metal into the oxide, oxide formation takes place at an external surface and a metal vacancy is left behind at the metal/scale interface. Vermilyea (114) has advanced a simple mechanism whereby adherence of the scale to the metal is retained by plastic readjustment of the oxide equivalent to the movement of an edge dislocation at the metal surface. Since wustite does exhibit plasticity, such type of mechanism would account for the many observations on growth of the scales exhibiting adherent compact layers. In many instances, however, voids are formed in the wustite layer even at high temperatures. Several mechanisms for either sorption of vacancies or

their condensation to voids have been considered by many authors. Contributions by Moreau and Cagnet (91), Dunnington et al (113), and Tylecote and Mitchell (92) deal extensively with this subject.

Regions of a scale where voids destroy the adherence of wustite to the metal substrate were observed in the early investigation by Pfeil (85). Subsequent work has shown that this feature becomes pronounced above certain scale thicknesses which is dependent on the shape and grade of iron specimens and the exposure conditions. A mechanism similar to that introduced by Dunnington et al (113) is believed to account for the condensation of vacancies to voids whereby a critical degree of vacancy supersaturation at the metal interface is required. This degree of supersaturation is approached more easily near the edges of plate specimens and on wires where the curvature of the scale restricts the plastic flow of wustite (115, 116). These voids often appear, also, earlier at surfaces of roughened and fully annealed specimens (117,118). In the first stage of formation, the small cavities act as barriers to iron migration across wustite. When these cavities enlarge to distinct blisters, oxygen could possibly be transported across a scale despite the absence of oxide fracture. A striking example of blister formation in a scale formed on a cylindrical specimen is shown in Fig. 18. Engell and Wever (116) have advanced observations to show that wustite actively forms beneath these regions by transport of oxygen when magnetite acts as the upper cavity surface. These authors and Birchenall (119) have analyzed the anomalous oxidation kinetics to be expected during this type of scale growth.

It has been realized for a long time that residual impurities in iron or impurities incorporated into the scale from the atmosphere play a profound role on the development of a Pfeil type scale (120-130). Most recently Maldy (125) has carried out studies of broad scope on the influence of residual impurities in the metal. Ultra-pure iron tends to
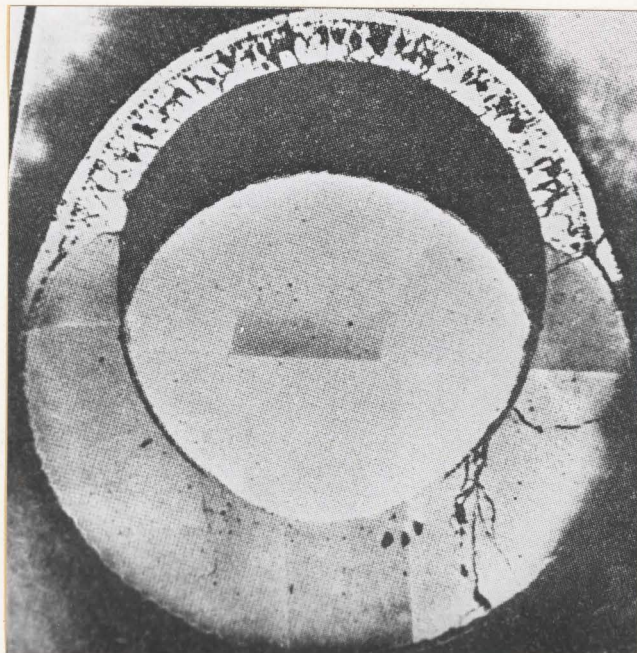
Figure 18

Cross-Section of an Iron Wire oxidized in Oxygen at 1atm. Pressure.

(From Reference 116)

retain a planar interface and a compact scale during oxidation. Metallic impurities noble to iron tend to segregate at the surface especially at grain boundaries whilst less noble impurities are selectively oxidized within the metal and most intensely at grain boundaries. These properties lead to complex processes involving polygonization of wustite, recrystallization of iron, irregularities in the metal interface and finally condensation of vacancies to voids. In addition to the influence of trace amounts of carbon and hydrogen in the metal, Rahmel and Toboloski (127, 128) and Tuck et al (129,130) advance results to show that these elements are incorporated into the scale from oxidizing atmospheres containing carbon dioxide or water vapor. These impurities also influence scaling kinetics and morphological development of the scales. Consequently, the authors propose that one possible mechanism for this behavior is the reaction of carbon or hydrogen with wustite to form CO_2-CO or H_2O-H_2 atmospheres within the pores. These atmospheres remain oxidizing due to the oxygen activity gradient across the scale. Enhanced scaling is then encountered by inward gaseous transport of oxygen, cyclic oxidation of iron at the inner surface and of the reduced gas at the outer surface of pores. It is apparent, accordingly, that mechanisms for the influence of impurities on scaling kinetics are complicated and not well understood but their elaboration is essential for more effective development of high temperature ferrous technology.

CHAPTER III

EXPERIMENTAL TECHNIQUES

3.1 Introduction

This chapter will deal with the preparation of the specimens, the oxidation apparatus, X-ray diffraction and scanning electron microscopy studies.

3.2 Specimen Preparation

The iron mainly used in this study was ultrahigh purity iron (Fe = 99.999%) from Gallard-Schlesinger; the chemical composition of this metal is given in Table III-1. In some of the experiments 99.996% purity iron and Ar mco iron were also used. The specimens were cut from the original rod by a diamond wheel. They were in the form of discs approximately 1cm in diameter and 1mm to 0.3mm thick. To prepare a specimen for oxidation, it was mounted in bakelite and abraded on a silicon carbide paper, this was followed by polishing on a wax lap impregnated with 15μ alumina. The final polishing was done on 6μ and 1μ diamond wheels with kerosene as lubricant. The specimen was then cleaned with petroleum ether, removed from the mount and electropolished in 5% perchloric acid in glacial acetic acid solution in order to remove the damaged surface layer. Upon the removal of a specimen from the electropolishing bath it was washed in distilled water and acetone. Finally the sample was sealed in a quartz tube containing high purity argon and annealed

41

Table III-1

Spectrochemical analysis of high-purity iron (in ppm).

Al	Cd	Cr	Co	Cu	Mg	Mn	Mo	Si	Ti	V
tr	nd	tr	nd	10	30	tr	tr	30	tr	tr

tr = trace

nd = not detected

at 800°C for 18 hours. It was then allowed to cool to room temperature. After annealing grain size varied from 0.03 to 0.3mm which corresponds to ASTM standard grain size No. 5. The sample was cleaned with petroleum ether and stored under acetone until required.

3.3 Oxidation Apparatus

The assembly for determining weight changes of a specimen during oxidation is shown pictorially in Fig. III, 1. This assembly consisted mainly of a Cahn R. G. Electrobalance represented in Fig. III, 2. High purity research grade oxygen was used as the reacting gas, the total impurity content being less than 25ppm. During an experiment in the pressure range 2.5×10^{-3} to 10 torr a calibrated oxygen leak was continuously open and oxygen pumped through the reaction tube. The oxygen pressure was controlled at both ends of this reaction tube by means of calibrated Edward High vacuum Pirani gauges (H1 and H2 Fig. III,2). This measurement providing the pressure gradient in the tube from which we can deduct the oxygen pressure near the specimen. After the introduction of oxygen, up to 3 min. was necessary before the establishment of the correct pressure. But from 10 to 152 torr instead of using a controlled leak, in order to maintain a constant pressure, we utilized an oxygen reservoir of 15 1. Immediately before an oxidation test a specimen was weighed in a Mettler microbalance and its surface area was computed by measuring the specimens dimensions with a micrometer. The sample was finally slightly electropolished and
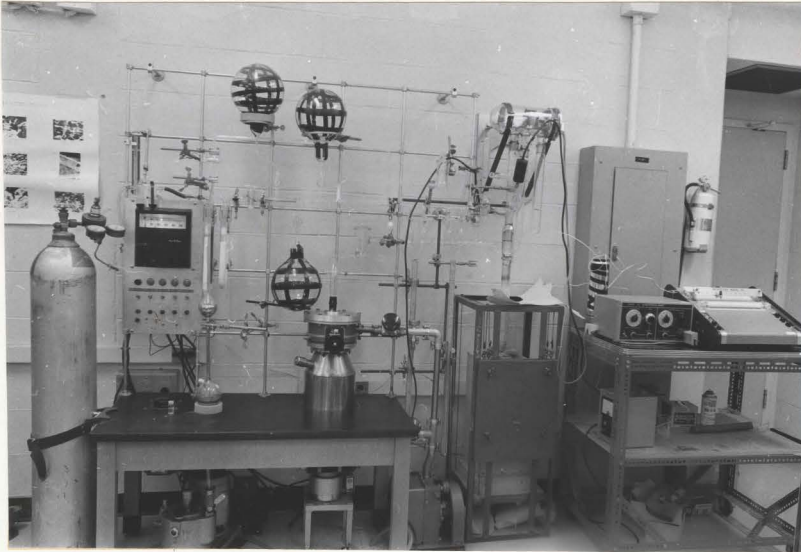
Figure III, 1

Photograph of the apparatus
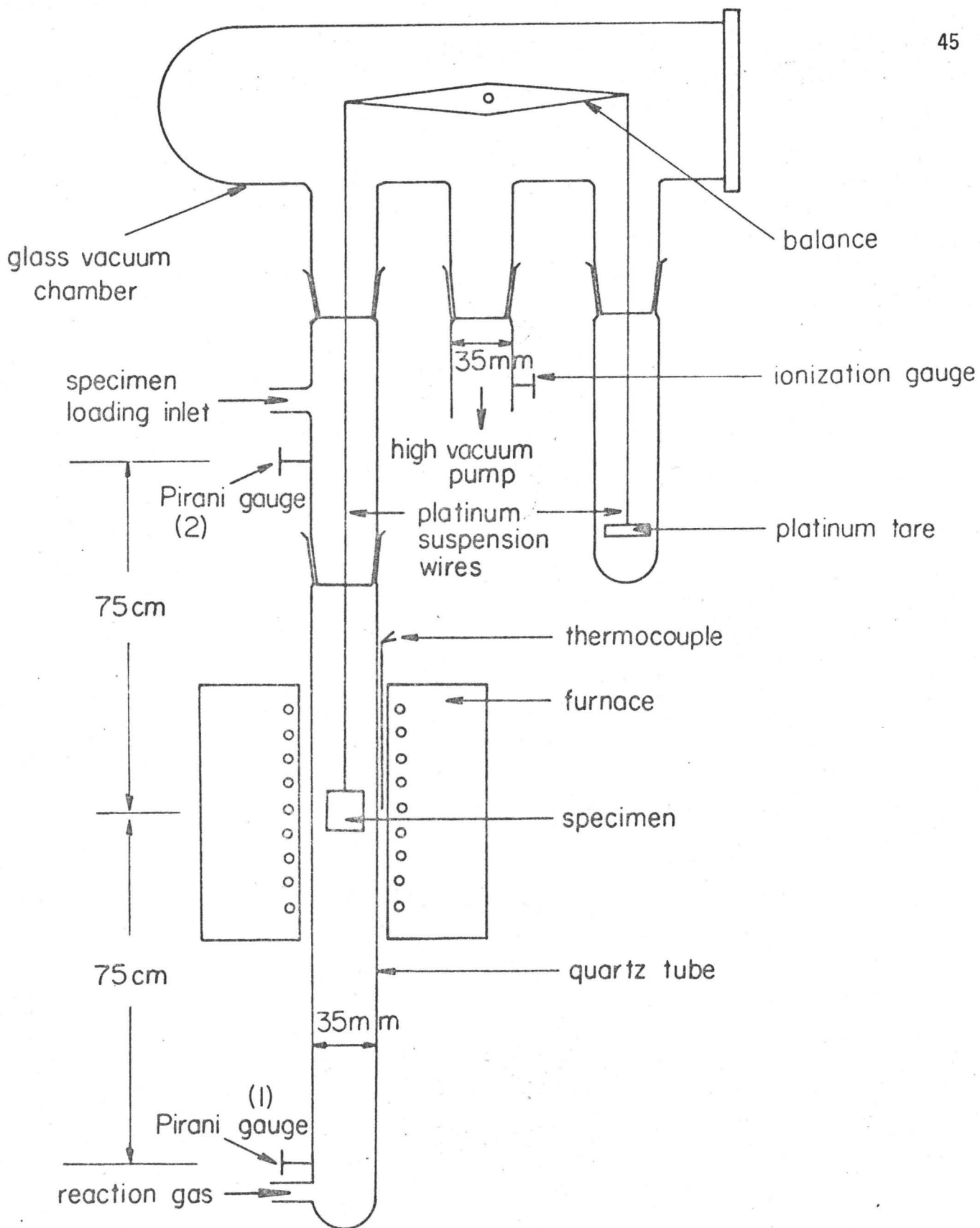
Figure III, 2

The assembly containing a Cahn continuously recording R. G.

Microbalance. The oxygen pressure is determined by Pirani gauges at

positions (1) and (2).

introduced in the oxidation assembly which was evacuated to 10^{-5} torr. The heated furnace was then raised around the reaction tube. After waiting 10 min. for stabilization of temperature, oxygen was admitted to the assembly and the growth of the oxide layer continuously recorded. The introduction of oxygen implies a buoyancy effect on the specimen. This effect was corrected after a calibration run with an inert sample having the same size as the specimen. At the end of the oxidation test the assembly was rapidly evacuated and at the same time the furnace moved down. The specimens were occassionally cooled under the experimental oxygen pressure. However, no difference was found between the results obtained with these two processes. Temperature was controlled to $\pm 2°C$ during the experiment.

3.4 Optical Metallography

Oxidized specimens for microscopic examination were mounted in room-setting epoxy resin and metallographically polished as described above. An ethyl alcohol solution containing 5% concentrated hydrochloric acid was used as an etchant to distinguish wustite from magnetite.

3.5 X-Ray Diffraction and Scanning Electron Microscopy

Identification of the oxide constituents was carried out by reflection X-ray examinations using Cu-Kα irradiation with a graphite monochrometer and the preferred orientation of wustite in a scale determined by reflecting Mo-Kα X-ray irradiation from the surface of a rotating specimen. Morphological features of the scales were determined by optical and scanning electron microscopy.

CHAPTER IV

EXPERIMENTAL RESULTS

4.1 Introduction

The results obtained from the various experimental tests will be presented in this section in the usual manner; that is, in the form of graphs, tables and photomicrographs.

4.2 Kinetics and Morphological Development of the Oxide Scale on Iron at 800°C in Oxygen at 2.5×10^{-3} to 3.0×10^{-1} Torr Pressure

4.2.1 Oxidation Kinetics

The kinetic curves for specimens exposed at 800°C and oxygen pressure from 2.5×10^{-3} to 3.0×10^{-1} torr are shown in Fig. IV, 1 and IV, 2 as weight change (MgO/cm^2) vs time (min) for periods up to 125 min ($1MgO/cm^2 = 7.2\mu FeO$). The curves of the weight change were constructed using the original dimensions of a specimen. Five runs at 1.2×10^{-1} torr were reproducible within ±5%. A typical curve exhibited initially a region wherein the reaction rate continually increased, followed by a region of linear reaction behavior and finally by a region of continually decreasing rate. Considering Fig. IV, 1 and IV, 2, the effect of oxygen pressure on reaction behavior is important particularly during the first hour of exposure.

47

Figure IV, 1

Oxidation curves for iron exposed at 800°C to oxygen over the pressure range 2.5×10^{-3} – 3.0×10^{-1} torr for periods up to 125 min. A curve is also given for oxidation in dry air at 1 atm pressure.
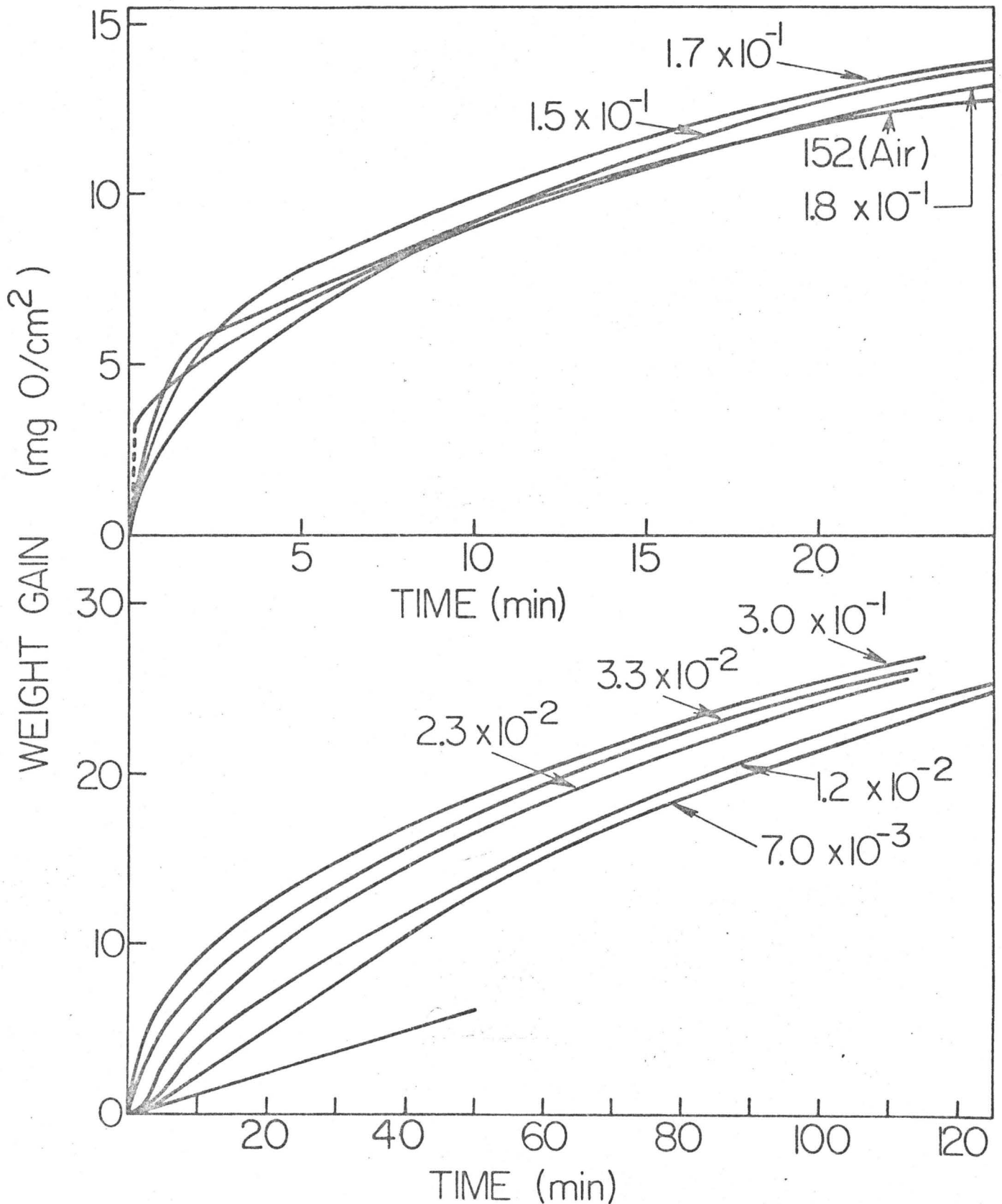
Oxidation curves for iron exposed at 800°C to oxygen over

the pressure range $2.5 \times 10^{-3} - 3.0 \times 10^{-1}$ torr for periods of 10 min.

3.3×10^{-2}

1.5×10^{-1}

2.3×10^{-2}

1.2×10^{-2}

7.0×10^{-3}

2.5×10^{-3} torr

WEIGHT GAIN (mg O/cm^2)

TIME (min.)
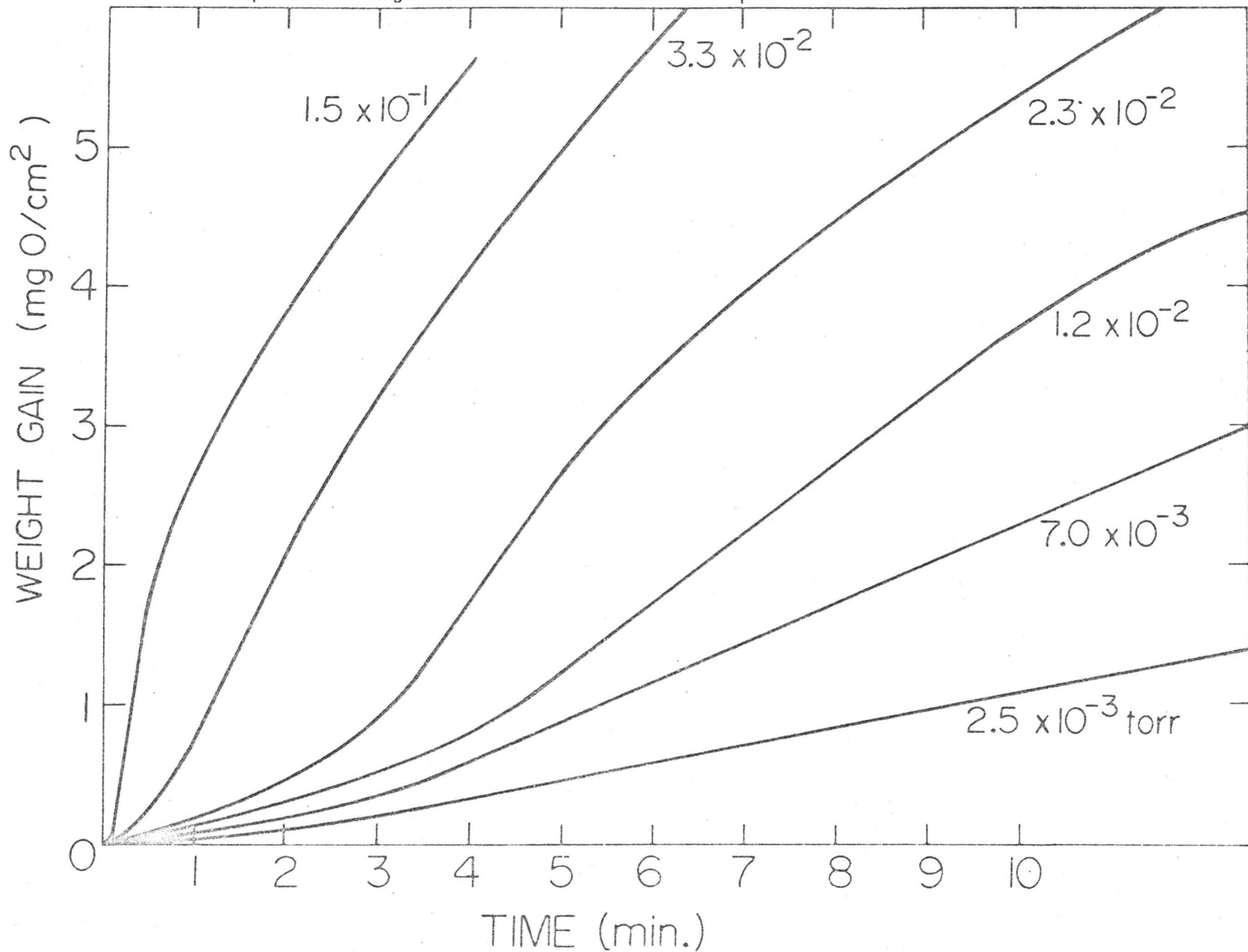
4.2.2 Morphological Development of the Oxide Scale

4.2.2.1 Initial Stage

It was found that small wustite crystals developed over a thin base film, their shape and population being dependent upon the orientations of the underlying metal grains (Fig. IV, 3). These crystals grew laterally and vertically to a uniformly thick layer during the initial period of continually increasing oxidation rate before onset of linear kinetics. A detailed shape of these nuclei is illustrated by Fig. IV, 4.

4.2.2.2 Region of Linear Reaction Behavior

4.2.2.2 (a) Oxide Structure and Preferred Orientation

The metal was covered by a uniformly thick wustite scale during the period of linear reaction kinetics and a subsequent part of the interval described by the continously decreasing rate. As can be seen in Fig. IV, 5 which represents an unetched cross section of the specimen, the thickness of the scale is very uniform and a good contact with the metal was generally found. Cooling pores may be observed at the Fe/FeO interface, but as we will show it was easy to distinguish a cooling void and a separation at the reaction temperature. The latter being always accompanied by transformation of wustite to a higher oxide. Etching of the scale revealed the large grain size of wustite which exhibits a preferential direction of growth (Fig. IV, 6). Examination of a scale 10μ thick showed a strong preferred orientation of the (311) wustite face parallel to the metal surface. Five thicker scales approximately 50μ thick

X1000
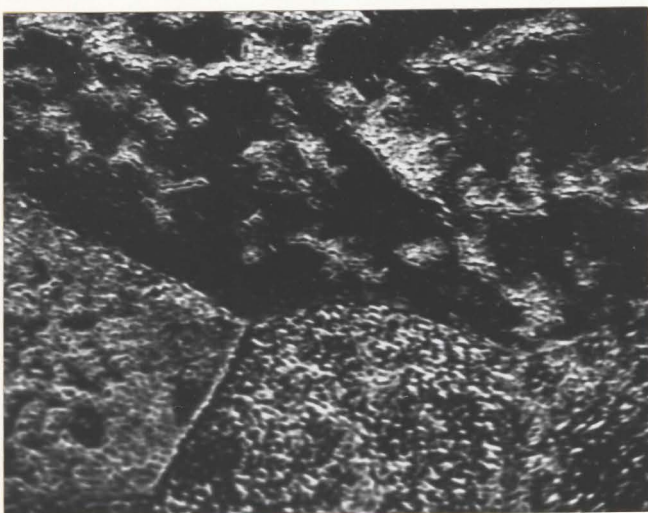
×750

Oxidation time: 1 min.
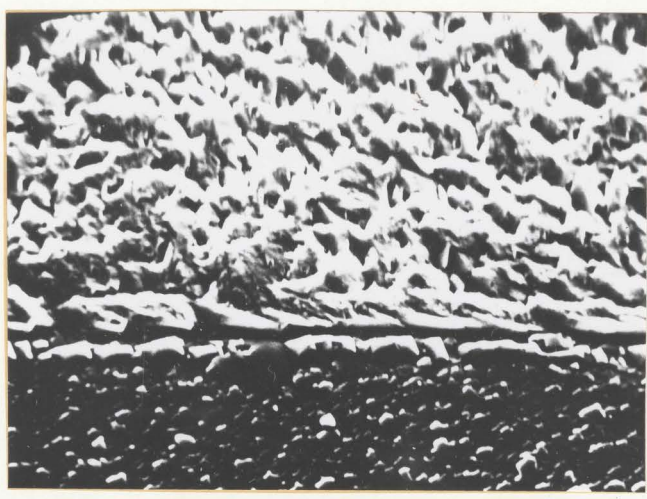
X1600
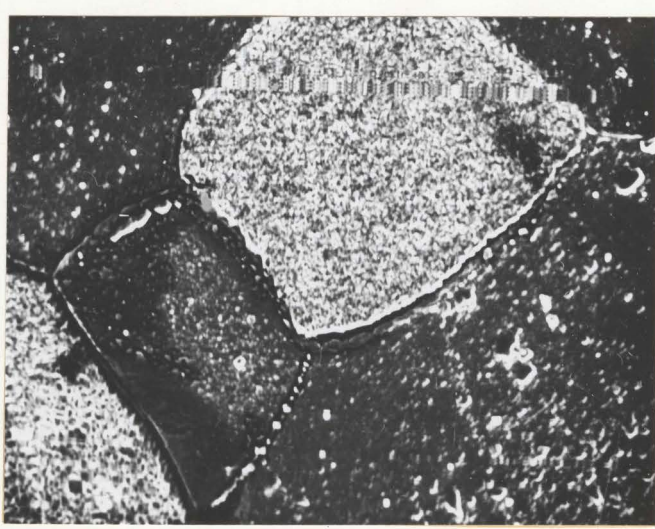
X390

Oxidation time: 3 min.

Figure IV, 3

Scanning electron micrograph of wustite crystals on iron after
an exposure in oxygen at 2.5×10^{-3} torr.
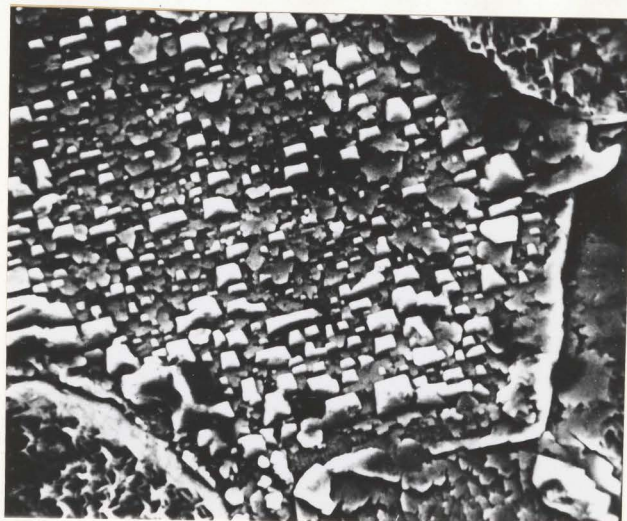
X1600
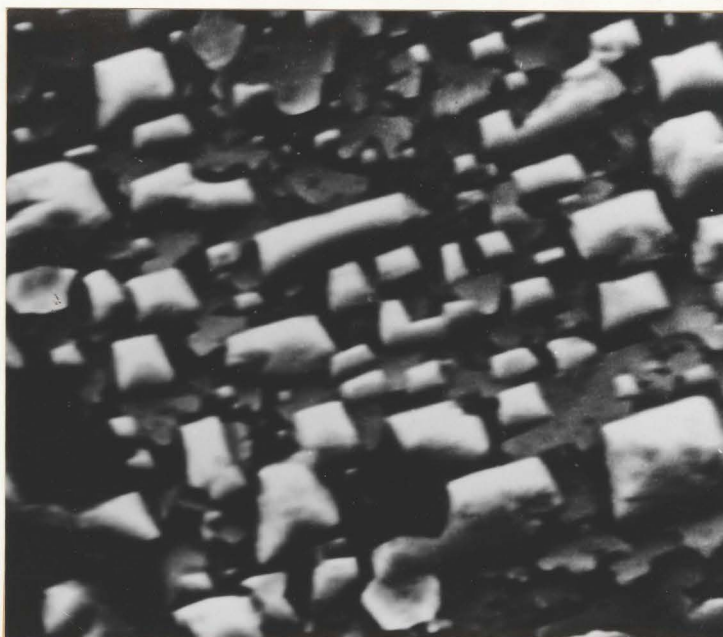
X3900

Figure IV, 4

Scanning electron micrograph of wustite crystals on iron after an exposure for 3 min. in oxygen at 2.5×10^{-3} torr.
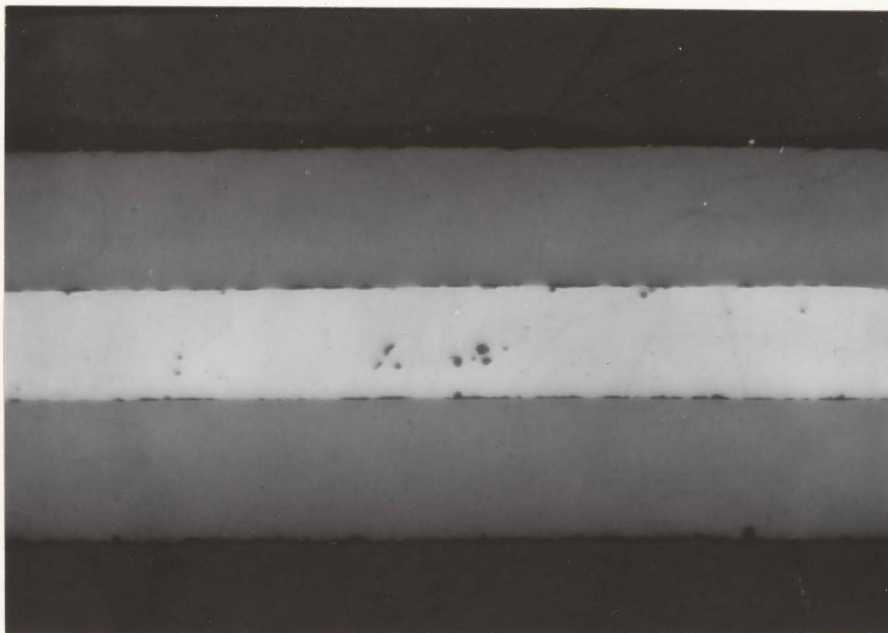
Figure IV, 5

Cross-section of the wustite scale on iron exposed for 30 min. in oxygen at 2.5×10^{-2} torr (X160).

Figure IV, 6

Cross-section of the etched wustite scale shown in Fig. IV, 5(X400).

showed the (110), (100) and (311) faces of wustite lying in decreasing order of parallel orientation with the metal surface.

4.2.2.2 (b) Surface Topology of the Oxide Scale

Examination of the scale surface with a scanning electron microscope showed that the small crystallites initially formed tend to coalesce and grow forming bigger grains with specific geometrical shapes, Fig. IV, 7. Then grains which developed by both lateral and vertical growth of platelets caused the formation of a very oriented topology. Ledge formation on the crystallite is also observed which is typical for a fast growing scale (147). Fig. IV, 8 represents a larger magnification of the sample surface showing the top of platelets with smooth faces on rough contour.

4.2.2.3 Region of Decreasing Rate and Nucleation of Magnetite

Magnetite was nucleated and it grew to cover the wustite layer in the early period of decreasing oxidation rate which became of shorter duration with increasing oxygen pressure. Using the scanning electron microscope, it was definitely established that the wustite layer was completely covered by magnetite during the first 60 min. at pressures in the range $7x10^{-3}$-$3.3x10^{-2}$ torr. Fig. IV, 9 represents the aspect of a part of the sample at the beginning of the nucleation period. Small crystallites of magnetite, which tend to form on the top of the ledges previously described, already cover a large grain of wustite. Fig. IV, 10 shows a more advanced stage of this nucleation process; the irregularly shaped magnetite crystals due to their lateral expansion tend to cover all of the
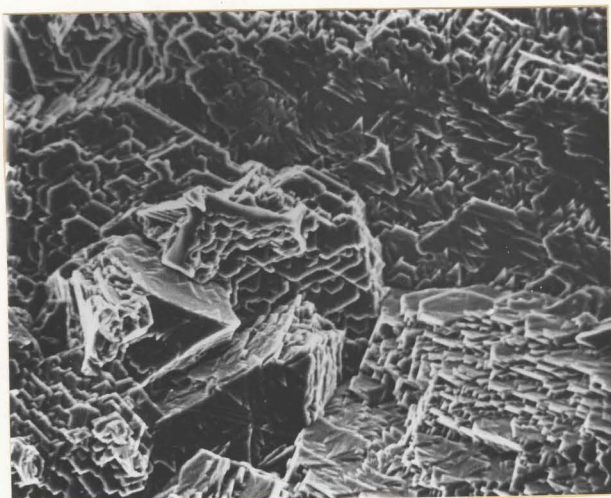
X440
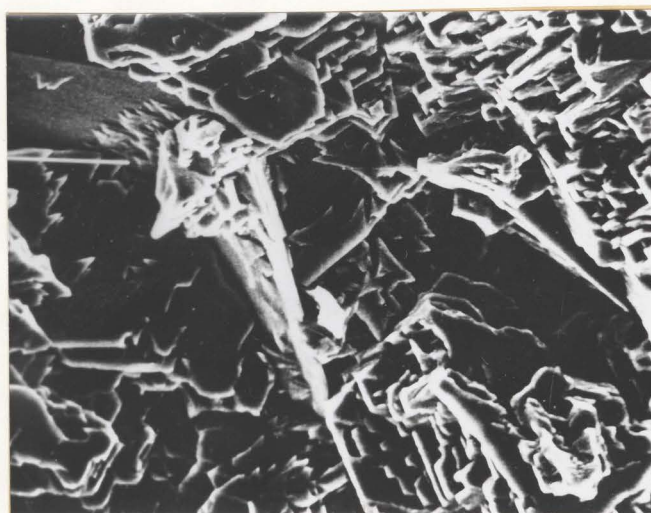
X900
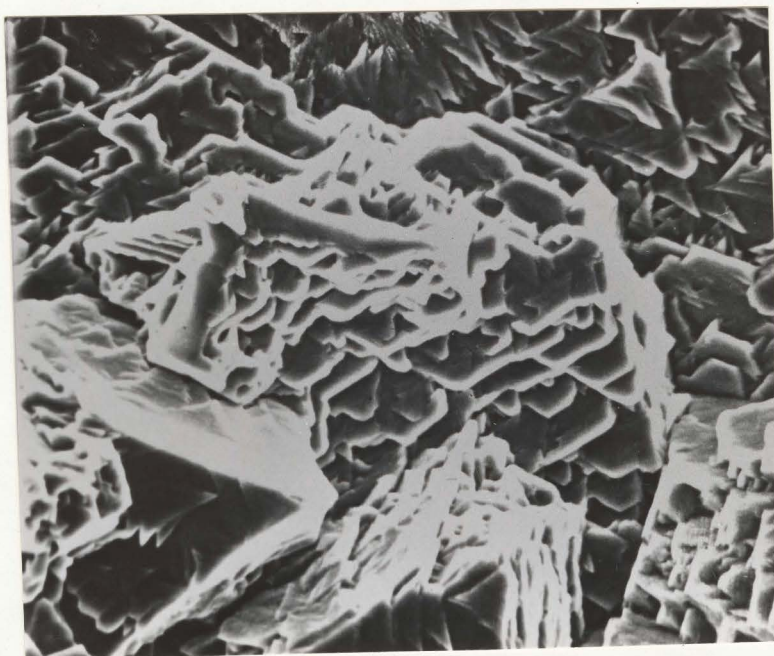
X1000

Figure IV, 7

Scanning electron micrograph of the surface of a wustite

scale formed on iron exposed for 20 min. in oxygen at 4×10^{-2} torr.
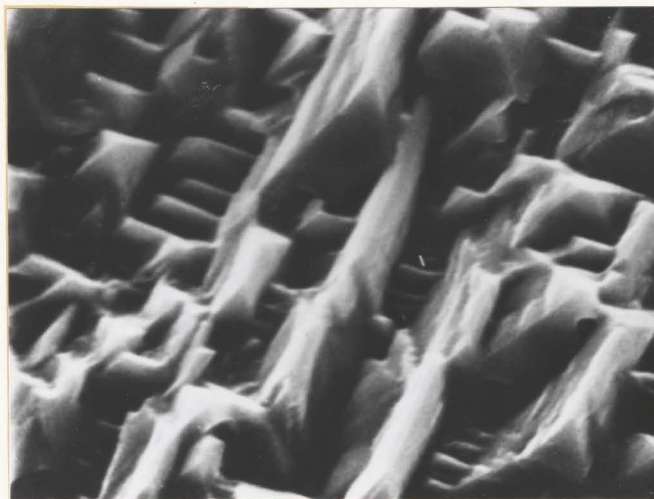
Figure IV, 8

Scanning electron micrograph of the surface of a wustite
scale formed on iron exposed for 20 min. in oxygen at 4×10^{-2} torr (X4400).
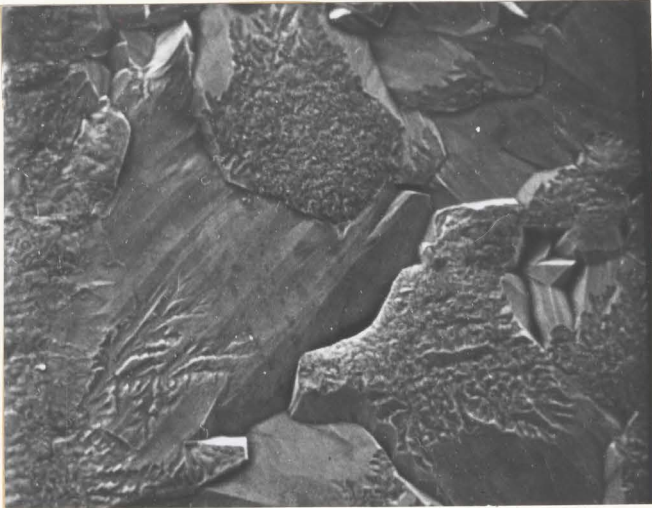
X200

X150

X500

Figure IV, 9

Scanning electron micrograph of scale surface showing partial coverage of wustite by magnetite. Exposure: 30 min. in oxygen at 3.0×10^{-2} torr.
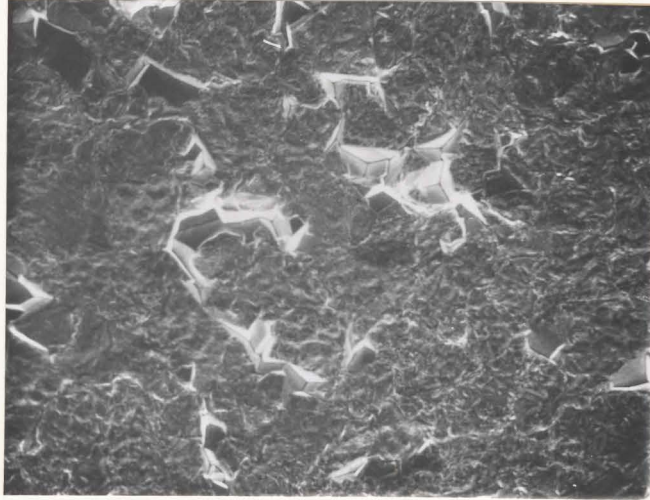
X200
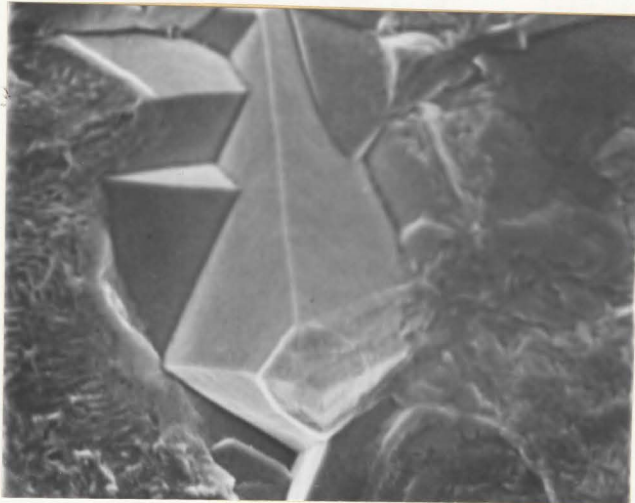
X750

Figure IV, 10

Scanning electron micrograph of scale surface showing partial coverage of wustite by magnetite. Exposure: 50 min. in oxygen at 1.5x 10^{-1} torr.

wustite surface, and only a few facetted wustite grains with a beautiful geometrical shape remain on the sample. At the end of the nucleation step the specimen exhibits a bright aspect to the eye. After that the small crystallites of magnetite had developed, the surface topology was uneven and exhibited a oriented mosaic Fig. IV, 11. In the lower pressure range, i.e. between 2.5×10^{-3} and 3.3×10^{-2} torr, even after 3 hours of oxidation the relative thickness of the magnetite layer was so small that it was impossible to observe this oxide by optical microscopy of a cross section. The presence of magnetite could be only detected by either X-ray or electron diffraction. Generally none of the cross sections of the oxidized specimens showed any tendency of loss of contact between scale and metal. But even if it happened very rarely, the particular case of non-adherence of the scale revealed interesting features. At an area where the wustite scale separated nucleation and growth of magnetite occured at the outer part and after cooling Fe_3O_4 precipitated in the FeO phase, (Fig. IV, 12). A higher magnification of the external part of the scale (Fig. IV, 13) showed that hematite is also formed on the top of magnetite. By examination of the surface of the specimen, we can therefore respectively study the formation of magnetite on wustite and hematite on magnetite. Regions of nonadherence exhibit circular shape (Fig. IV, 14). A higher magnification of boundary 1 shows the difference in grain size and topology of the wustite and magnetite regions. At higher magnification, boundary 2 shows the presence of small Fe_2O_3 nuclei on the Fe_3O_4
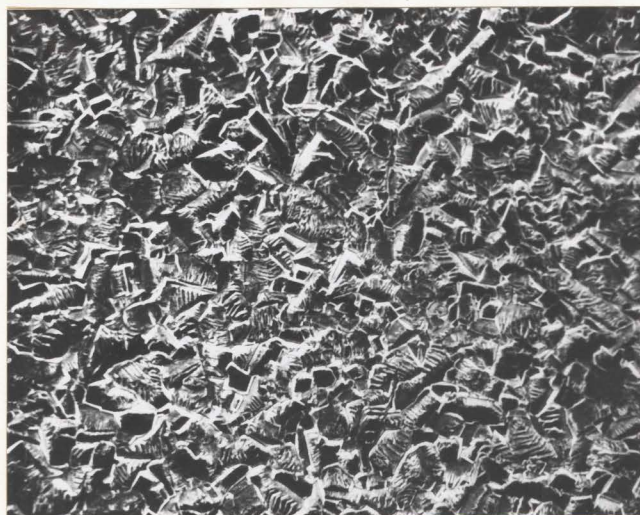
X130

X1000

Figure IV, 11

Scanning electron micrograph of the magnetite layer formed on wustite. Exposure: 120 min. in oxygen at 3.0×10^{-1} torr.
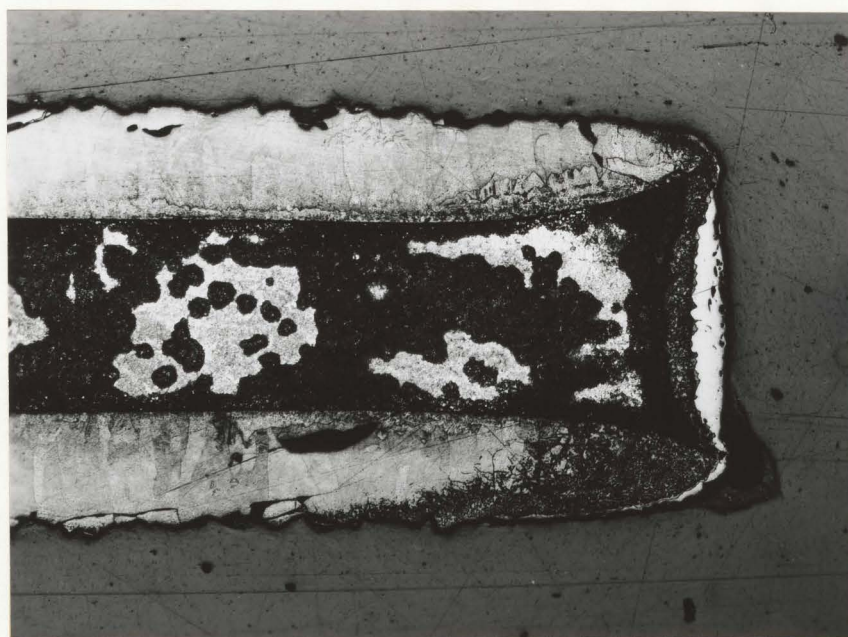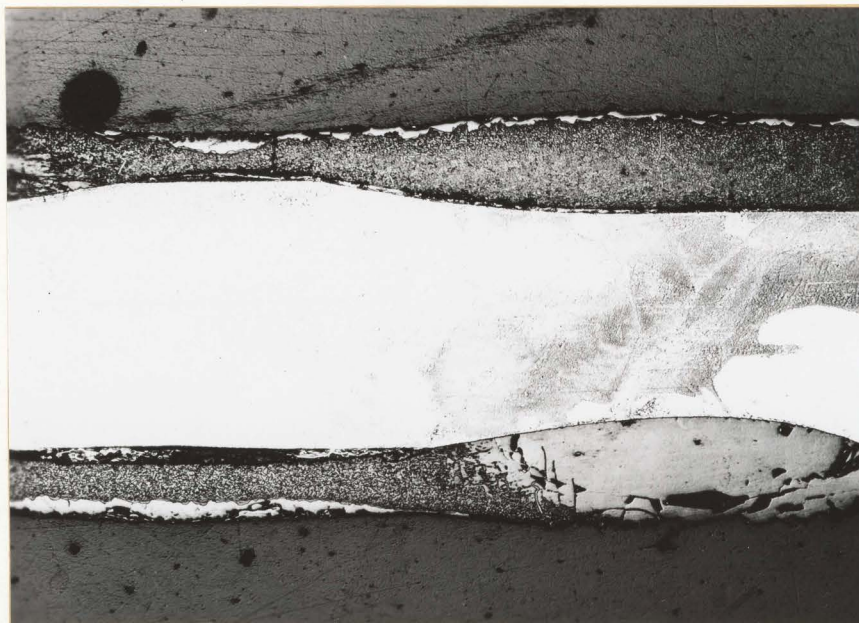
Figure IV, 12

Cross-section of a separated wustite scale on iron exposed
for 240 min. in oxygen at 3.0×10^{-3} torr (X50).
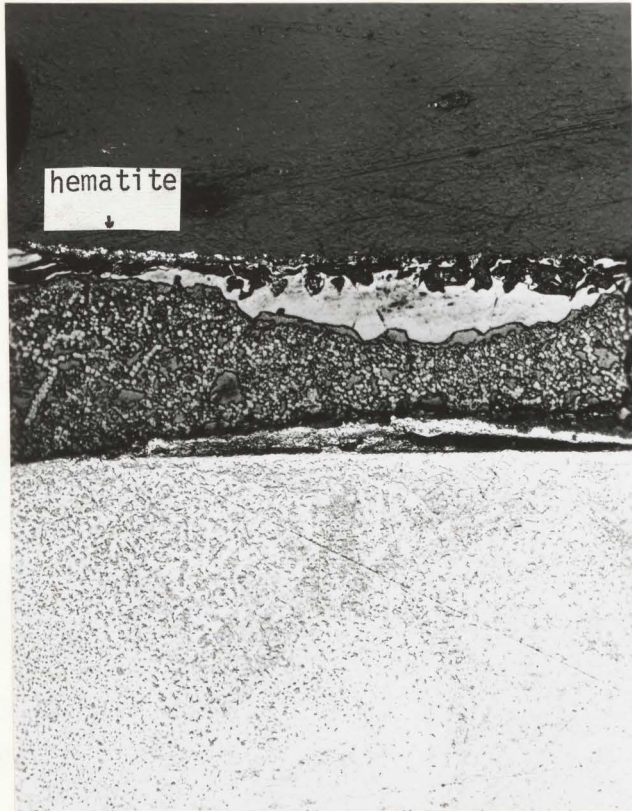
Figure IV, 13

Magnification from Fig. IV, 12 (X200)
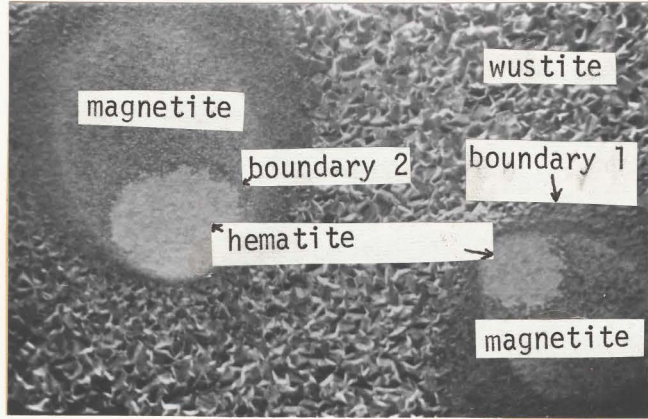
X20

(a)
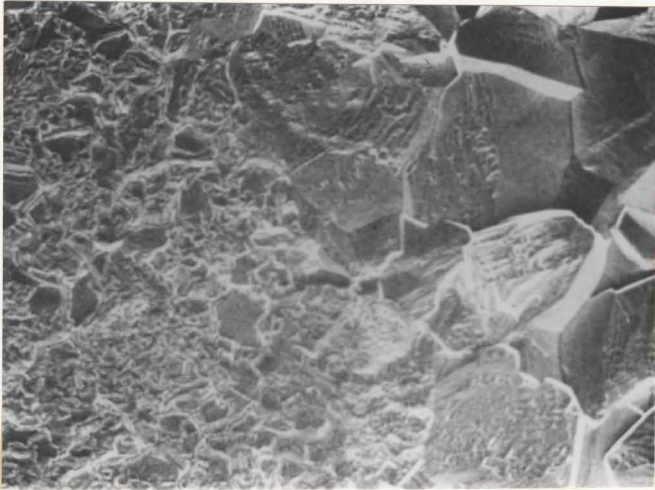
Boundary 1 (X200)

(b)
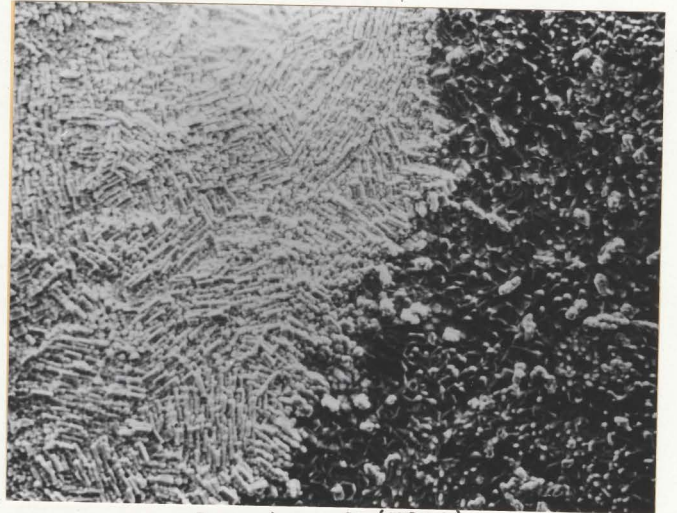
Boundary 2 (X200)

(c)

Figure IV, 14

Scanning electron micrograph of the surface of the separated
scale shown in Fig. IV, 12.

surface. The size and topology of Fe_3O_4 and Fe_2O_3 are very different since the first oxide consists of very small cubic crystallites and the second oxide is formed with strongly oriented plates as illustrated Fig. IV, 15.

4.3 The Kinetics and Morphological Development of the Oxide Scale on Iron at High Temperature in the Pressure Range 0.3 to 760 Torr

4.3.1 Oxidation Kinetics

The oxidation curves for specimens exposed at 800°C in the pressure range 0.3 to 760 torr are shown in Fig. IV, 16. The weight change was evaluated using the original dimensions of a specimen. These curves were reproducible to approximately 5%. According to the results represented in Fig. IV, 16 the oxidation rate does not seem to be pressure dependent and apparently decreases after the first few minutes of reaction.

4.3.2 Morphological Development of the Oxide Scale

Depending upon pressure and time the oxidation products are different. Generally at the beginning of oxidation a duplex scale is obtained consisting of wustite and magnetite. As illustrated by Fig. IV, 17, wustite comprises more than 95% of a scale. Normally 25% of the FeO layer exhibits Fe_3O_4 precipitates. Near the edges, however, contact was not maintained. Wustite then became saturated with oxygen and shows a complete precipitation zone, the magnetite layer being also thicker than on an adherent scale Fig. IV, 18. Fig. IV, 19, represents the topography of the specimen showing the

X1000
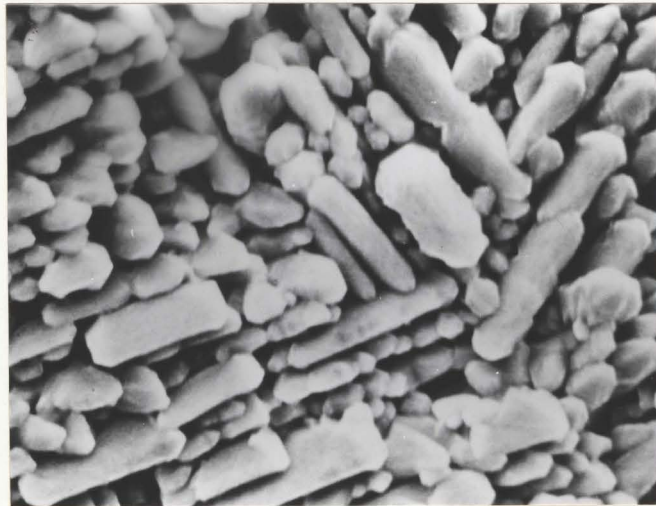
X2000

Figure IV, 15

Higher magnification from Fig. IV, 14c.

Figure IV, 16

Oxidation curve for iron exposed at 800°C to oxygen over

the pressure range 0.3 to 152 torr for periods up to 150 min.
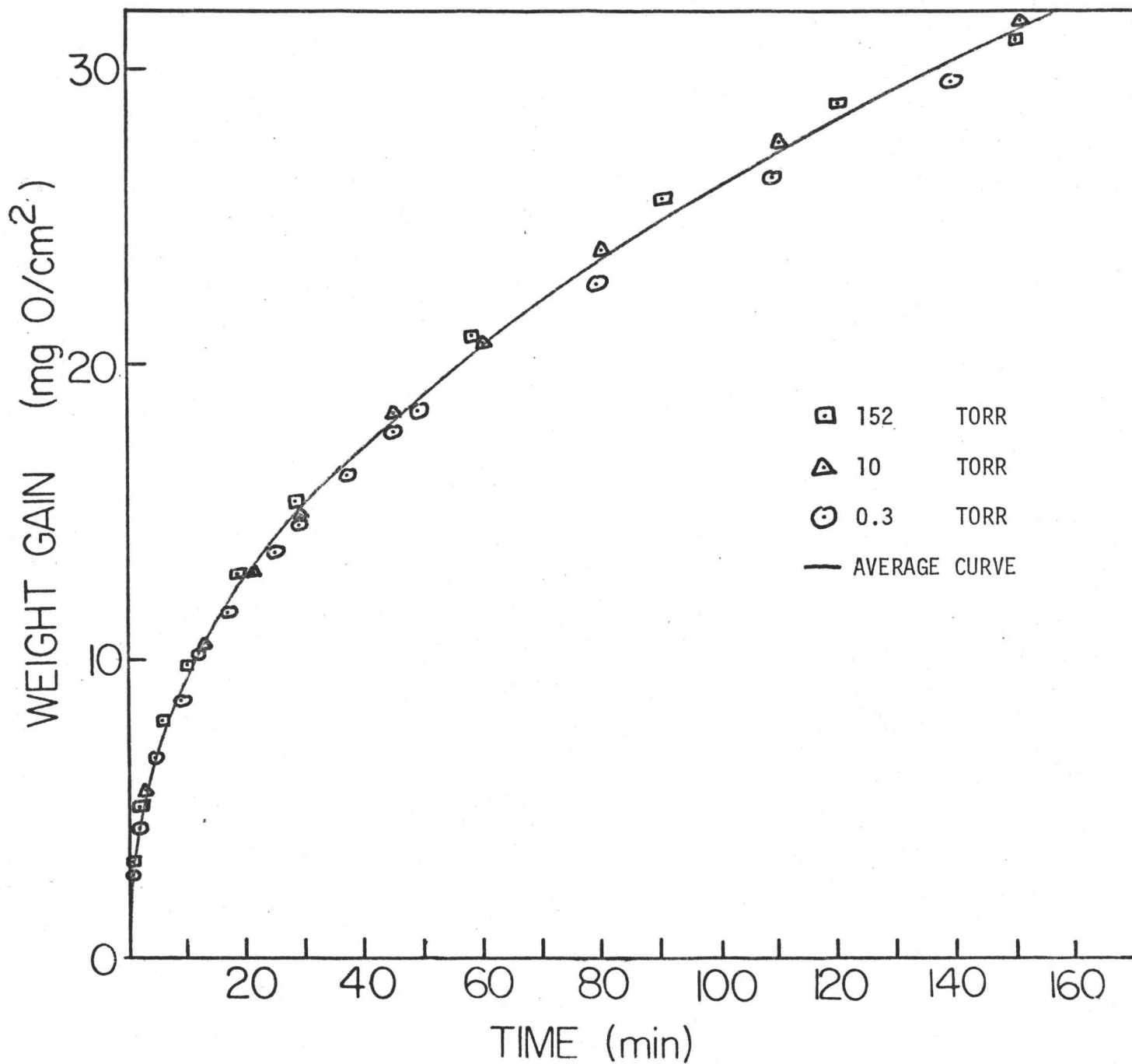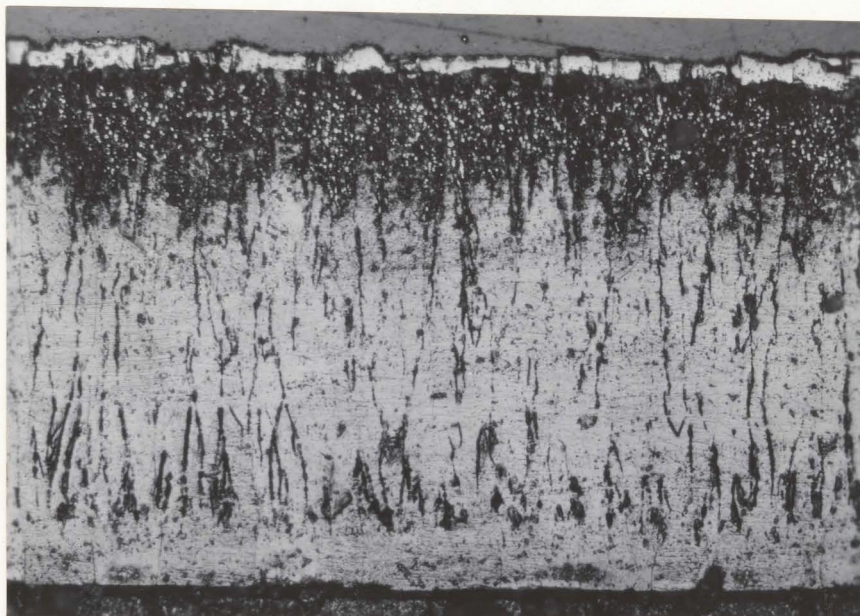
X250

(X800)

Figure IV, 17

Cross-section of wustite-magnetite scale on iron exposed for
170 min. in oxygen at 3.0×10^{-1} torr.
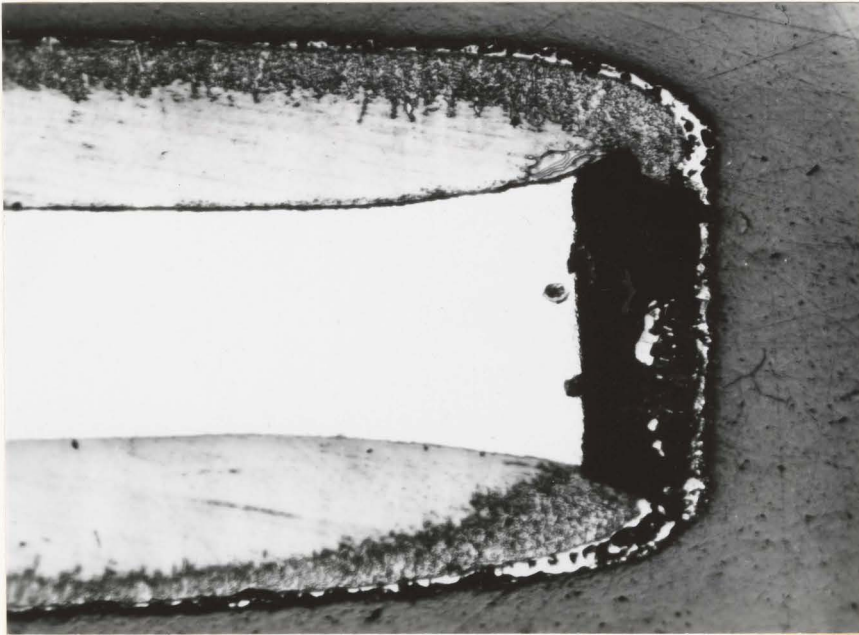
X80
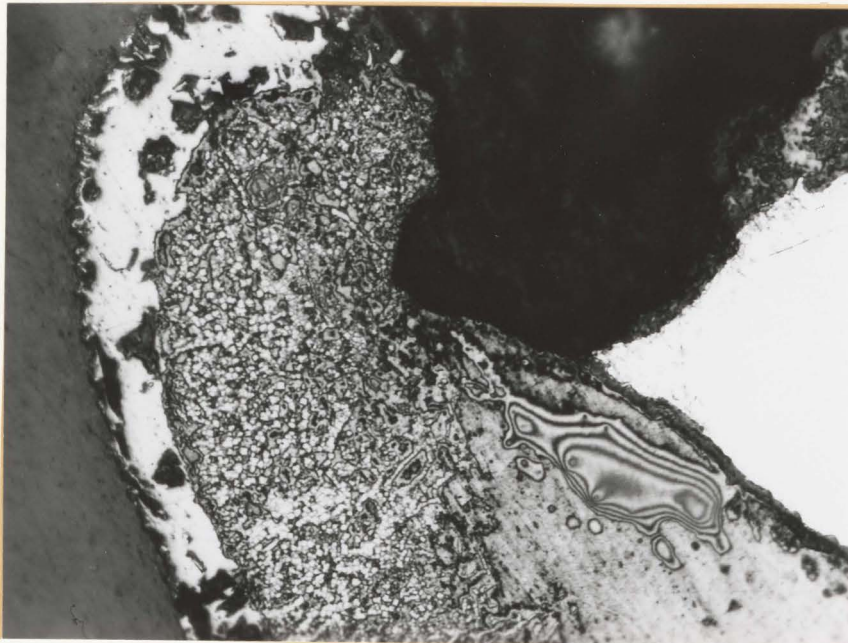
X320

Figure IV, 18

Cross-section of wustite-magnetite scale on iron exposed

for 170 min. in oxygen at 3.0×10^{-1} torr.

Exposure: 20 min. at 800°C in oxygen at 0.30 torr (X1650).
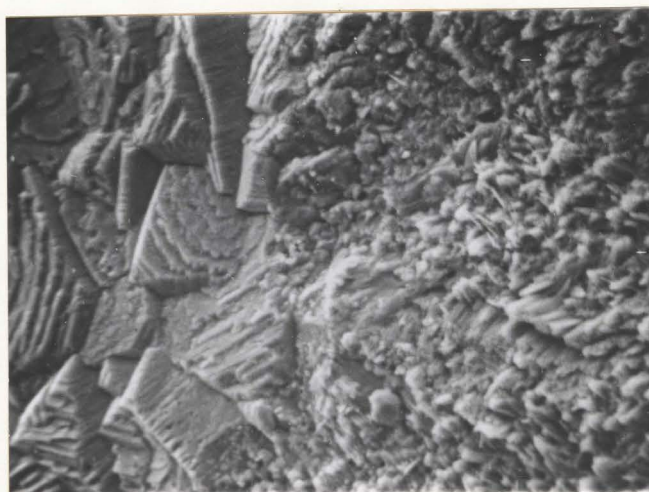
Exposure: 30 min. at 800°C in oxygen at 0.30 torr (X750).

Figure IV, 19

Scanning electron micrograph of the magnetite layer formed on wustite.

magnetite grains of very irregular shape. Near the edges the topology was occassionally different as magnetite appears in the form of needles.

Hematite is nucleated on the magnetite surface after a certain time which is pressure dependent. Its appearance is illustrated in Fig. IV, 20. Nucleation seems to preferentially occur near grain boundaries. The nuclei extend laterally under the form of large islands and finally hematite covers the entire surface. These islands are shown in Fig. IV, 21. The formation of Fe_2O_3 was also at a more advanced stage near the edges where contact has been lost. Hematite formed by a mechanism involving the vertical and lateral growth of whiskers. These whiskers are even formed on adherent scale Fig. IV, 22 and they can appear either under the form of platelets Fig. IV, 23 or under the form of needles Fig. IV, 24. In order to obtain more information about the phenomena of whisker formation we carried out a study concerning the effect of different parameters, i.e., time, oxidant agent, temperature, oxygen pressure and metal purity. These results are represented in Fig. IV, 25 and Table IV, 1.

The growth of hematite whiskers may be summarized by the following steps. At 800°C and in laboratory air under atmospheric pressure, needles of approximately 0.7 μ in length and 0.06 μ in diameter grow on the specimen surface after 1 min. of oxidation (Fig. a). They generally appear in colony forming islands (Fig. b). For the same conditions but after 2 min. of oxidation the whiskers increased in density, length and diameter (Fig. c). Finally the previous islands developped laterally until a very dense forest of

Figure IV, 20

Scanning electron micrograph of the hematite nuclei formed on magnetite (X800). Exposure: 40 min. in oxygen at 5.0×10^{-1} torr.
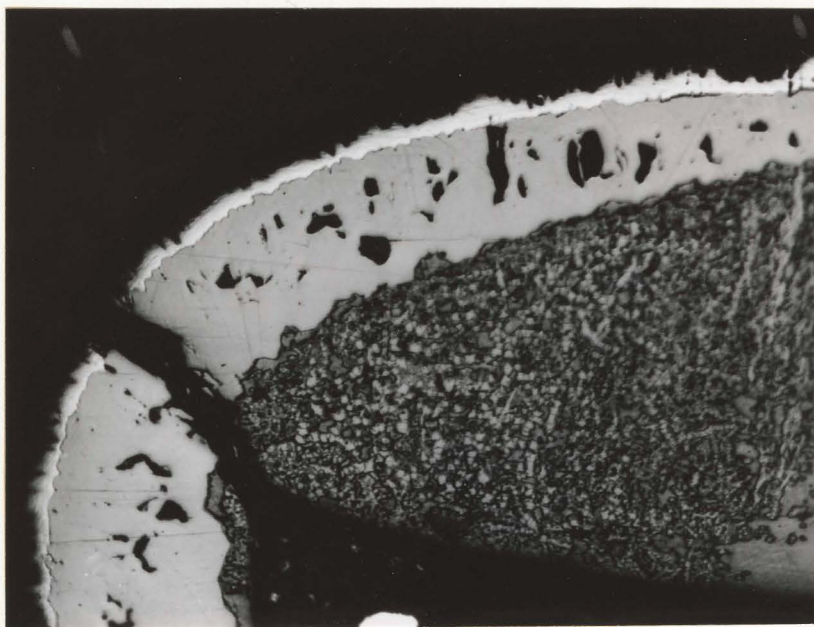
Figure IV, 21

Cross-section of the multilayer scale on iron exposed for 150
min. in oxygen at 5.0×10^{-1} torr (X320).
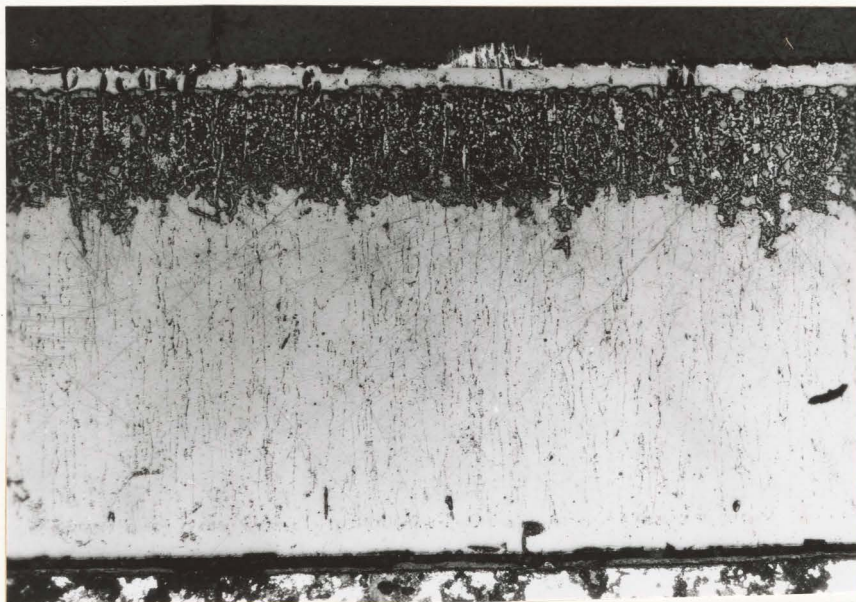
X180
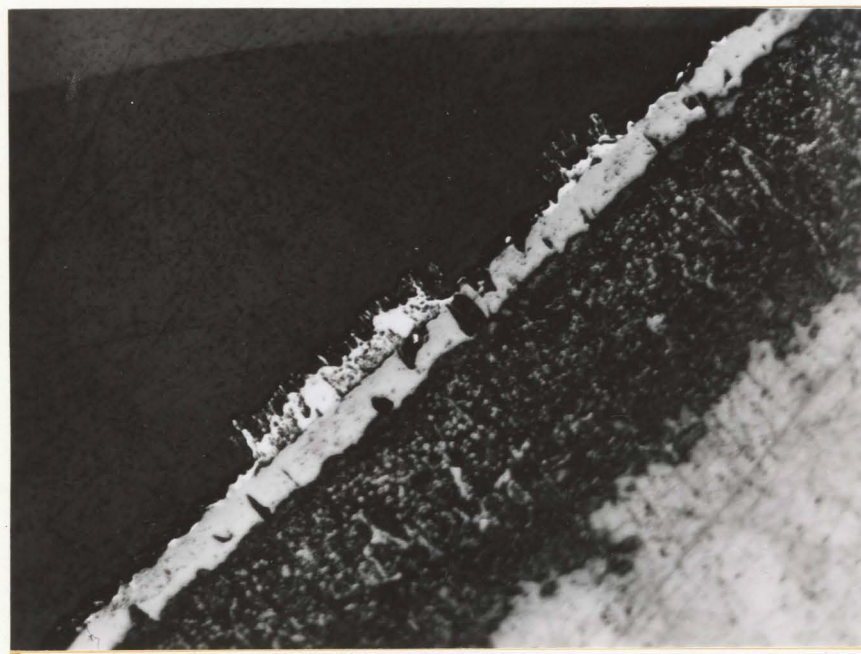
X320

Figure IV, 22

Cross-section of the multilayer scale on iron exposed for 230 min. in oxygen at 10 torr.

X8500
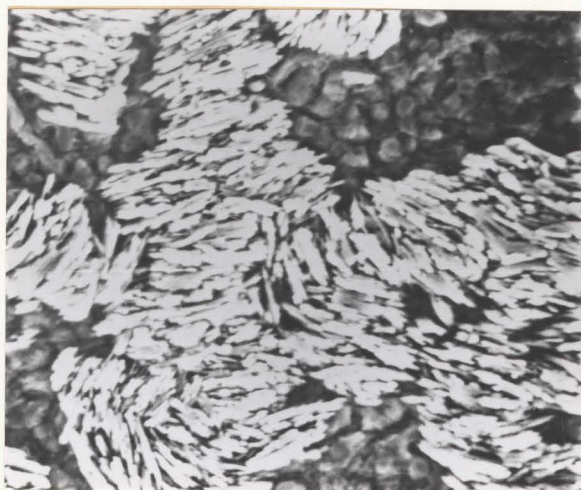
X900

Figure IV, 23

Scanning electron micrograph of scale surface showing platelets.

Exposure: 230 min. at 800°C in oxygen at 10 torr.

Figure IV, 24a

Cross-section of the multilayer scale on iron exposed for
330 min. at 800°C in air at 760 torr. (X320).

Figure IV, 24b

Scanning electron micrograph of the surface of hematite whiskers.
Exposure: 90 min. at 840°C in air at 760 torr (X4900).
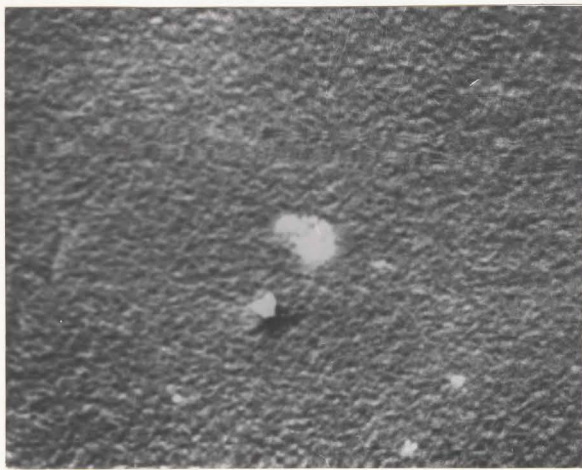
(a)

(b)

(c)
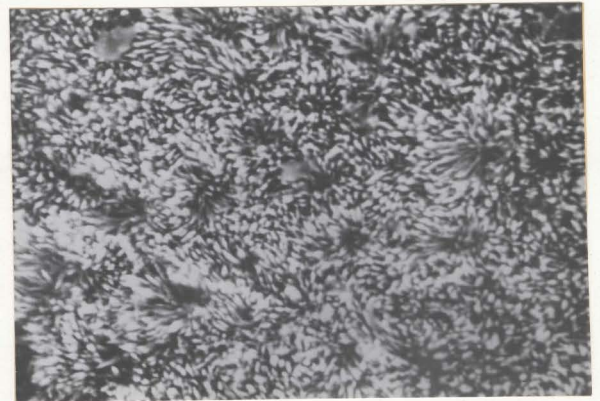
(d)
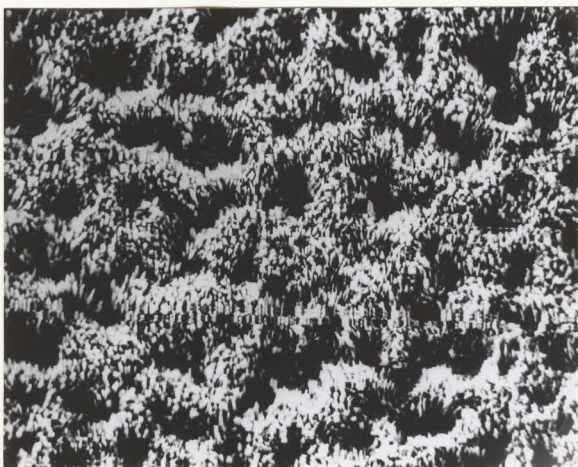
(e)

(f)

Figure IV, 25

(g)

(h)

(i)

(j)

(k)

Figure IV, 25 (continued)
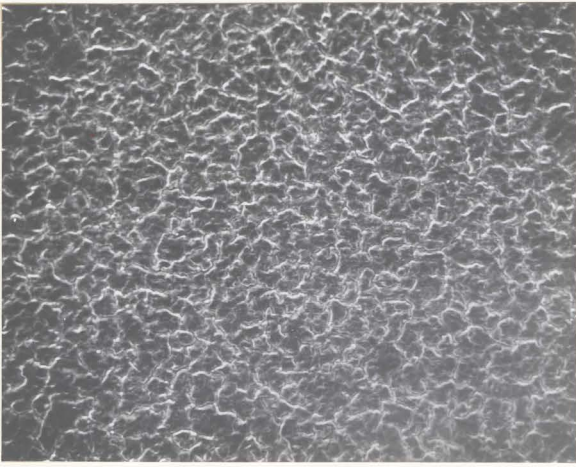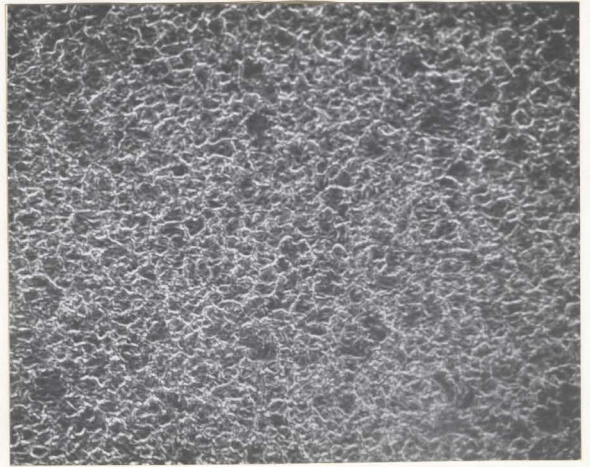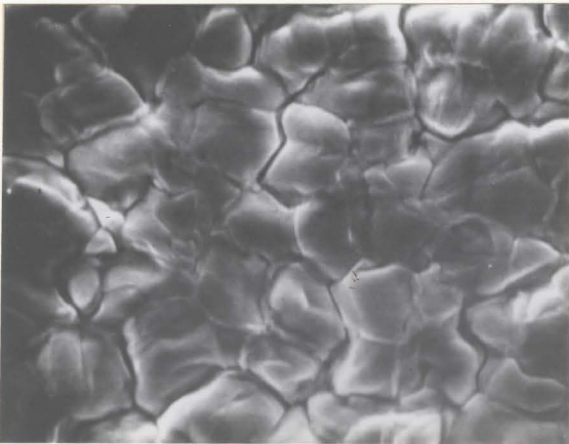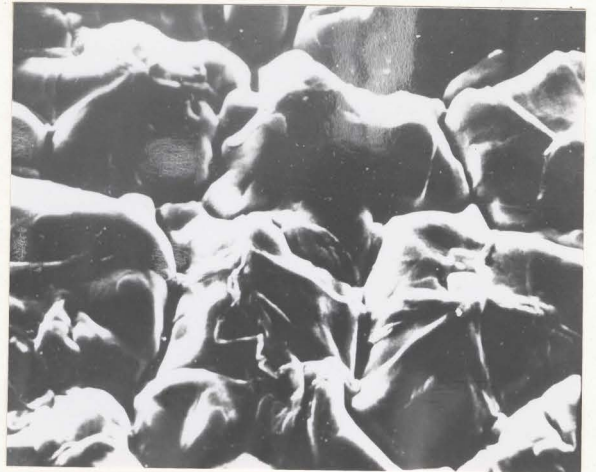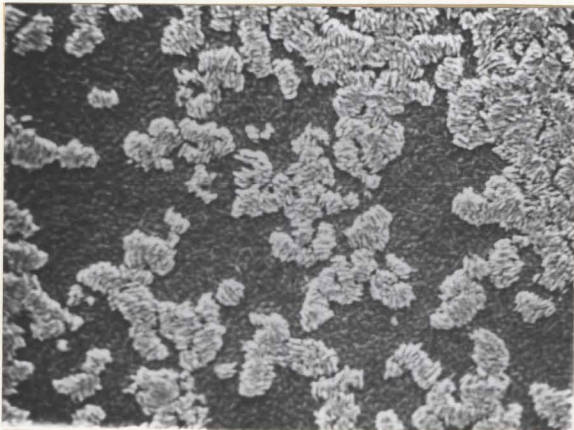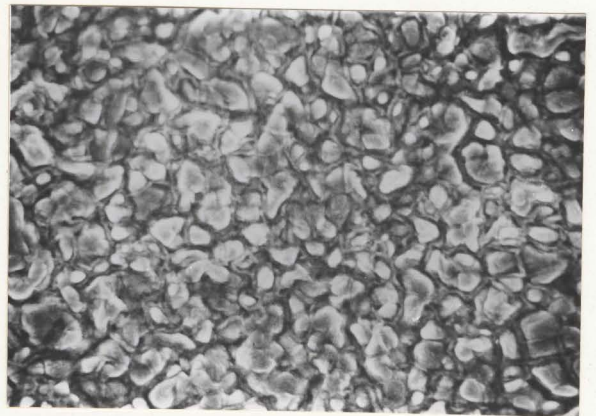
(l)

Table IV-1

Effect of different parameters on the phenomena of whisker formation.

Oxidation time (minutes)	Oxidant agent	Temperature (°C)	Pressure (Torr)	Metal Purity	Corresponding name in Fig.IV,25	Magnification
1	Laboratory air	800	760	H.P.	(a)	X8300
1	"	"	"	"	(b)	X410
2	"	"	"	"	(c)	X4300
60	"	"	"	"	(d)	X750
60	"	830	"	"	(e)	X470
96	"	840	"	"	(f)	X980
15	"	860	"	"	(g)	X180
60	"	"	"	"	(h)	X180
60	"	"	"	"	(i)	X1800
15	"	990	"	"	(j)	X1700
230	oxygen	800	10	"	(k)	X180
60	Laboratory air	"	760	Armco	(1)	X980

needles covered the entire surface and this state occurs after
approximately 1 hr. for the conditions described previously (Fig. d).
The same results are obtained in dry oxygen. If the temperature is
increased to 830°C whiskers still cover the entire specimen
surface after 1 hr., but it seems from the dark area of Fig. e that
their density of population is less important than at 800°C. Never-
theless at 840°C only a few areas are invaded by small needles, the
remainder of the surface being covered by regularly shaped grains
growing perpendicularly to the specimen surface Fig. f. At 850°C
the density of whiskers decreases again and finally at 860°C no
whiskers are observed on the specimen surface which exhibits only
regular grains of hematite (Fig. g, h and i). This structure is
always found in the temperature range 860 to 1000°C (Fig. j). How-
ever at 800°C when the oxygen pressure is only 10 torr, even after
4 hrs. the sample surface is not completely covered with whiskers
(Fig. k). Finally we will mention that whisker formation is in-
dependent of surface preparation since the same results were
obtained with 1 µ diamond polish, annealed and electropolish
specimens. But it is interesting to note that during the first
minutes of oxidation whiskers appeared preferentially at eventual
polishing strike or at marks of finger print. On the other hand
we do not observe whisker formation on Armco iron oxidized 1 hr. at
800°C in laboratory air under atmospheric pressure (Fig. 1).

Examination of the scale cross sections with an optical micro-
scope shows that the oxide layers are very compact and adherent to

the metal substrate (Fig. IV, 26). Contact at the Fe/FeO interface
is maintained by plastic deformation of the oxide scale. This
implies the generation of important stresses which leads to complex
processes involving polygonization of iron and wustite as illustrated
by Fig. IV, 27. However the iron-oxide interface is very planar,
its detailed microscopic shape being a function of the metal purity.
From the measurements of relative thicknesses of the different
layers given in Table IV, 2 we can see that our results are generally
in agreement with those previously advanced by Paidassi (87). How-
ever when whisker formation is observed this phenomena is associated
with an important increase of the relative thickness of hematite
Fig. IV, 28, the proportion of FeO and Fe_3O_4 in the scale remaining
constant.

4.4 The Kinetics and Morphological Development of the Oxide Scale on Iron at 1.5×10^{-2} torr in the Temperature Range 750 to 1000°C

4.4.1 Introduction

We reported before for the case of iron oxidation at 800°C and
at pressures ranging between 2.5×10^{-3} to 3.0×10^{-1} torr that the kinetic
curves exhibited a region of linear behavior and a part where the
oxidation rate decreased with time. After this investigation con-
cerning the pressure influence on the reaction rate, we decided to
study the temperature effect in order to gain more information about
the rate determining process. A detailed analysis of the kinetics
results should lead to a complete interpretation of the reaction
mechanism and a further insight into the oxidation characteristics
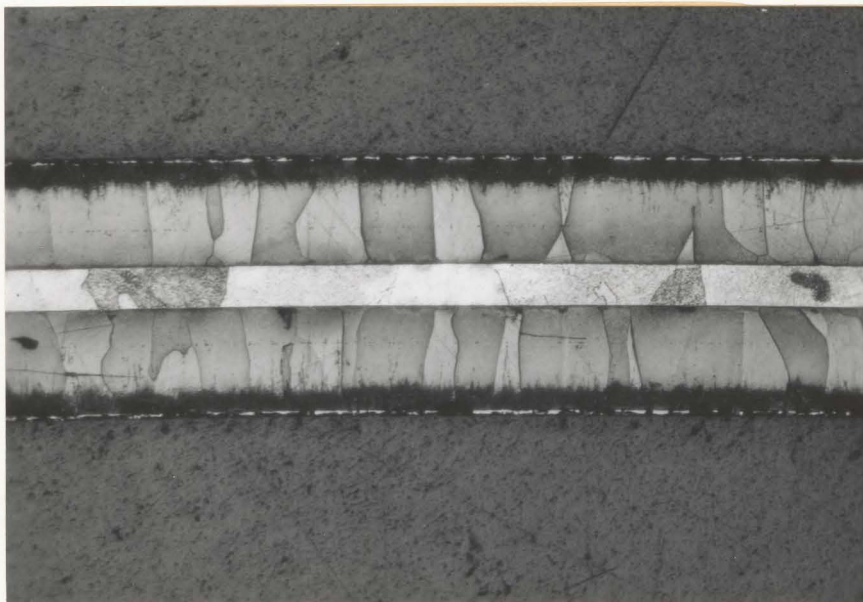
X80
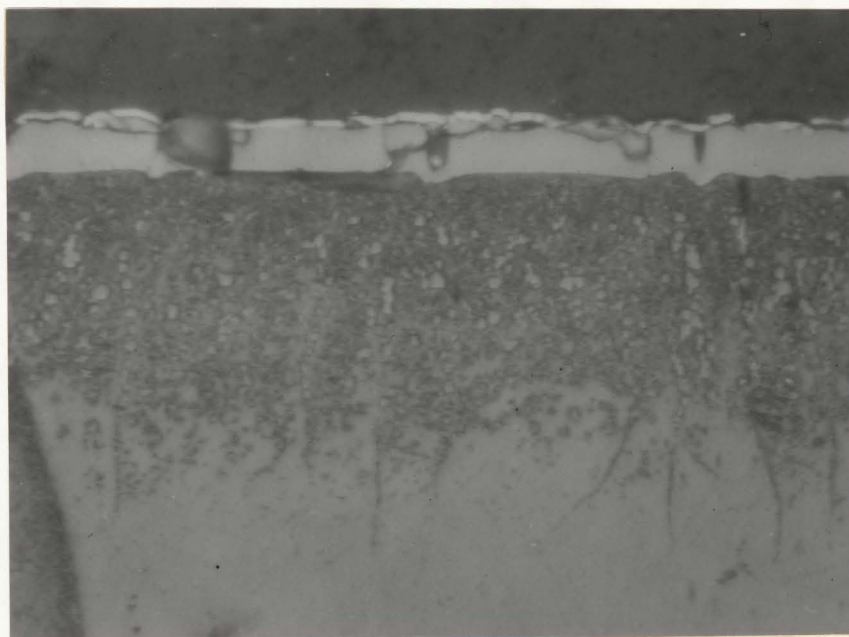
X800

Figure IV, 26

Cross-section of the multilayer scale on iron exposed for 13
min. at 960°C in air at 760 torr.
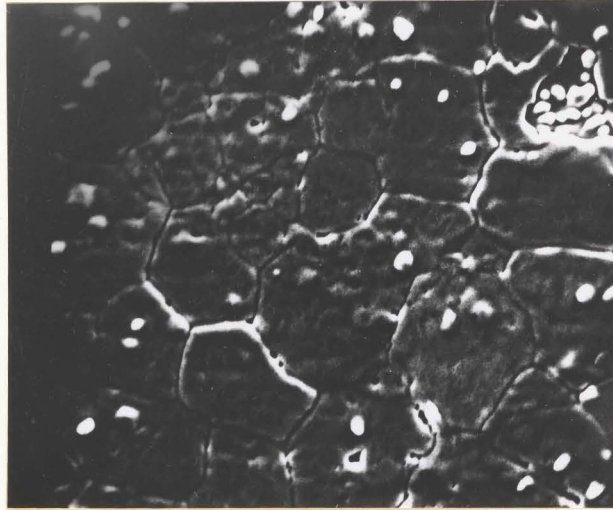
Polygonization of Iron (X900)
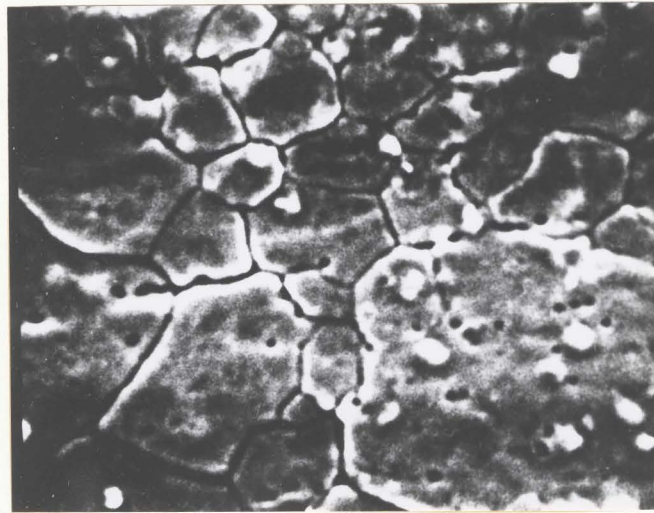
Polygonization of wustite (X1400)

Figure IV, 27

Scanning electron micrograph of the Fe/FeO interface after an exposure for 60 min. at 800°C in air at 760 torr.

Table IV-2

Relative Thicknesses of the Oxides

No whiskers	Present results	Literature (87)
Fe_2O_3	0.7%	0.9%
Fe_3O_4	3.8%	3.7
FeO	95.5%	95.4%

Whiskers Formation		
Fe_2O_3	4.8%	
Fe_3O_4	3.6%	
FeO	91.6%	

Formation of a Duplex Scale (FeO + Fe_3O_4)		
Fe_3O_4	3.70%	
FeO	96.30%	
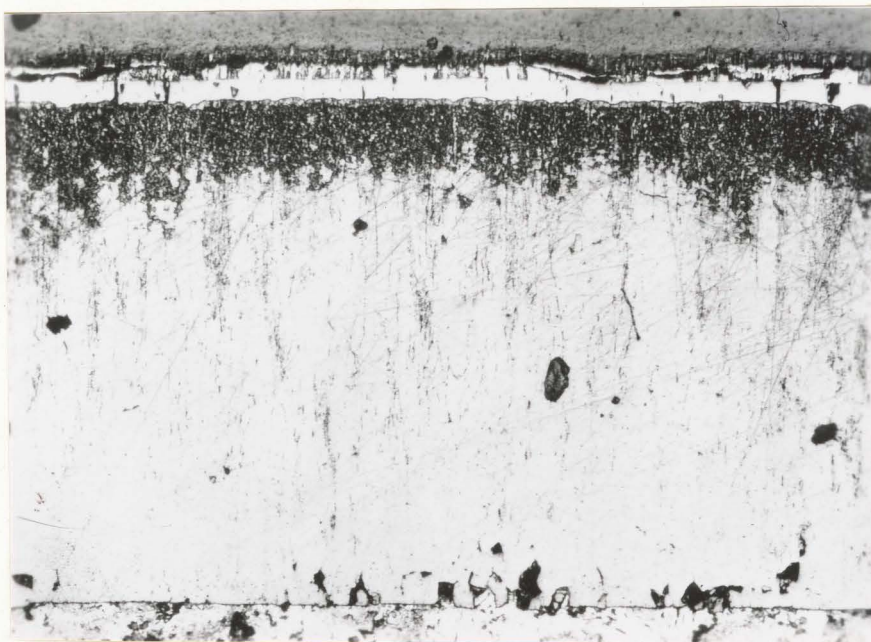
Figure IV, 28

Cross-section of the multilayer scale on iron exposed for
330 min. at 800°C in air at 760 torr (X160).

of α and γ iron.

4.4.2 Oxidation Kinetics

The oxidation curves for specimen exposed to research grade oxygen at 1.5×10^{-2} torr pressure in the temperature range 750° to 1000°C are shown in Fig. IV, 29. The weight change was evaluated using the original dimensions of the specimen. These curves were reproducible to approximately, 5% in the α iron region (T<910°C), and 10% in the γ iron region (T>910°C). According to Fig. IV, 29 the results obtained are analogous to those advanced previously at 800°C. for the same pressure. The duration of the linear region increases considerably with temperature. If we consider Fig. IV, 30 which represents the first minutes of oxidation we can see that the temperature effect on the linear reaction rate does not seem to be very important.

4.4.3 Morphological Development of the Oxide Scale

Our observations are generally similar to the results advanced previously at 800°C, i.e., oxidation during the first stage is associated with growth of small crystals as it is shown in Fig. IV, 31. During the region of linear behavior and a subsequent part of the oxidation curve described by the continuously decreasing rate the specimens were covered with an oxide scale consisting only of wustite. The wustite/oxygen interface is of very irregular shape during the first minutes of oxidation (Fig. IV, 32) but become more uniform after a certain period (Fig. IV, 33). Etching of the scale revealed the large grain size (40 to 60 μ) of wustite which exhibits
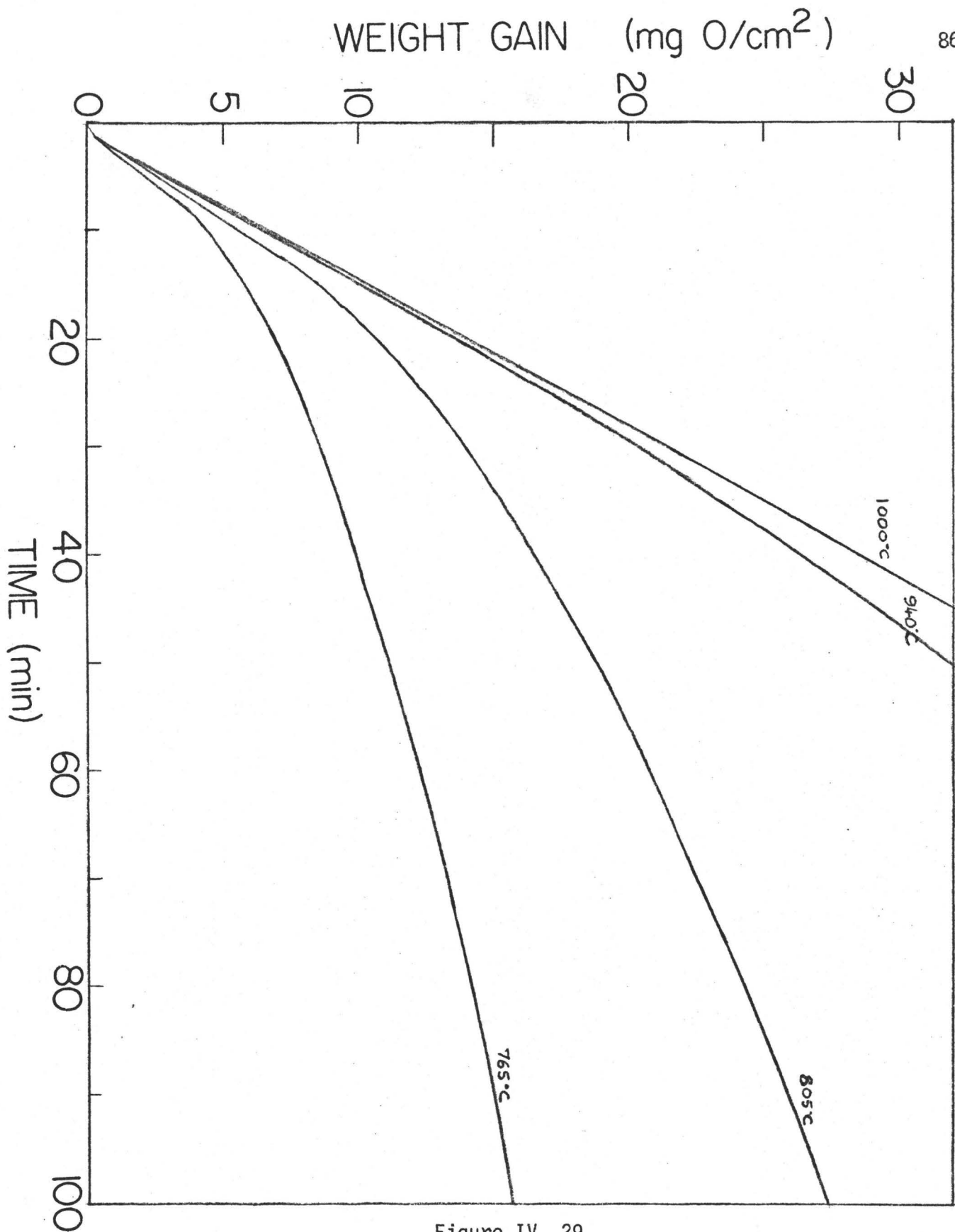
Figure IV, 29

Oxidation curves for iron exposed to oxygen at 1.5×10^{-2} torr
pressure over the temperature range 750°-1000°C for periods up to 100
min.

Figure IV, 30

Oxidation curves for iron exposed to oxygen at 1.5×10^{-2} torr

pressure over the temperature range 750°-1000°C for periods of 10 min.
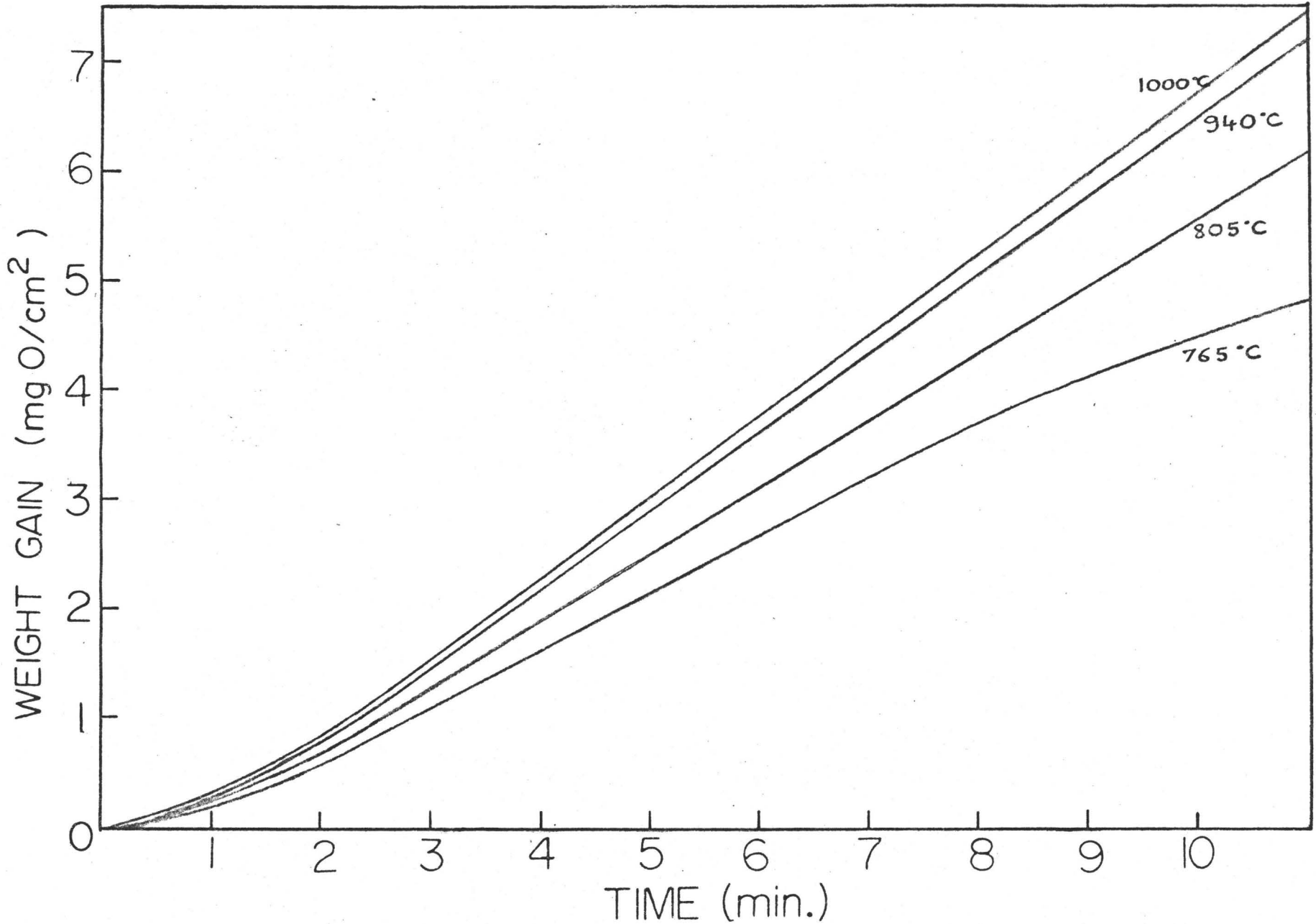
Figure IV, 31

Scanning electron micrograph of wustite crystals on iron after
an exposure for 5 min. at 1000°C in oxygen at 2.5×10^{-3} torr (X1700).
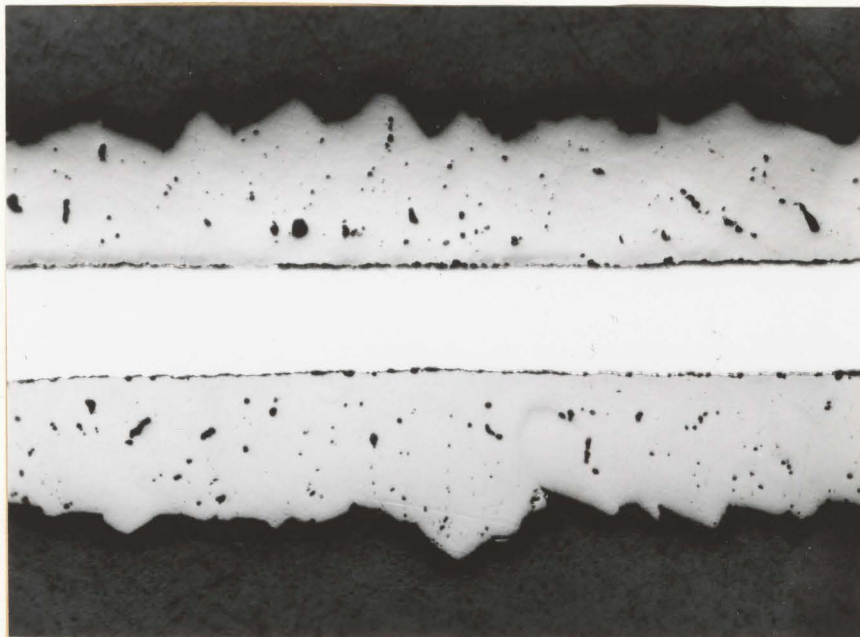
Figure IV, 32

Cross-section of the wustite scale on iron exposed for 15 min.
at 1000°C in oxygen at 10^{-1} torr (X160).
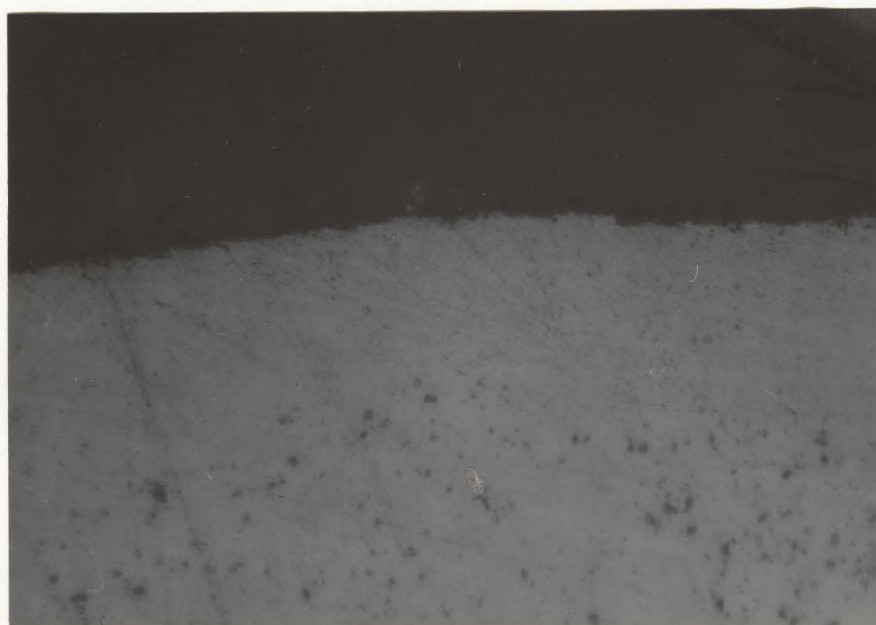
Figure IV, 33

Cross-section of the wustite scale on iron exposed for 90 min.
at 950°C in oxygen at 1.5×10^{-2} torr (X800).

a strong preferential direction of growth (Fig. IV, 34). Study of a scale 10_μ thick obtained at 1000°C showed a preferred orientation of the (100) wustite face parallel to the metal surface. On the other hand no specific texture was found in very thick scale ($\gtrsim 500_\mu$). Examination of scale surface with a scanning electron microscope showed the morphology of the very large wustite grains Fig. IV, 35.

After a certain time which is strongly correlated to the temperature magnetite is nucleated on the wustite surface. Since this nucleation process is very slow at temperatures as high as 1000°C, it was therefore possible to observe the formation of the first Fe_3O_4 nuclei. As it is shown on Fig. IV, 36 these nuclei are of very specific shape and are formed on a uniform base film. They grow laterally to completely cover the wustite surface. The details of these different steps is illustrated by Fig. IV, 36 to IV, 38 where we can see that the magnetite grains are large enough to be discernable even if Fe_3O_4 does not entirely cover the FeO surface. However if wustite is sufficiently saturated with oxygen the development of a magnetite layer is still very slow as it is shown on Fig. IV, 39.

Figure IV, 34

Cross-section of the etched wustite scale shown in Fig. IV, 32 (X400).

Figure IV, 35

Scanning electron micrograph of the surface of a wustite scale formed on iron exposed for 180 min. at 1000°C in oxygen at 1.5×10^{-2} torr (X70).
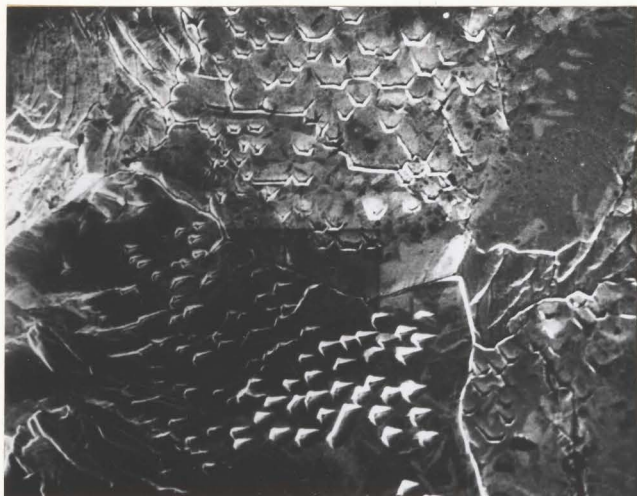
X150
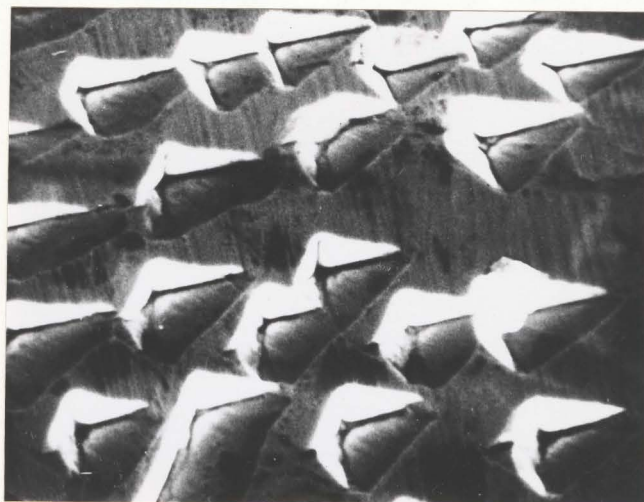
X750

X800

X1500

Figure IV, 36

Scanning electron micrograph of magnetite crystals on wustite
after an exposure for 180 min. at 1000°C in oxygen at 1.5×10^{-2} torr.

X15
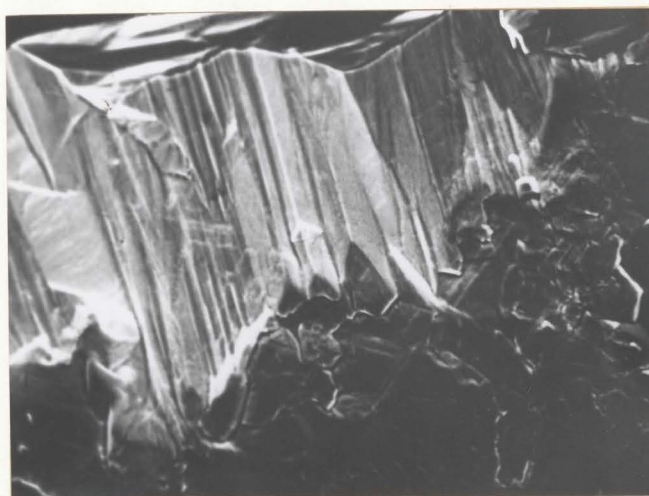
X400

Figure IV, 37

Scanning electron micrograph of scale surface showing partial coverage of wustite by magnetite. Exposure: 120 min. at 940°C in oxygen at 1.5×10^{-2} torr.
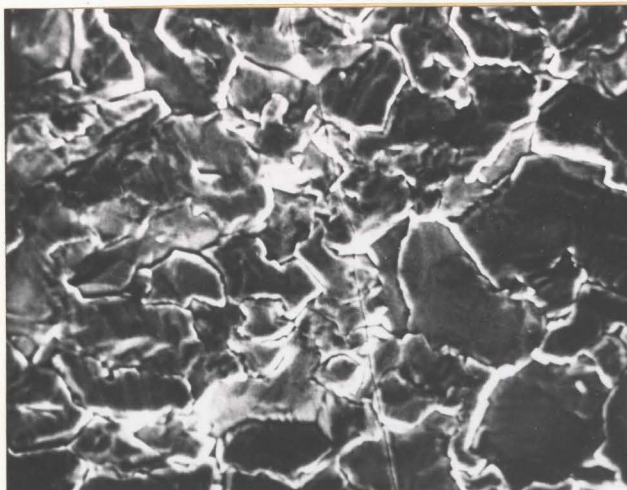
Figure IV, 38

Scanning electron micrograph of the magnetite layer formed
on wustite. Exposure: 120min. at 940°C in oxygen at 1.5×10^{-2} torr (X750).

Figure IV, 39

Cross-section of a completely oxidized sample. Exposure:
60 min. at 900°C in oxygen at 1.5×10^{-2} torr (X260).

CHAPTER V

ANALYSIS AND DISCUSSION OF EXPERIMENTAL RESULTS

5.1 Introduction

We have previously divided the presentation of our results in three sections which we will also discuss separately. Then from these discussions a general model will be proposed concerning the mechanism of iron oxidation at high temperature.

5.2 Oxidation at 800°C in the Pressure Range 2.5×10^{-3} to 3.0×10^{-1} Torr

5.2.1 The Phenomena of Magnetite Formation

The dissociation pressures of wustite, magnetite and hematite at 800°C are 1.01×10^{-16}, 2.21×10^{-15} and 3.96×10^{-7} atm, respectively (10, 11). Formation of these oxides is therefore thermodynamically feasible under the experimental conditions chosen. There is a general agreement that the growth of the wustite layer occurs by outward diffusion of iron ions via vacant sites in the iron sub-lattice. Consequently FeO is formed at the FeO/O_2 interface, during the first period of oxidation according to equation (5-1).
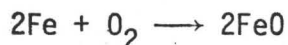
$$2Fe + O_2 \longrightarrow 2FeO \qquad\qquad 5-1$$

Since iron migrates rapidly through a thin wustite scale, an over supply of iron ions react with any Fe_3O_4 that may form to yield FeO according to the following equations,

$$6FeO + O_2 \longrightarrow 2Fe_3O_4 \qquad\qquad 5\text{-}2$$

$$Fe_3O_4 + Fe \longrightarrow 4FeO \qquad\qquad 5\text{-}2'$$

And the proportion of Fe_3O_4 in the scale will depend on the balance between reactions (5-2) and (5-2'). After a sufficiently long oxidation time or if wustite is not adherent on the metal the supply of oxygen absorbed exceeds the amount of iron diffusing to the wustite surface and reaction (5-2) becomes faster than reaction (5-2'). We observe then the formation of both FeO and Fe_3O_4.

The kinetic results show that the oxidation behavior of iron at 800°C in oxygen at pressures ranging from 2.5×10^{-3} to 3.0×10^{-1} torr exhibits the same general features as in carbon dioxide (67)(71-74). The kinetic curves consist of a short acceleration period, a region of linear behavior and finally a period of decreasing rate associated with the nucleation and growth of Fe_3O_4.

5.2.2 The Acceleration Period

As it was previously suggested by Charbonnier, Bardolle and Mollimard (63)(64) this acceleration period is associated with the nucleation and growth of FeO on the surface of iron. Since the period was very short in time we could not do a proper kinetic exploitation of this part. It would appear that the wustite crystals formed grow laterally and vertically over a thin base oxide film to cover the surface with a layer of wustite.

5.2.3 The Region of Linear Behavior

During this period the weight increase per unit area is proportional to the time t, and we can define a linear rate constant K_L such as,

$$\frac{\Delta p}{s} = K_L \cdot t. \qquad\qquad 5\text{-}3$$

These linear kinetics suggest that wustite grows according to an interfacial control reaction. Fig. V, 1 shows K_L as a function of the oxygen pressure. We have just reported the pressure dependence on K_L in the pressure range 2.5×10^{-3} to 3.3×10^{-2} torr, because even at 3.3 to 10^{-2} torr the kinetics followed a linear law only during 1 min., and for higher pressure the linear region was shorter than 30 sec. (Fig. IV, 2). Therefore it was difficult to give a physical significance to such a short period which could be just a transition between an acceleration period, due to both nucleation and establishment of the correct pressure, and the region of decreasing rate. According to Fig. V, 1 the linear rate constant is directly proportional to the oxygen pressure. In consequence the expression,

$$K_L = \alpha(K_L)_{theor} = \alpha P_{O_2} / (2\pi mkT)^{\frac{1}{2}} \qquad\qquad 5\text{-}4$$

is used to calculate the fraction of impinging oxygen molecules, α, incorporated into wustite. $(K_L)_{theor}$ represents the rate constant assuming that all impinging molecules react, k is Boltzmann's

Figure V, 1

Plot of the linear oxidation constant for wustite formation
on iron at 800°C vs oxygen pressure over the range $2.5 \times 10^{-3} - 3.3 \times 10^{-2}$ torr.
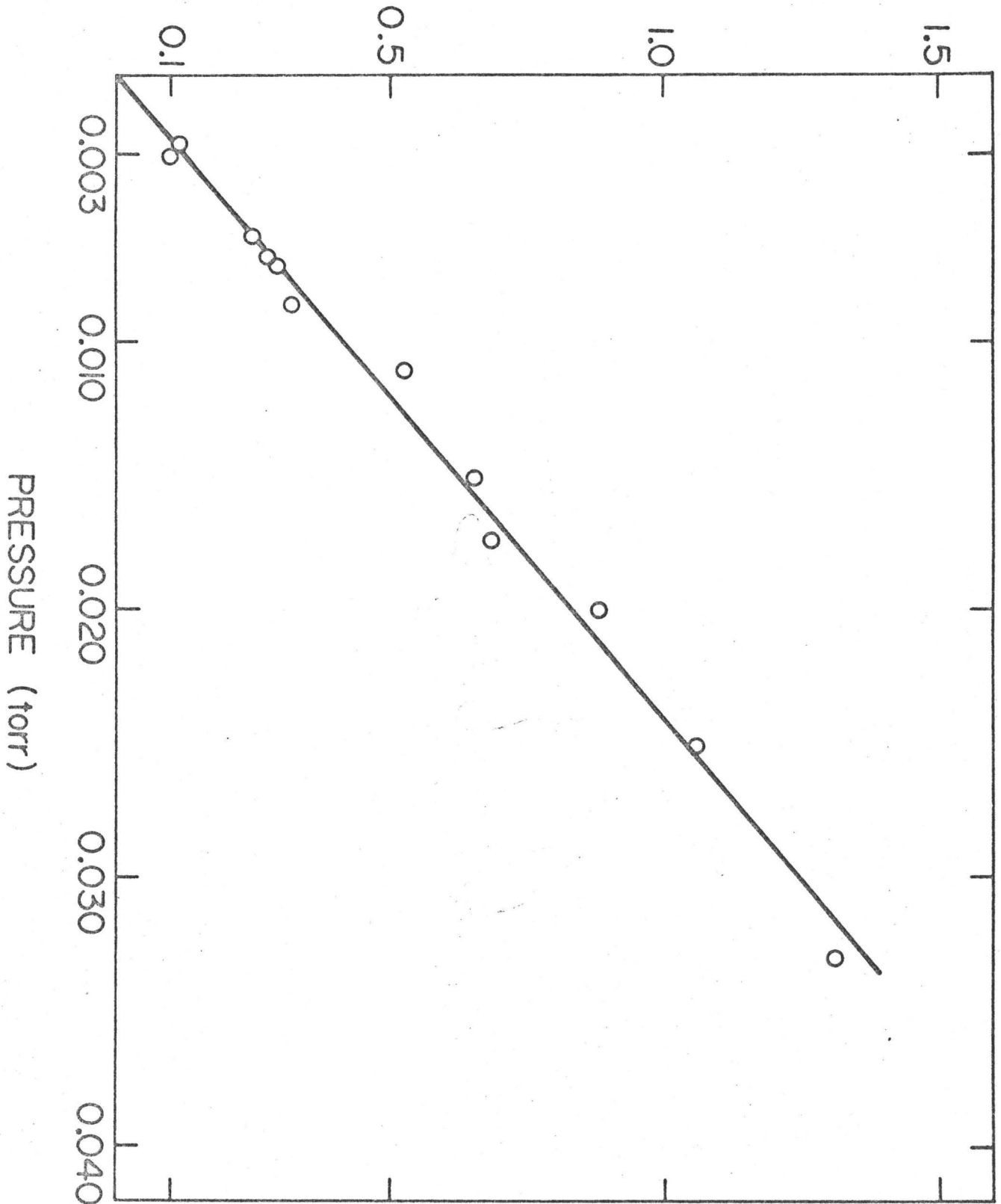
constant, m is the mass of an oxygen molecule and T is the temperature in °K. The calculated values, Table V, 1, demonstrate that the fraction of impinging molecules adsorbed is only 6.7% independent of pressure. These results are consistent with the conclusion that the rate controlling step during linear kinetics involves a non-dissociative oxygen adsorption mechanism.

5.2.4 The Region of Decreasing Rate

The oxidation curves have been plotted in parabolic form in Fig. V, 2. A typical curve exhibits a transition from linear to parabolic kinetics. It is to be noted that the periods for this transition decrease with increasing pressure. Above 1.5×10^{-1} torr, the transition also occurs at progressively smaller weight gains with increasing pressure presumably due to more rapid nucleation and growth of magnetite. Results are also included for oxidation in dry air in order to show that the rate of parabolic scaling remains pressure independent up to 1 atm.

Since wustite accounts for at least 95% of the scale thickness, the overall scaling rate can be identified with the growth rate of the wustite layer alone which is given by the following expression derived by Wagner,

$$Kr = \bar{C}_2 \int_{a'_0}^{a''_0} \frac{Z_1^2}{|Z_2|} D_1 \, d\ln a_0. \qquad 5\text{-}5$$

where $\bar{C}_2$ is the average composition of wustite, D_1 is the self diffusion coefficient for iron, Z_1 and Z_2 are the valencies of iron and oxygen, a'_0 and a''_0 are respectively the oxygen activities at the inner

Table V-1

Sticking coefficient, $\alpha = K_L/(K_L)_{theor}$, for oxygen on wustite at 800°C.

Pressure x 10^3 (Torr)	α
2.5	0.077
2.9	0.058
3	0.055
6	0.069
6.8	0.067
7	0.067
7 }	0.068
8.5	0.062
12	0.079
17.4	0.065
23	0.067
25.2	0.063
33	0.066

Average value:

$\alpha = 0.067 \pm 0.012$
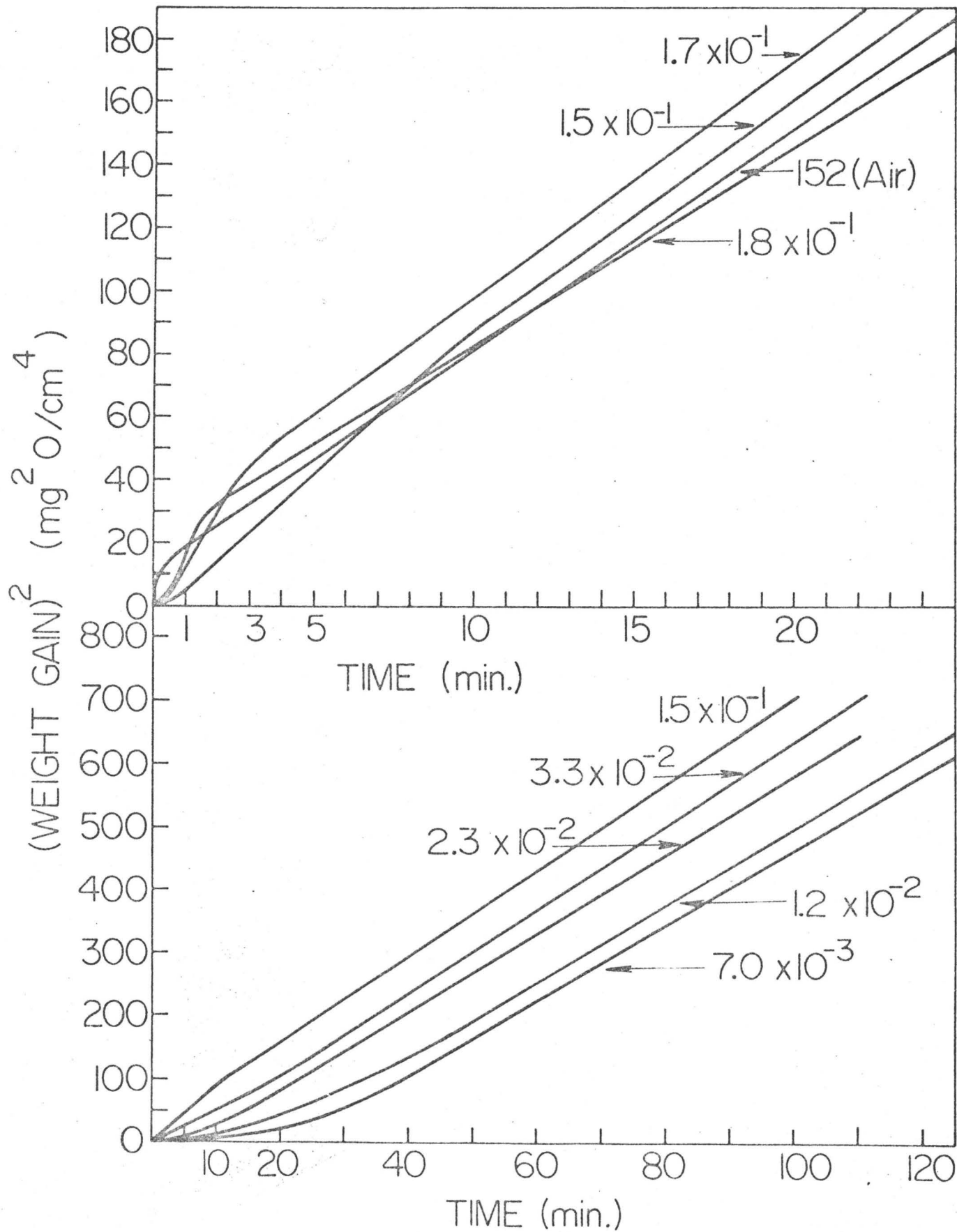
Figure V, 2

The oxidation curves plotted in parabolic form: $(\frac{\text{weight gain}}{\text{unit area}})^2$ vs time.

and outer interface. If a thin layer of magnetite is formed a'_o and a''_o are respectively given by the decomposition pressure of FeO and Fe_3O_4, the reaction rate is then independant of the ambient oxygen pressure. This behavior is precisely shown by the plot in Fig. V, 3 for the values of the parabolic constant vs pressure. The values from this investigation lie in agreement to a previously determined value for zone-refined iron. They are also equal to calculated values, within the accuracy of the calculation, using independent iron diffusivity measurements in wustite in equation (5-5) (40, 72).

5.3 Oxidation at High Temperature in the Pressure Range 0.30 to 760 Torr

5.3.1 Oxidation Kinetics

The kinetic results plotted in parabolic manner Fig. V, 4 show that except during a period ranging between 20 and 30 mins. the oxidation process obeyed a parabolic law. Within the interval of error these parabolic curves having the same slope, the reaction rate is not dependent upon oxygen pressure between 0.3 and 760 torr. The values of the different parabolic constants are given in Table V, 2 and we can see that our results are in close agreement with those previously advanced by Paidassi (87) and Schmall et al (88). However the rate constants determined and calculated by Himmel et al (40) are at least 30% lower.

In the early stages of an oxidation test, it is very difficult to avoid specimen overtemperature resulting from the exothermicity of the chemical reaction. And the anomalous oxidation behavior observed

Figure V, 3

A plot of the parabolic oxidation constants vs oxygen pressure. The references are designated by the numbers in brackets.
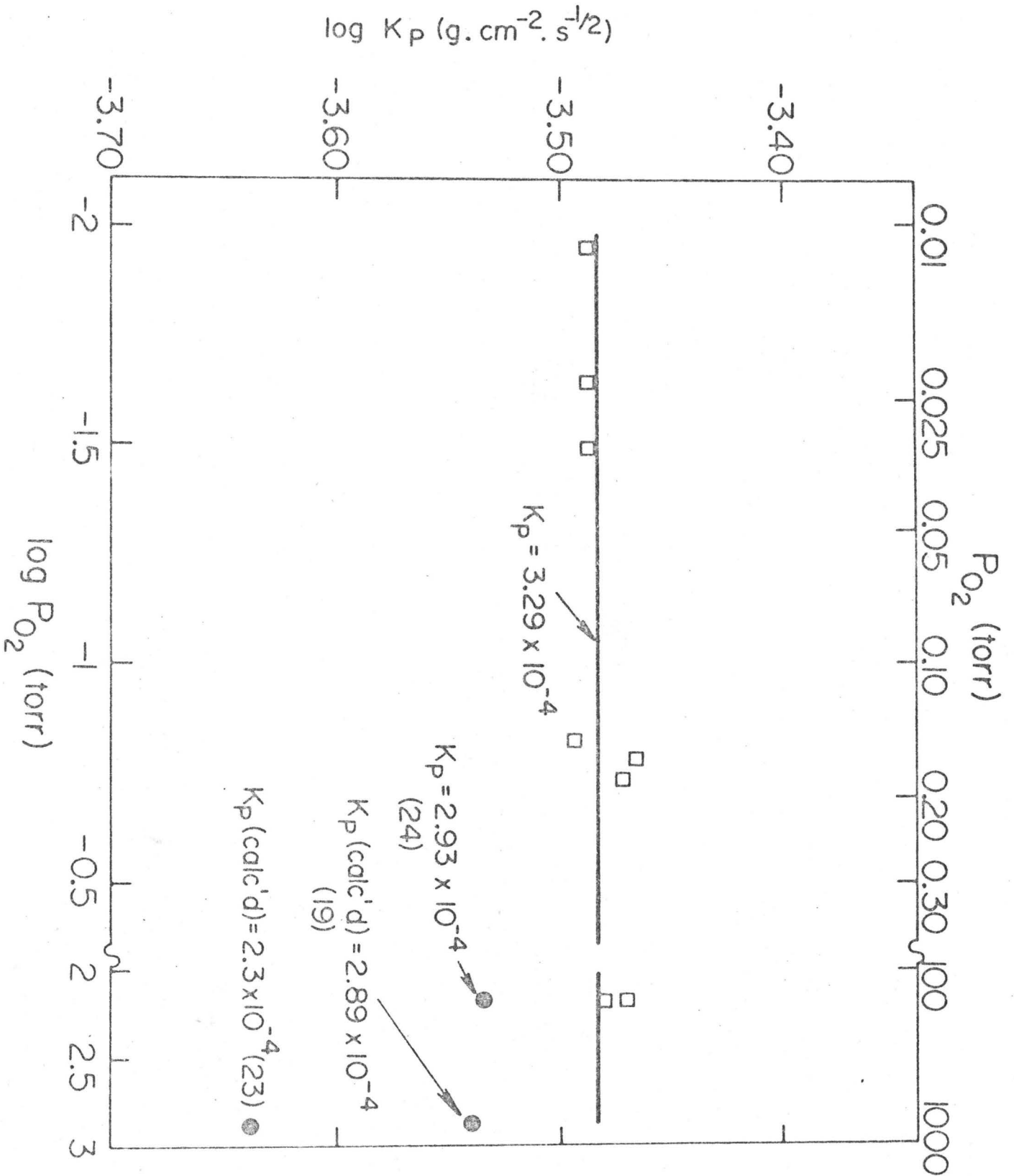
Figure V, 4

The oxidation curves plotted in parabolic form: $\left(\frac{\text{weight gain}}{\text{unit area}}\right)^2$

vs time.
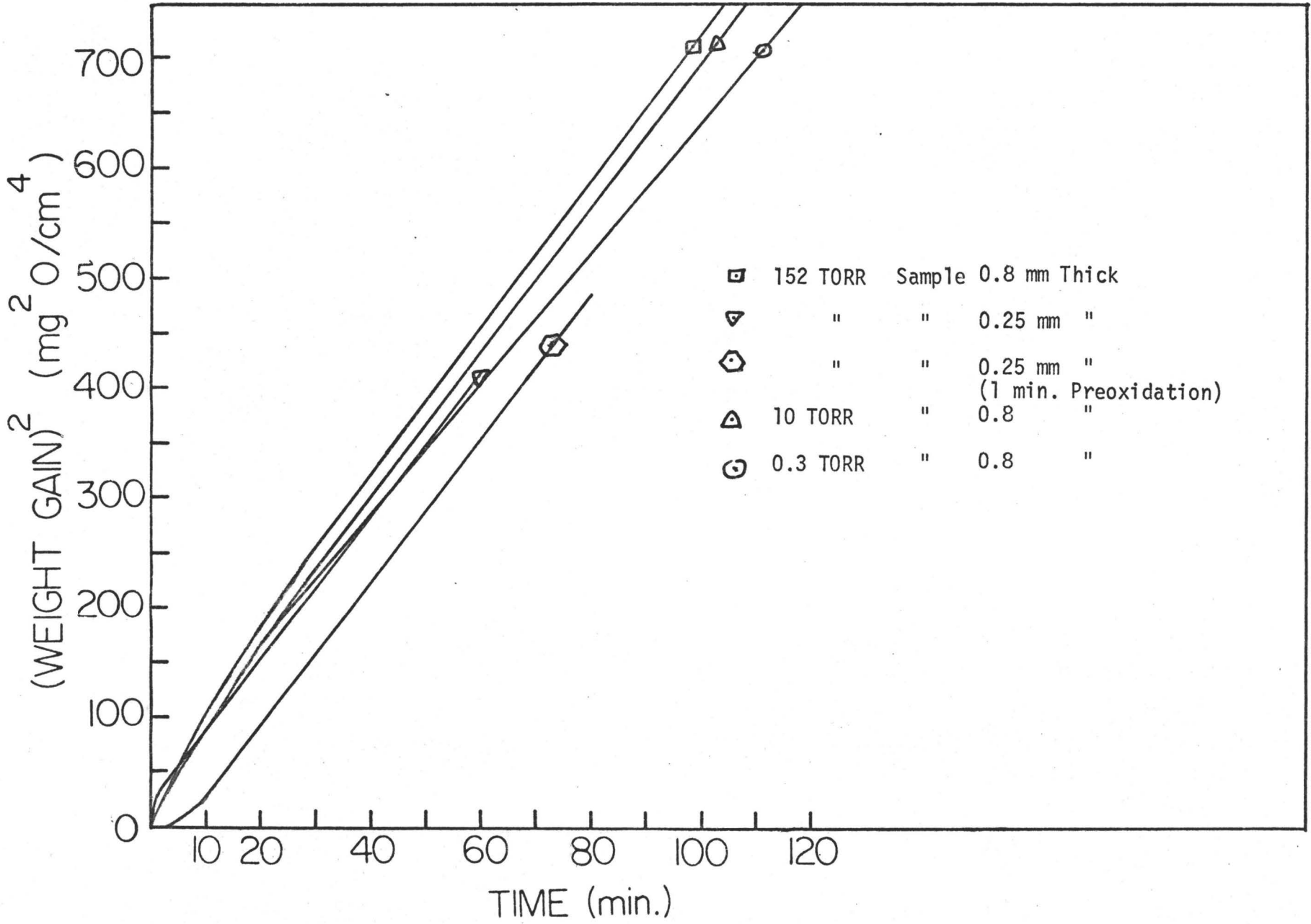
Table V-2

Measured parabolic rate constants for oxidation of iron.

Oxygen pressure (Torr)	K_p $(g.O\ cm^{-2}.s^{-\frac{1}{2}})$
0.3	3.14×10^{-4}
0.5	3.19×10^{-4}
10	3.33×10^{-4}
152	3.35×10^{-4}
152[*]	2.93×10^{-4}
760[**]	2.94×10^{-4}

*   From reference (87).

** From reference (88).

during the first minutes of oxidation is believed to be due to an "heating effect" (138). In order to support these findings we have also plotted on Fig. V, 4 results obtained with specimen 0.25 mm thick. With these specimens the magnitude of the temperature excess is more important than for specimen 0.8mm thick and the "heating effect" ends after only 1 min. of oxidation. If the samples are preoxidized during 1 min. the anomalous accelerated rate is not observed.

5.3.2 The Phenomena of Hematite Formation

After a few minutes of reaction a duplex scale consisting of FeO and Fe_3O_4 is obtained. The equilibrium dissociation pressure of hematite being at 800°C of the order of 4×10^{-7} torr, Fe_2O_3 formation is thermodynamically feasible, the reaction equation involved is

$$2Fe_3O_4 + \frac{1}{2}O_2 \longrightarrow 3Fe_2O_3 \qquad\qquad 5\text{-}6$$

If we suppose that the diffusing species in magnetite are iron ions (86), Fe_3O_4 formation only takes place according to the following reaction

$$4Fe_2O_3 + Fe \longrightarrow 3Fe_3O_4 \qquad\qquad 5\text{-}7$$

Consequently hematite is only nucleated on the magnetite when reaction (5-6) becomes faster than reaction (5-7) and therefore when

the supply of oxygen adsorbed exceeds the amount of iron diffusing
to the magnetite surface. This occurs after a certain period tc
which decreases when the oxygen pressure increases (tc $\simeq$ 3 hrs. if
po_2 = 0.3 torr and tc < 1 min. if po_2 = 760 torr). Then the Fe_2O_3
nuclei developped with a very preferred orientation of growth.
They are observed under the form of whiskers having, needles, blades
or platelets shape. This whisker development phenomena was studied
by Gulbransen (139) and Talbot and Bigot (140) upon exposing iron in
H_2O/H_2 atmospheres the temperature ranging between 350 and 550°C.
In oxygen or air at normal pressure in our temperature range, whisker
formation was reported by Paidassi (112) and Takagi (111), but never
such a big density of population was mentioned. In fact this
whisker growth phenomena is strongly dependent upon the metal purity
and therefore the observed density seems to be due to the high purity
of our iron (99.999). This argument is supported by the recent re-
sults of Jansson and Vannerberg (141) who upon oxidizing 99.998% iron
samples at 625°C obtained a very dense forest of whiskers. They
cover such an appreciable part of the Fe_2O_3 surface that, according
to the previous authors, oxidation became more difficult. Never-
theless our results do not support this last point of view since
Fig. V, 4 the oxidation curve obtained at 0.3 torr (without whisker
growth) is identical to this obtained under 152 torr (with whisker
growth). But on the other hand we will emphasize the important in-
crease of the relative thickness of hematite when whiskers formation
is observed. In fact lattice diffusion of either iron or oxygen in

hematite occurs at a much lower rate than lattice diffusion of iron in magnetite. Consequently the relative thickness of hematite must be lower than the relative thickness of magnetite in the multilayer scale. Nevertheless we only observe this when whiskers are not formed on the specimen surface. This means that when whiskers are observed diffusion of either cations or anions in hematite proceeds more rapidly than lattice diffusion i.e. by short-circuit diffusion. This idea is supported by the following facts. Whiskers formation occurs at low temperature (T less than 860°C) where the grain size of hematite is very small. On the other hand the activation energy advanced in the literature for the parabolic growth of hematite during oxidation of iron in atmospheric air (87) is much smaller than the values determined in the diffusion studies (40 Kcal/Mole compared to 77.9, 100, 112 and 146 Kcal/Mole). This first diffusion process must be retarded by the presence of impurities in hematite. That is the reason why the preceding phenomena are not observed during oxidation of Armco iron.

Finally since the growth of whiskers is pressure dependent we believe that their formation occurs at the Fe_2O_3/O_2 interface according to the mechanism illustrated Fig. V, 5. It follows from the previous remarks that during oxidation of iron in oxygen or air at atmospheric pressure hematite grows by short-circuit diffusion of iron. This conclusion being in agreement with the recent work of Holt and Himmel (142) who concluded from their diffusion measurements that iron was the mobile specie in Fe_2O_3. We will equally mention

— *Model of oxide platelet growth on iron*
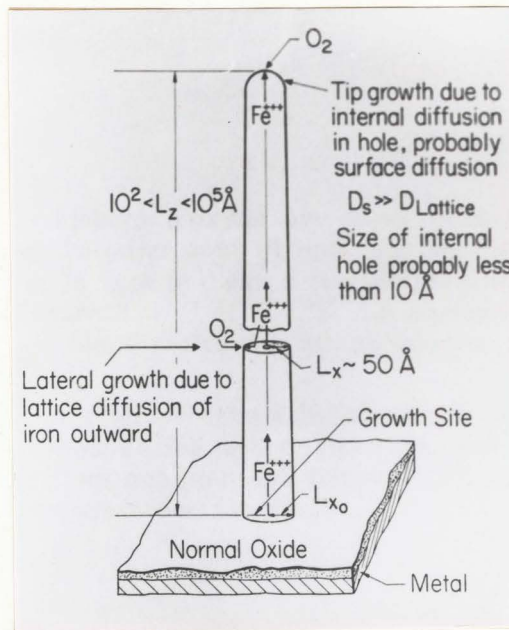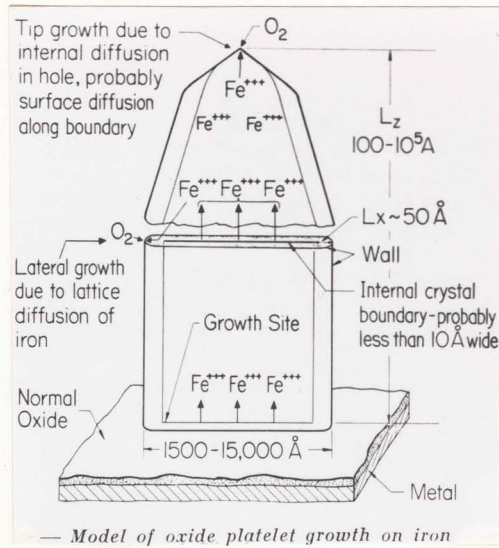
Model of needle growth

Figure V, 5

Model of Oxide whiskers growth. (From Reference 139)

that structural evidence has also been placed forward, by Arkharov
and Agapova (99), which indicates that iron is the predominant
migrating species in hematite when it is formed as the external
layer in a scale containing wustite. This mechanism given for
whisker growth of hematite from magnetite is that originally advanced
by Gulbransen (139). To this time, however, the rapid diffusion
channel for vertical growth of whiskers has not been defined. The
internal channel described as a tubular hole less than 10Å in
diameter must be closely associated with the crystallography to be
expected for a line defect or a crystal boundary in the oxide since
molecular or atomic oxygen is not believed to diffuse inward during
outward growth of a whisker.

5.4 Oxidation at Pressure Ranging between 2.5×10^{-3} to 3×10^{-1} Torr
     in the Temperature Range 750° to 1000°C.

The oxidation curves obtained at 1.5×10^{-2} torr in the
temperature range 750° to 1000°C exhibit the same form as the curve
obtained at 800°C, the region of linear behavior becoming longer
with increasing temperature. Consequently α and γ iron oxidize
according to the same mechanism. This idea being is supported by the
fact that at 1000°C (*) the magnitude of the linear rate constant was
also proportionally dependent on pressure. The only noticed dif-
ference in the oxidation behavior of α and γ iron was the change in
thin scale texture ((311) at 800°C and (100) at 1000°C). Values of
the linear oxidation constants, K_L, at temperatures in the range

(*) This was reported to be still valid at 950°C and 900°C (143).

750-1000°C were obtained from the linear section of the oxidation curves in Fig. IV, 29 and IV, 30. Their Arrhenius plot gave us an activation energy of approximatively 6 Kcal. $Mole^{-1}$. This value can be compared with the 7 ± 1 Kcal. $Mole^{-1}$ found by Charbonnier and Bardolle (64) for the linear oxidation of iron in the temperature range 800°-1000°C in oxygen at $9x10^{-5}$ torr pressure.

At temperatures as high as 1000°C nucleation and growth of magnetite could be observed. The magnetite crystals seem to develop, as the wustite nuclei in the early exposures stage, over a thin base film. The similarity between the two processes, i.e., nucleation of wustite or magnetite, consist also in the fact that the first nuclei were only observed after a certain induction period.

5.5 General Model for the Mechanism of Oxidation of Iron at High
     Temperature

According to our observations, the mechanism of iron oxidation can be divided into the following steps:

1. Nucleation and growth of wustite on iron.

2. Development of uniformly thick wustite scales according to an interfacial control reaction due to a weakly activated process involving the non-dissociative adsorption of oxygen.

3. Parabolic growth of wustite scales by means of outward diffusion of iron via vacancies.

4. Nucleation and growth of magnetite on wustite.

5. Parabolic growth of a duplex scale consisting of wustite and magnetite by means of outward diffusion of iron.

6. Nucleation and growth of hematite on magnetite.

7. Parabolic growth of a multilayer scale consisting of wustite, magnetite and hematite by means of outward diffusion of iron.

CHAPTER VI

CONCLUSIONS

1.1   Iron exposed to oxygen in the pressure range 2.5×10^{-3} – 3.0×10^{-1} torr the temperature ranging between 750 and 1000°C exhibits initially an increasing oxidation rate followed by a stage of linear kinetics before onset of parabolic kinetics. The first oxidation stage is associated with the growth of wustite crystals over an oxide base film whilst linear kinetics governs the growth of a uniformly thick wustite scale. At 800°C this scale exhibits a textured structure containing the (110), (100) and (311) faces of wustite in the predominant parallel orientations with the metal surface. The magnitude of the linear rate constant was proportionally dependent on pressure due to reaction control by a non-dissociative oxygen adsorption. The activation energy for this process was approximatively 6 Kcal/Mole, in agreement with the value of 7 Kcal/Mole advanced by previous authors.

1.2   After a certain time depending upon temperature and pressure magnetite was nucleated on the wustite surface. This process seems to exhibit the same general features as the phenomena of nucleation and growth of wustite.

1.3   Parabolic kinetics, which were not dependent upon oxygen pressure, governed growth of duplex scales containing layers of wustite and magnetite for exposures up to 125 min. Magnetite comprised less than 5% of scale thickness. Value of the parabolic

113

constant at low pressures were equal to those at pressures near 1 atm because the iron flux for scale growth was directly related to the iron vacancy concentration gradient in wustite established by the oxygen activities at the Fe/FeO and FeO/Fe$_3$O$_4$ interfaces.

2.1   At 800°C in the pressure range 3.0×10^{-1} to 760 torr magnetite was nucleated on the wustite surface after a period less than 10 min. therefore the oxidation rate was found to be independent of pressure.

2.2   After a certain time depending upon temperature and pressure hematite was nucleated on the magnetite surface. Then for temperatures less than 860°C the hematite nuclei developed by a mechanism involving the vertical and lateral growth of whiskers. This process was found to be strongly dependent upon temperature, oxygen pressure and metal purity.

2.3   According to our experimental results scaling of iron at high temperature must be attributed to outward diffusion of iron across the entire scale.

REFERENCES

1. J. Paidassi, "L'Oxydation des Métaux", p.13-116, editor J. Bénard, Gauthier-Villars Paris, 1964.

2. U. R. Evans, "The Corrosion and Oxidation of Metals", Edwin Arnold, London, 1960.

3. K. Hauffe, "Oxidation of Metals", Plenum Press, New York, 1965.

4. O. Kubaschewski and B. E. Hopkins, "Oxidation of Metals and Alloys", Butterworths, London, 1962.

5. P. Kofstad, "High Temperature Oxidation of Metals", Wiley, New York, 1966.

6. M. Hansen, "Constitution of Binary Alloys", McGraw-Hill, Inc., New York (1958).

7. R. Sifferlen, "Insolubility of Oxygen in α-Iron Purified by Zone Melting", C. R. Acad. Sci. Fr., $\underline{247}$, 1608 (1952).

8. M. T. Hepworth, R. P. Smith and E. T. Turkdogan, "Permeability, Solubility and Diffusivity of Oxygen in b.c.c. Iron", Trans. A.I.M.E., $\underline{236}$, 1278 (1966).

9. J. H. Swisher and E. T. Turkdogan, "Solubility, Permeability and Diffusivity of Oxygen in Solid Iron", Trans. A.I.M.E., $\underline{239}$, 426 (1967).

10. G. G. Charette and S. N. Flengas, "Thermodynamics Properties of the Oxides of Iron, Nickel, Lead, Copper and Manganese by e.m.f. Measurements", J. Electrochem. Soc., $\underline{115}$, 796 (1968).

11. P. E. C. Bryant and W. W. Smeltzer, "The Dissociation Pressure of Hematite", J. Electrochem. Soc., $\underline{118}$, 1409 (1969).

12. L. S. Darken and R. W. Gurry, "The System Iron-Oxygen: I. The Wustite Field and Related Equilibria. II. Equilibrium and Thermodynamics of Liquid Oxide and Others Phases", J. Am. Chem. Soc., $\underline{67}$, 1398 (1945); $\underline{68}$, 798 (1946).

13. N. G. Schmahl, D. Hennings and C. Rubelt, "Decomposition Equilibria in the System $Fe_2O_3-Fe_3O_4$", Arch. Eisenhutten ., $\underline{40}$, 375 (1969).

14. B. E. F. Fender and F. D. Riley, "Thermodynamic Properties of $Fe_{1-x}O$. Transitions in the Single Phase Region", J. Phys. Chem. Solids, $\underline{30}$, 793 (1969).

15. J. Campserveux, G. Boureau, C. Picard and P. Gerdanian, "Determination of the Limits of the Iron Protoxide Field at High Temperature", Rev. Int. Hautes Temp. Refract., $\underline{6}$, 165 (1969)

16. G. Lehmann, "Defects and Phase Magnitude of Wustite", Ber. Bunsenges Phys. Chem., $\underline{73}$, 349 (1969).

17. J. Manenc, J. Bourgeot and T. Herai", X-ray Diffraction Study of the Preprecipitation State of Wustite", C. R. Acad. Sci. Fr., $\underline{258}$, 4263 (1964).

18. P. Vallet and P. Raccah, "Limits of the Domain of Solid Wustite and the Resulting Phase Diagram", C. R. Acad. Sci. Fr., $\underline{258}$, 3679 (1964).
"Contribution to the Thermodynamic Study of Wustite", Mem. Sci. Rev. Met., $\underline{62}$, 1 (1965).

19. M. Kleman, "Thermodynamic Properties of FeO in Solid Form", Rev. Metall., $\underline{62}$, 457 (1965).

20. C. Carel, D. Weigel and P. Vallet, "Dilatometry of Varieties of Wustite and a Metastable Triple Point between the Three Varieties", C. R. Acad. Sci. Fr., 258, 3281, (1964).

"Variation of the Crystalline Parameter of Three Varieties of Solid Wustite within Their Respective Domains of Existence", C. R. Acad. Sci. Fr., 260, 4325 (1965).

21. C. Wagner and E. Koch, "Electrical Conductivity of Oxides of Cobalt and Iron", Z. Phy. Chem., B32, 439 (1936).

22. S. Takeuchi and K. Igari, "Statistical Thermodynamical Studies on Fundamental Reactions Concerning Steelmaking II: Oxidation and Reduction Equilibrium of Wustite with Gas Phases", Sci. Rep. Res. Inst. Tokyo Univ., A4, 164 (1952).

23. D. M. Smyth, "Deviation from Stoichiometry in MnO and FeO", J. Phys. Chem. Solids, 19, 167 (1961).

24. H. G. Sockel and H. Schmalzried, "Coulometric Titration of Transition Metal Oxides", Rev. Bunsenges. Phys. Chem., 72, 745 (1968).

25. D. S. Tannhauser, "Conductivity in Iron Oxides", J. Phys. Chem. Solids, 23, 25 (1962).

26. G. H. Geiger, R. L. Levin and J. B. Wagner, Jr., "Studies on the Defect Structure of Wustite using Electrical Conductivity and Thermoelectric Measurements", J. Phys. Chem. Solids, 27, 947 (1966).

27. B. Swaroop and J. B. Wagner, Jr., "On the Vacancy Concentrations of Wustite near the P to N Transition", Trans. A.I.M.E., 239, 1215 (1967).

28. D. M. Laptev, "Thermodynamics of Wustite", Russian J. Phys. Chem., 43, 1757 (1969).

29. G. G. Libowitz, "Nonstoichiometry in Chemical Compounds", Prog. Solid State Chem., 2, 216 (1965).

30. P. Kofstad and A. Z. Hed, "Defect Structure Model for Wustite", J. Electrochem. Soc., 115, 103 (1968).

31. W. L. Roth, "Defects in the Crystal and Magnetic Structures of Ferrous Oxide", Acta Cryst., 13, 140 (1960).

32. F. B. Koch and M. E. Fine, "Magnetic Properties of Fe_xO as Related to the Defect Structure", J. Appld. Phys., 38, 1470 (1967).

33. D. J. Elias and J. W. Linnett, "Oxidation of Metals and Alloys, Part 3: Mossbauer Spectrum and Structure of Wustite", Trans. Far. Soc., 65, 2673 (1969).

34. M. S. Seltzer and A. Z. Hed, "Analysis of the High Temperature Electrical Properties of Wustite", J. Electrochem. Soc., 117, 815 (1970).

35. H. J. Goldschmidt, "The Crystal Structures of Fe, FeO and Fe_3O_4 and their Interrelations J. Iron Steel Inst., 146, 157 (1942).

36. E. J. W. Verwey and P. W. Haayman, "Electronic Conductivity and Transition Point of Magnetite", Physica, 8, 979 (1941).

37. S. G. Bhatt and H. D. Merchant, "Influence of Stoichiometry on Lattice Parameters in Iron Oxide (Fe_3O_4), Nickel Oxide (NiO), and Nickel-Iron Ferrite", J. American Ceram. Soc., 52, 452 (1969).

38. J. Smut, "Structure of Wustite and the Variation of its X-ray Diffraction Intensities with Composition", J. Iron Steel Inst., 204, 237 (1966).

39. D. J. M. Bevan, J. P. Shelton and J. S. Anderson, "Properties of Some Simple Oxides and Spinels at High Temperatures", J. Chem. Soc., 2, 1729 (1948).

40. L. Himmel, R. F. Mehl and C. E. Birchenall, "Self-Diffusion of Iron in Iron Oxides and the Wagner Theory of Oxidation", Trans. A.I.M.E., 197, 827 (1953).

41. R. Lindner, "Diffusion of Radioactive Iron in Iron Oxide and Zinc-Iron Spinel", Arkiv. Kemi, 4, 481 (1952).

42. W. C. Hagel, "Oxygen-Ion Diffusion in Hematite", Trans. A.I.M.E., 236, 179 (1966).

43. P. Hembree and J. B. Wagner, Jr., "The Diffusion of Fe_{55} in Wustite as a Function of Composition at 1100°C", Trans. A.I.M.E., 245, 1547 (1969).

44. H. J. Engell "The Concentration Gradient of Iron-Ion-Vacancies in Wustite Scaling Films and the Mechanism of Oxidation of Iron", Acta Met., 6, 439 (1958).

45. P. Desmarescaux and P. Lacombe, "Self-Diffusion of Iron in Wustite", Mem. Sci. Rev. Met., 60, 899 (1963).

46. P. Desmarescaux and P. Lacombe, "Role of Cations in the Electrical Conductivity of Wustite", Mem. Sci. Rev. Met., 61, 157 (1964).

47. P. E. Childs, L. W. Laub and J. B. Wagner, Jr., "Chemical Diffusion in Non-Stoichiometric Compounds", Proc. Br. Ceramic Soc., 19, 29(1971).

48. P. J. Harrop, "Self-Diffusion in Simple Oxides", J. Materials Sc., 3, 206 (1968).

49. S. M. Klotsman, A. N. Timofeyev and I. S. Trakhtenberg, "The Problem of the Measurement of Diffusion Coefficients in Oxide Phases", Phys. Metals Metallogr., 10, 93 (1960).

50. V. I. Izvekov, "Diffusion of Fe in Magnetite", Inzh. Fiz. Akad. Nauk. Belorus, S.S.R., 1, 64 (1958).

51. V. I. Izvekov, N. S. Gorbunov and A. A. Babad-Zakhryapin, "Diffusion of Iron in Hematite", Fiz. Metal. i Metalloved., 14, 33 (1962). Phys. Metals Metallogr., 14, 195 (1962).

52. W. D. Kingery, D. C. Hill and R. P. Nelson, "Oxygen Mobility in Polycristalline $NiCr_2O_4$ and $\alpha-Fe_aO_3$", J. Amer. Ceram. Soc., 43, 473 (1960).

53. J. Bardolle and J. Bénard, "The Existence of a Process of Germination in the Controlled Oxidation of Iron at Elevated Temperatures", C.R. Acad. Sci. Fr., 232 (1951).

54. J. Bardolle and J. Bénard, "A Study of The Mechanism of Oxidation or Iron Single Crystals" Rev. Met. 49, 613 (1952).

55. J. Bénard, "L'Oxydation des Métaux", Vol.I, p. 74, editor J. Bénard, Gauthier-Villars, Paris, 1962 .

56. E. A. Gulbransen, W. R. McMillan, K. F. Andrew, "Electron Optical Study of Oxidation of High Purity Iron at Low Oxygen Pressures". Trans. A.I.M.E., 200, 1027 (1954).

57. E. A. Gulbransen and K. F. Andrew, "Oxide Nucleation and the Substructure of Iron", J. Electrochem. Soc., 106, 511 (1959).

58. R. F. Mehl, E. L. McCandless and F. N. Rhines, "Orientation of Oxide Films on Metals", Nature, London, 134, 1009 (1934).

59. T. N. Rhodin, Jr., W. H. Orr and D. Walton, "Nucleation and Growth of Oxide on Metals", Mem. Sci. Rev. Met., LXII, 67 (1965).

60. J. Bénard, Acta Met., 8, 272 (1960).

61. G. E. Rhead, "Surface Diffusion and the Growth of Oxide Particles on Metal Surfaces", Trans. Far. Soc., 61, 797 (1965).

62. J. F. Chittum, "Reverse Pit Theory of Oxidation Nuclei", Mem. Sci. Rev. Met., LXII, 67 (1965).

63. J. C. Charbonnier, J. Bardolle and D. Mollimard, "Nucleation Kinetics during Controlled Oxidation of Iron", Rev. Metall., 7, 107 (1967).

64. J. C. Charbonnier and J. Bardolle, "Kinetics of the Controlled Oxidation of Iron at High Temperatures", Mem. Sci. Rev. Met., LXV, 423 (1968).

65. J. Bardolle and B. Blaise, "Wustite Crystal Formation on a Crystal of Iron", Mem. Sci. Rev. Met., LXII, III (1965).

66. J. Paidassi, Bul. Soc. Chilena Quim., 5, 46 (1953); reference 1, page 79.

67. J. Paidassi and D. Fuller, "Constitution and Morphology of the Superficial Oxidation Film of Iron in Water Vapor at Elevated Temperatures", C.R. Acad. Sci. Fr., 246, 604, (1958) J. Paidassi and M. Hoogewys, "Constitution and Morphology of the Oxidation Film on Iron in Carbon Dioxide at High Temperatures", C.R. Acad. Sci. Fr., Ser. C., 270, 1229 (1970). M. Hoogewys, J. Paidassi and R. Darras, "Kinetics of the Reaction on Iron with Carbon Dioxide at Atmospheric Pressure and High Temperatures", C.R. Acad. Sci. Fr., Ser. C., 271, 97 (1970).

68. K. Fischbeck, L. Neundeubel and F. Salzer, "The Reactivity of Crystal Forms", Z. Elektrochem., 40, 517 (1934).

69. K. Hauffe and H. Pfeiffer, "Kinetics of Wustite Formation in the Oxidation of Iron", Z. Metallkunde., 44, 27 (1953).

70. V. I. Arkharov, V. P. Mar'evich, M. Reinkhol, and M. I. Simonova, "Structure of Iron Scale, XI: Scale Formed on Oxidation of Iron by Carbon Dioxide", Fiz. Metal. Metalloved, 5, 251 (1957).

71. W. W. Smeltzer, "The Oxidation of Iron in Carbon Dioxide-Carbon Monoxide Atmospheres", Trans. A.I.M.E., 218, 674 (1960).

72. W. W. Smeltzer, "The Kinetics of Wustite Scale Formation on Iron", Acta Met., 8, 377 (1960)

73. F. S. Pettit, R. Yinger and J. B. Wagner, Jr., "The Mechanism of Oxidation of Iron in Carbon Monoxide-Carbon Dioxide Mixtures", Acta. Met., 8, 617 (1960).

74. F. S. Pettit and J. B. Wagner, Jr., "Transition From the Linear to the Parabolic Rate Law during the Oxidation of Iron to Wustite in $CO-CO_2$ Mixtures", Acta. Met., 12, 35 (1964).

75. H. J. Grabke, "Kinetics of Oxygen Transport from Carbon Dioxide to the Surface of Iron", Proc. Intern. Congr. Catalysis, 3rd., Amsterdam, 2, 928 (1964).

76. E. T. Turkdogan, W. M. McKewan and L. Zwell, "Rate of Oxidation of Iron to Wustite in Water Hydrogen Gas Mixtures", J. Phys. Chem., $\underline{69}$, 327 (1965).

77. M. Billy and P. Raynaud, "Kinetics of Iron Oxidation by Water Vapor at Elevated Temperature", Ind. Chim. Belge., $\underline{32}$, 417 (1967).

78. H. Pfeiffer and C. Laubmeyer, "Dependence of the Oxidation of Iron at 1000"C on Oxygen Pressure and the Problem of Matter Transport in Fe_2O_3", Z. Elektrochem., $\underline{59}$, 579 (1955).

79. L. A. Morris and W. W. Smeltzer, "The Kinetics of Wustite Scale Formation on Iron Nickel Alloys", Acta. Met., $\underline{15}$, 1591 (1967).

80. H. J. Grabke, K. J. Best and A. Gala, "Oxygen Exchange from CO_2-CO and H_2O-H_2 Mixtures to Metals and Oxides", Werkstoffe u. Korrosion, $\underline{21}$, 911 (1970).

81. J. Bénard and J. Talbot, "The Kinetics of the Reaction of Oxidation of Iron in its Initial Phase", C. R. Acad. Sci. Fr., $\underline{226}$, 912 (1948).

82. B. Chattopadhyay and J. C. Measor, "Initial Oxidation of Pure Iron and the Effect of the Allotropic Transformation", Brit. Corrosion J., $\underline{4}$, 216 (1969).

83. J. C. Measor and K. K. Afzulpurkar, "Initial Oxidation Rate of Pure Iron and the Effect of the Curie Temperature", Phil. Mag, $\underline{10}$, 817 (1964).

84. N. B. Pilling and R. E. Bedworth, "Oxidation of Metals at High Temperatures", J. Inst. Metals, $\underline{29}$, 529 (1923).

85. L. B. Pfeil, "The Oxidation of Iron and Steel at High Temperatures", J. Iron and Steel Inst., $\underline{119}$, 501 (1929).

86. M. H. Davies, M.T. Simnad, and C. E. Birchenall, "On the Mechanism and Kinetics of the Scaling of Iron". Trans. A.I.M.E., $\underline{191}$, 889 (1951).

87. J. Paidassi, "Oxidation of Iron in Air between 700 and 1250°C"., Rev. Met., $\underline{LIV}$, 569 (1957).

88. N. G. Schmahl, H. Baumann, and H. Schenck, "The Temperature Dependence of Scaling of Pure Iron in Oxygen", Arch. Eisenhutten ., $\underline{29}$, 83 (1958).

89. C. Wagner,"Theory of the Tarnishing Process", Z. Physik. Chem., $\underline{B21}$, 25 (1933).

90. M. H. Davies, M. T. Simnad and C. E. Birchenall, "A Corrected Interpretation of the Mechanism of Growth of Magnetite During Oxidation", Trans. A.I.M.E.; $\underline{197}$, 1250 (1953).

91. J. Moreau and M. Cagnet, "Growth and Structure of Oxide Films on Iron at Elevated Temperatures", Rev. Met., $\underline{55}$, 1091 (1958).

92. R. F. Tylecote and T. E. Mitchell, "Marker Movement in the Oxidation of Iron", J. Iron Steel Inst., $\underline{196}$, 445 (1960).

93. C. Wagner, "Diffusion and High Temperature Oxidation of Metals", Atom Movements, Am. Soc. Metals, Cleveland, p. 153 , 1951.

94. A. Rahmel and H. J. Engell, "Effect of Oxygen on Oxidation Velocity of Pure Iron", Arch. Einsenhutten, $\underline{30}$, 743 (1959).

95. P. Belin, "Kinetics of Oxidation of Iron at High Temperature in the Presence of Oxygen at Low Pressure ", Corrosion et anti-corrosion, 7, 384 (1959). "Investigation of the Kinetics of Oxidation of Iron at High Temperature and Low Oxygen Pressure", Corrosion et anti-corrosion ; 8, 96 (1960); 8, 140 (1960).

96. N. G. Schmahl, H. Kuppersbusch and H. Schenck, "Oxidation of Pure Iron and Iron-Silicon Alloys as a Function of Oxygen Pressure", Arch. Eisenhuttenw, 34, 115 (1963).

97. K. Hauffe, Metalloberfl., A8, 97 (1954); reference 3, p. 285.

98. V. I. Tikhomirov, "Theory of Rate of Oxidation of Iron and Ferrous Alloys at High Temperatures, I: Oxidation of Iron under Conditions of Two-Layer Scale Formation", Uchenye Zapiskileningrad-Gosudarst-Univ. 175, Ser. Khim. Nauk, 14, 168 (1954).

99. V. K. Arkharov and Y. V. Agapova, "Structural Features of the Hematite of Iron Scale related to the Conditions under which It was Formed", Fiz. Metal. Metallowed., 20, 384 (1965).

100. V. K. Arkharov and B. S. Borissov, "On Texture in Iron Scale, IX: Electron Diffraction Investigation of Textures in the Hematite layer at Different Stages of the Oxidation of Iron in Air", Phys. of metals and Metallogr. 4, 58(1957).

101. Y. V. Agapova and V. K. Arkharov, "X-Ray Diffraction Analyses of the Hematite in Iron Scale", Fiz. Metal Metalloved, 28, 841 (1969).

102. N. G. Schmahl, H. Baumann and H. Schenck, "The Scaling of Pure Iron and Scaling in General", Arch. Eisenhuttenw., 27, 707 (1956). "Over-Temperatures Occuring during the Scaling of Pure Iron and their Theoretical Treatment", Arch. Eisenhuttenw., 29, 41(1958).

103. D. Caplan, "Overtemperature in Metal Scaling", J. Electrochem. Soc., 107, 359 (1960).

104. G. Valensi, "L'Oxydation Des Métaux", Vol. I, P. 173, Editor J. Bénard, Gauthier-Villars, Paris, 1962 .

105. P. D. Dankov and P. V. Churaev, "The Deformation Effect of the Surface Layer of a Metal upon Oxidation", Dokl. Akad. Nauk., SSSR, 73, 1221 (1950).

106. D. Bruce and P. Hancock, "Influence of Mechanical Properties of Surface Oxide Films on Oxidation Mechanisms. I: A Vibrational Technique to Study the Nature and Growth of Thermally Formed Oxide Films on Metals. II. Mechanical Properties and Adhesion of Surface Oxide Films on Iron and Nickel Measured during Growth", J. Inst. Metals, 97, 140, 148 (1969).

107. A. T. Gordon, G. Bitsianes and T. L. Joseph, "Thermal Expansion Coefficients for Iron and its Oxides from X-ray Diffraction Measurements at Elevated Temperature", Trans A.I.M.E., 233, 1519 (1965).

108. D. L. Douglass, "The Role of Oxide Plasticity on the Oxidation Behavior of Metals: a Review", J. Oxidation Metals, 1, 127 (1969).

109. J. Stringer, "Stress Generation and Relief in Growing Oxide Films", Corrosion Sci., 10, 513 (1970).

110. J. D. Mackenzie and C. E. Birchenall, "Plastic Flow of Iron Oxides and the Oxidation of Iron", Corrosion, 13, 783 (1957).

111. R. Takagi, "Growth of Oxide Whiskers on Metals at High Temperature", J. Phys. Soc., Japan, 12, 1212 (1957).

112. J. Paidassi, "On Growth of Hematite Needles in the Scales Formed on Iron During High Temperatures Oxidation", Acta. Met., 6, 778 (1958).

113. B. W. Dunnington, F. H. Beck and M. G. Fontana, "The Mechanism of Scale Formation on Iron at High Temperature", Corrosion, 8, 2 (1952).

114. D. A. Vermilyea, "On the Mechanism of the Oxidation of Metals", Acta Met. 5, 492 (1957).

115. D. W. Juenker, R. A. Meussner and C. E. Birchenall, "Cavity Formation in Iron Oxides", Corrosion, 14, 57 (1958).

116. H. Engell and F. Wever, "Some Basic Problems of the Formation and Adherence of Scale on Iron", Acta Met., 5, 695 (1957).

117. A. G. Eubanks, D. G. Moore and W. A. Pennington, "Effect of Surface Roughness on Oxidation Rate of Iron", J. Electrochem. Soc., 109, 382 (1967).

118. D. Caplan and M. Cohen, "Effect of Cold Work on the Oxidation of Iron from 400-650°C", Corrosion Science, 6, 321 (1966).

119. C. E. Birchenall, "Kinetics of Formation of Porous or Partially Detached Scales", J. Electrochem. Soc., 103, 619 (1956).

120. R. Collongues and G. Chaudron, "Study of the Structure and of the Properties of the Wustite Scale Formed on the Surface of High Purity Iron, Rev. Met., 49, 699 (1952).

121. R. Collongues, R. Sifferlen and G. Chaudron, "Study of the Oxidation of High Purity Iron and of the Ways in which Ferrous Oxide Decomposes", Rev. Met. 50, 727 (1953).

122. M. R. Sifferlen, "Solubility of Oxygen in Iron and Structure of the Oxidation Interface", Mem. Sci. Rev. Met., LXV, 413 (1968).

123. F. K. Peters and H. J. Engell, "The Adhesion of Scale on Steel", Arch. Eisenhuttenw, 30, 275 (1959).

124. R. F. Tylecote, "The Adherence of Oxide Films on Metals", J. Iron Steel. Inst., 195, 280 (1960).

125. J. Maldy, "The Structure of the Iron-Iron Oxide Interface. Role of the Residual Impurities", Mem. Sci., Rev. Met., LXII, 379, 439 (1965).

126. H. Dlaska, H. Trenkler, "Oxidation of Pure Iron and Iron Carbon Alloys in Carbon-Dioxide, Steam, Oxygen and Different Flue Gas Atmosphere at 900°-1300°C", Berg-Huettenmaenn. Monatsh, 113, 313 (1968).

127. A. Rahmel and J. Toboloski, "The Influence of Water Vapor and Carbon Dioxide on the Oxidation of Iron in Oxygen at High Temperature", Werkstoffe u. Korrosion, 16, 662 (1965).

128. A. Rahmel and J. Toboloski, "Influence of H_2O and CO_2 on the Oxidation of Fe in O_2 at High Temperature", Corrosion Science, 5, 333 (1965).

129. C. W. Tuck, "Oxidation Behavior of Iron-Silicon Alloys Between 800 and 1000°C in Carbon Monoxide-Carbon Dioxide Mixtures", Intern. Congr. on Metallic Corrosion, 1st., London, Eng. page 221 (1961).

130. C. W. Tuck, "Oxidation Behavior of Iron-Silicon Alloys Between 800° and 1000°C in Carbon Monoxide - Carbon Dioxide Mixtures", Int. Congr. on Metallic Corrosion, 1st., London, Engl., p. 221 (1961).

131. W. E. Boggs, R. H. Kachik and G. E. Pelissier, J. Electrochem. Soc., 112, 539 (1965).

132. W. E. Boggs, R. H. Kachik and G. E. Pelissier, J. Electrochem. Soc., 114, 32 (1967).

133. M. J. Graham and M. Cohen, J. Electrochem. Soc., 116, 1430 (1969).

134. D. Caplan, M. J. Graham and M. Cohen, Corrosion Science, 10, 1 (1970).

135. R. J. Hussey and M. Cohen, Corrosion Science, 11, 699 (1971).

136. R. J. Hussey and M. Cohen, Corrosion Science, 11, 713 (1971).

137. N. G. Schmahl, H. Baumann and H. Schenck, Arch. Eisenhutten., 29, 147 (1958).

138. A. G. Goursat, Thèse Doct. Chimie Physique, Poitiers, (1970).

139. E. A. Gulbransen, in "Processus de Nucléation dans les Réactions des Gaz sur les Métaux et Problèmes Connexes" published in Mem. Sci. Rev. Met., LXII, 253 (1965).

140. S. Talbot and J. Bigot, ibid., 261 (1965).

141. L. Jansson and N. G. Vannerberg, Oxidation of Metals, 3, 453 (1971).

142. J. B. Holt and L. Himmel, J. Electrochem. Soc., 116, 1569 (1969).

143. R. J. Hussey and G. R. Wallwork, Private communication.